MODERN PROBLEMS IN STATISTICAL PHYSICS OF BOSE-EINSTEIN CONDENSATION AND IN ELECTRODYNAMICS OF FREE ELECTRON LASERS

A Dissertation

by

KONSTANTIN DORFMAN

Submitted to the Office of Graduate Studies of
Texas A&M University
in partial fulfillment of the requirements for the degree of

DOCTOR OF PHILOSOPHY

May 2009

Major Subject: Physics

MODERN PROBLEMS IN STATISTICAL PHYSICS OF BOSE-EINSTEIN CONDENSATION AND IN ELECTRODYNAMICS OF FREE ELECTRON LASERS

A Dissertation

by

KONSTANTIN DORFMAN

Submitted to the Office of Graduate Studies of
Texas A&M University
in partial fulfillment of the requirements for the degree of

DOCTOR OF PHILOSOPHY

Approved by:

Chair of Committee,	Vitaly Kocharovsky
Committee Members,	Glenn Agnolet
	Alexey Belyanin
	Peter Kuchment
Head of Department,	Edward Fry

May 2009

Major Subject: Physics

ABSTRACT

Modern Problems in Statistical Physics of Bose-Einstein Condensation
and in Electrodynamics of Free Electron Lasers. (May 2009)
Konstantin Dorfman, B.S., Nizhny Novgorod State University;
M.S., Texas A&M University
Chair of Advisory Committee: Dr. Vitaly Kocharovsky

In this dissertation, I have studied theoretical problems in statistical physics and electrodynamics of Bose particles, namely, mesoscopic effects in statistics of Bose-Einstein condensate (BEC) of atoms and electromagnetic waveguide effects of planar Bragg structures in Free Electron Lasers.

A mesoscopic system of a trapped gas of Bose atoms is the most difficult for the theoretical analysis in quantum statistical physics since it cannot be studied by neither a quantum mechanics of the simple microscopic systems of one or very few atoms nor a standard statistical physics of the macroscopic systems that implies a thermodynamic limit.

I present analytical formulas and numerical calculations for the moments and cumulants of BEC fluctuations in both ideal and weakly interacting gas.

I analyze the universal scaling and structure of the BEC statistics in a mesoscopic ideal gas in the critical region. I present an exactly solvable Gaussian model of BEC in a degenerate interacting gas and its solution that confirms the universality and constraint-cut-off origin of the strongly non-Gaussian BEC statistics.

I consider a two-energy-level trap with arbitrary degeneracy of an upper level and find an analytical solution for the condensate statistics in a mesoscopic ideal gas. I show how to model BEC in real traps by BEC in the two-level or three-level traps.

I study wave propagation in the open oversized planar Bragg waveguides, in par-

ticular, in a planar metal waveguide with corrugation. I show that a step perturbation in a corrugation phase provides a high selectivity over transverse modes.

I present a new Free Electron Laser (FEL) amplifier scheme, in which the radiation is guided by the planar Bragg structure with slightly corrugated walls and a sheet electron beam is traveling at a significant angle to the waveguide axis. By means of nonlinear analysis, I demonstrate that the proposed scheme provides an effective mode filtration and control over the structure of the output radiation and allows one to achieve amplification up to 30 dB in the existing FEL machines.

To my beloved parents Evgeniy Dorfman and Tatiana Bystrova

ACKNOWLEDGMENTS

I would like to thank everybody who has inspired, encouraged, and helped me in my work towards Ph.D. although it is nearly impossible to come up with a complete list.

In particular, I would like to express my gratitude to my advisor, Dr. Vitaly Kocharovsky, for his guidance and patience. I would like to thank the members of the Ph.D. committee, Dr. Glenn Agnolet, Dr. Alexey Belyanin, and Dr. Peter Kuchment, for their endurance and patience.

The Physics Department of Texas A&M University is also gratefully acknowledged.

Finally, I wish to thank my parents for their love, encouragement, understanding, and patience.

TABLE OF CONTENTS

CHAPTER Page

CHAPTER Page

LIST OF FIGURES

FIGURE Page

FIGURE Page

FIGURE Page

FIGURE Page

FIGURE Page

FIGURE Page

FIGURE Page

CHAPTER I

INTRODUCTION

The dissertation consists of two parts. In the first part I study theoretical problems in statistical physics of Bose atoms, namely, mesoscopic effects in statistics of Bose-Einstein condensate (BEC) of atoms. In the second part I discuss electrodynamics of Bose particles, in particular, electromagnetic waveguide effects of planar Bragg structures in Free Electron Lasers.

A. Phenomenon of the Bose-Einstein condensation

In 1924-1925 Einstein published two papers [1, 2] where he generalized the work of Bose [3] on the quantum statistics of photons to the case of an ideal gas with a fixed number of atoms. In the second paper he predicted the condensation of atoms to the lowest energy state. At high enough temperature the distribution function of atoms in the momentum space for a large box trap is:

$$\bar{n}_p = \left(\exp\left[\frac{\epsilon(p) - \mu}{T} \right] - 1 \right)^{-1}, \qquad T > T_c, \tag{1.1}$$

where $\mu \leq 0$ is a chemical potential of a gas and $\epsilon(p) = p^2/2m$ is an atomic energy as a function of momentum $\mathbf{p}$. It was shown that the distribution becomes different below the temperature of the phase transition

$$T_c = 3.31 \frac{\hbar^2}{m} n^{2/3}, \tag{1.2}$$

where n is the number density of the gas and the degeneracy factor is assumed to be $g = 1$. Namely, below the critical temperature the mean number of atoms $\bar{n}_0$ with

---

The journal model is Physical Review Letters.

the zero momentum $\mathbf{p} = 0$ (the condensed atoms) is macroscopically large, that is proportional to the total number of particles N,

$$\bar{n}_0 = N\left[1 - \left(\frac{T}{T_c}\right)^{3/2}\right], \qquad T < T_c. \tag{1.3}$$

The noncondensed atoms with the momentum $\mathbf{p} \neq 0$ are distributed according to Eq. (1.1) with the zero chemical potential $\mu = 0$, i.e.,

$$\bar{n}_p = \left(\exp\left[\frac{\epsilon(p)}{T}\right] - 1\right)^{-1}, \qquad T < T_c. \tag{1.4}$$

The phenomenon of Bose-Einstein condensation (BEC) plays an important role in many physical systems, including superliquid helium, electrons in the superconductors, and excitons in the semiconductors. In all these cases BEC is mixed with a strong interaction or a complicated structure of the system itself. For example, there is no doubt, that the condensate exists in the superliquid ^{4}He, but the precise measurement of the number of condensed atoms from the neutron scattering data is not direct and involves complicated theoretical calculations.

The theory of BEC is related to the theories of superfluidity and second order phase transitions. Following the classical Landau theory of the second order phase transitions applied to the liquid Helium [4, 5], one can conclude that the occurrence of superfluidity in liquid helium involves a second order phase transition, which results in the qualitative change in the properties of the matter. From the microscopic point of view, a transition between the normal state and the superfluid state at the λ-point depends on the certain property of the momentum distribution of the actual particles; namely, in a superfluid, a macroscopically large number of particles have zero momentum, which means that these particles form Bose-Einstein condensate in the momentum space.

The theory of BEC is formulated in terms of $\hat{\Psi}$ operator, which can be written

in the interaction representation as follows:

$$\hat{\Psi}(\mathbf{r},t)=\frac{1}{\sqrt{V}}\sum_{\mathbf{p}}\hat{a}_{\mathbf{p}}\exp\{\frac{i}{\hbar}\mathbf{p}\cdot\mathbf{r}-\frac{i}{\hbar}\frac{p^2}{2m}t\}. \tag{1.5}$$

One can write the $\hat{\Psi}$ operator as:

$$\hat{\Psi}=\hat{\Xi}+\hat{\Psi}', \qquad \hat{\Psi}^{\dagger}=\hat{\Xi}^{\dagger}+\hat{\Psi}'^{\dagger}, \tag{1.6}$$

where the operators $\hat{\Xi}^{\dagger}$ and $\hat{\Xi}$ are the creation and annihilation operators of the particle in the condensate ignoring the non-commutativity of the operators $\hat{a}_0$ and $\hat{a}_0^{\dagger}$. In the thermodynamic limit, i.e. at $N\to\infty$, $V\to\infty$ and a finite given value of the number density N/V, the matrix elements of the $\hat{\Xi}$ operators can be written as:

$$\lim_{N\to\infty}\langle m,N|\hat{\Xi}|m,N+1\rangle=\Xi, \qquad \lim_{N\to\infty}\langle m,N+1|\hat{\Xi}^{\dagger}|m,N\rangle=\Xi^{*}, \tag{1.7}$$

where Ξ is a complex number. Since the remaining part, corresponding to the non-condensate, converts the state $|m,N\rangle$ into states orthogonal to it, one has zero matrix elements

$$\lim_{N\to\infty}\langle m,N|\hat{\Psi}'|m,N+1\rangle=\lim_{N\to\infty}\langle m,N+1|\hat{\Psi}'^{\dagger}|m,N\rangle=0 \tag{1.8}$$

and in the thermodynamic limit the difference between the states $|m,N\rangle$ and $|m,N+1\rangle$ disappears entirely. In this sense, the quantity Ξ becomes the mean value of the operator $\hat{\Psi}$ for that state [4, 5].

In the homogeneous liquid at rest, the quantity Ξ is independent of the coordinates and time, which can be proved by an appropriate choice of the phase of this complex quantity and by considering the Hamiltonian $\hat{H}'=\hat{H}-\mu\hat{N}$. Therefore,

$$\Xi=\sqrt{\bar{n}_0}, \tag{1.9}$$

where $\bar{n}_0$ is the mean number of the condensate particles per unit volume of the

liquid. In the case of the superfluid motion, which takes place in the liquid under the non-stationary and non-uniform (over distances large in comparison with the interatomic distances) external conditions, the BEC also takes place, but now one cannot assert that it occurs in the state with the zero momentum. The quantity Ξ, defined in Eq. (1.7), now is the function of the coordinates and time and represents the particle wavefunction in the condensate. It is normalized by the condition $|\Xi|^2 = \bar{n}_0$, and, therefore, can be expressed as:

$$\Xi(t, \mathbf{r}) = \sqrt{\bar{n}_0(t, \mathbf{r})}\exp(-i\Phi(t, \mathbf{r})). \tag{1.10}$$

The gradient of the phase of the condensate wavefunction determines the velocity of the superfluid motion

$$\mathbf{v}_s = (\hbar/m)\nabla\Phi. \tag{1.11}$$

Since there is a macroscopically large number of particles in the condensate, the wave function of this state becomes a classical macroscopic quantity.

The existence of the condensate changes dramatically the density matrix to the liquid

$$N\rho(\mathbf{r_1}, \mathbf{r_2}) = \langle m, N|\hat{\Psi}^\dagger(t, \mathbf{r_2})\hat{\Psi}(t, \mathbf{r_1})|m, N\rangle. \tag{1.12}$$

In the homogeneous liquid, this function depends only on the difference $\mathbf{r} = \mathbf{r_1} - \mathbf{r_2}$. Therefore, substituting the operator $\hat{\Psi}$ from Eq. (1.6) and using the properties of Eqs. (1.7) and (1.8), we get:

$$N\rho(\mathbf{r_1}, \mathbf{r_2}) = \bar{n}_0 + N\rho'(\mathbf{r_1}, \mathbf{r_2}). \tag{1.13}$$

The density matrix ρ' for the noncondensed particles tends to zero as $|\mathbf{r_1} - \mathbf{r_2}| \to \infty$, whereas the total density matrix ρ tends to the finite limit $\bar{n}_0/N$. This expresses the "long-range order" in a superfluid, which is not present in ordinary liquids, where one

always has $\rho \to 0$ as $|\mathbf{r_1} - \mathbf{r_2}| \to \infty$. The fact that Ξ is complex, means that the order parameter, which characterizes the symmetry of the system, has two components, and the effective Hamiltonian [4] of the system depends only on $|\Xi|^2$, i.e., is invariant under the transformation $\Xi \to e^{i\alpha}\Xi$ for any real phase α.

The empirical results concerning the λ-transition in liquid helium, seem to indicate, that there is no region in which the Landau mean-field theory of phase transitions [4-6] is valid. Hence, for superfluid liquid helium as well as for other BEC critical phenomena at $|T - T_\lambda| << T_\lambda$ one should employ the fluctuation theory of the phase transitions of the second kind to relate the temperature dependences of various quantities. In particular, the temperature dependence of the order parameter and, therefore, the condensate density $\bar{n}_0$ as $T \to T_\lambda$ is given by a critical index β [4, 6],

$$|\Xi| = \sqrt{\bar{n}_0} \propto (T_\lambda - T)^\beta. \tag{1.14}$$

The temperature dependence of the specific heat c_p is of special interest. One can employ the hypothesis of the scale invariance, which implies, that the characteristic length of the fluctuations is the correlation radius r_c of the fluctuations. In particular, the square of the superfluid velocity, obtained from Eq. (1.11) varies with temperature according to:

$$v_s^2 \propto 1/r_c^2 \propto (T_\lambda - T)^{2\nu}, \tag{1.15}$$

where ν is the critical index of the correlation radius. Considering the long-wavelength fluctuations, which in fact govern the singularity of the thermodynamic quantities at the transition point, one can assume that the kinetic energy close to the transition point varies with the temperature in the same way as the singular part of the thermodynamic potential of the liquid, i.e. as $(T_\lambda - T)^{2-\alpha}$, where α is a critical index of

the specific heat c_p. Thus, we find:

$$\rho_s v_s^2 \propto \rho_s (T_\lambda - T)^{2\nu} \propto (T_\lambda - T)^{2-\alpha}, \tag{1.16}$$

whence $\rho_s \propto (T_\lambda - T)^{2-\alpha-2\nu}$. Using the relation $3\nu = 2 - \alpha$ which follows from the hypothesis of scale invariance [4, 6], we have:

$$\rho_s \propto (T_\lambda - T)^{(2-\alpha)/3}, \tag{1.17}$$

which finally relates the temperature dependences of ρ_s and specific heat c_p near the phase transition point.

In order to derive the equation for the condensate wavefunction (order parameter) $\Xi(\mathbf{r}, t)$, one has to write the time evolution of the field operator $\hat{\Psi}(\mathbf{r}, t)$ using the Heisenberg equation of motion [7, 8]:

$$i\hbar \frac{\partial}{\partial t} \hat{\Psi}(\mathbf{r}, t) = \left[\hat{\Psi}, \hat{H}\right] = \left[-\frac{\hbar^2 \nabla^2}{2m} + V_{ext}(\mathbf{r}) + \int d\mathbf{r}' \hat{\Psi}^\dagger(\mathbf{r}', t) V(\mathbf{r} - \mathbf{r}') \hat{\Psi}(\mathbf{r}', t)\right] \hat{\Psi}(\mathbf{r}, t), \tag{1.18}$$

where a many-body Hamiltonian $\hat{H}$

$$\hat{H} = \int d\mathbf{r} \hat{\Psi}^\dagger(\mathbf{r}) \left[-\frac{\hbar^2 \nabla^2}{2m} + V_{ext}(\mathbf{r})\right] \hat{\Psi}(\mathbf{r}) + \frac{1}{2} \int d\mathbf{r} d\mathbf{r}' \hat{\Psi}^\dagger(\mathbf{r}) \hat{\Psi}^\dagger(\mathbf{r}') V(\mathbf{r} - \mathbf{r}') \hat{\Psi}(\mathbf{r}') \hat{\Psi}(\mathbf{r}). \tag{1.19}$$

includes a two-body interaction. Replacing the operator $\hat{\Psi}$ with the classical field Ξ and thus, considering only large distances $\mathbf{r} - \mathbf{r}'$, one can specify the interaction term in Eq. (1.18) in the simplest approximation. Assume that the gas of atoms is cold and dilute, and, therefore, only binary collisions at low energy are relevant. These collisions are characterized by a single parameter, the s-wave scattering length a, independently of the details of the two-body potential. Thus, one can replace the

interaction term $V(\mathbf{r}-\mathbf{r}')$ in Eq. (1.18) with the following expression:

$$V(\mathbf{r}-\mathbf{r}') = U_0\delta(\mathbf{r}-\mathbf{r}'), \tag{1.20}$$

where the coupling constant U_0 is related to the scattering length a as follows:

$$U_0 = \frac{4\pi\hbar^2 a}{m}. \tag{1.21}$$

The introduced above interaction term yields the following equation of motion for the order parameter Ξ:

$$i\hbar\frac{\partial}{\partial t}\Xi(\mathbf{r},t) = \left[-\frac{\hbar^2\nabla^2}{2m} + V_{ext}(\mathbf{r}) + U_0|\Xi(\mathbf{r},t)|^2\right]\Xi(\mathbf{r},t). \tag{1.22}$$

Eq. (1.22) is known as Gross-Pitaevskii (GP) equation. It is valid when the s-wave scattering length is much smaller than the average distance between atoms $a << (N/V)^{-1/3}$ (the criteria of dilute gas), and the mean number of atoms in the condensate is large, $N-\bar{n}_0 << N$. The GP equation can be used at low temperature to explore the macroscopic behavior of the system, characterized by variations of the order parameter over distances larger than the mean distance between atoms.

The experimental systems are the collections of individual neutral alkali-gas atoms, with a total number N ranging from a few hundred up to $\sim 10^{10}$, confined by magnetic and/or optical trap to a relatively small region of space. The achieved densities range from $\sim 10^{11} cm^{-3}$ to $\sim 5\times 10^{15} cm^{-3}$ with a temperature, in the region of interest, typically in the range between a few tens of nK and a few tens of μK.

An alkali atom in its ground state has a single valence electron in an ns^1 state outside one or more fully occupied shells. Therefore, the electronic state is a doublet. The only excited state that we are interested in is a np, since it is more favorable to this state to couple to the ground state in the sense of the radiation in optical regime. The wavelength λ of the transition $ns \rightarrow np^1$ lies in the range $5000-7000\ A^\circ$ and

the excited state lifetime is of the order of 20 nsec. Since for the alkali atoms the atomic number Z is odd, it means that for odd isotopic number A, the systems such as ^{87}Rb, ^{23}Na, ^{7}Li obey the Bose-Einstein statistics, whereas an even-A systems such as ^{6}Li or ^{40}K obey Fermi-Dirac statistics.

It is worth to outline the general features of the resulting effective potentials in which the atoms move, i.e. the trapping potentials. There are two types of trapping potentials, which are widely used in the experiments. The first type is based on the atom-laser interaction. The effect that has been principally exploited in the laser trapping of atoms in BEC regime is the so-called dipole effect, which relies on the interaction of the laser field with the electric dipole moment, which is induced in the atom. One can define the detuning of the laser frequency from the $ns \rightarrow np$ transition frequency as

$$\Delta = \hbar\omega_{las} - (\epsilon_{np} - \epsilon_{ns}) \equiv \hbar\omega_{las} - 2\pi\hbar c/\lambda. \tag{1.23}$$

The energy change in the atom is inverse proportional to the detuning Δ. A region of high laser intensity, thus, provides an attractive potential for $\Delta < 0$ ("red detuning") and a repulsive potential $\Delta > 0$ ("blue detuning"). However, there are different problems concerning this type of confinement such as sensitivity to the hyperfine-Zeeman splitting, the spontaneous emission, etc. which I do not discuss here.

The second type of the trap potential arises from the magnetic analogue of the Earnshaw theorem, which forbids the magnitude of the magnetic field $\mathbf{B}(\mathbf{r})$ to have a local maximum in free space. However, nothing forbids the occurrence of the local minimum, which can be provided by various methods. Virtually all non-laser assisted magnetic traps used in BEC experiments to date have had axial symmetry and a finite offset field, thus, it can be written in cylindrical coordinates as

$$|\mathbf{B}(\mathbf{r})| = B_0 + \frac{1}{2}\alpha\rho^2 + \frac{1}{2}\beta z^2. \tag{1.24}$$

The cooling process usually consists of two steps. First, the laser cooling technique is used. Then, the atoms are evaporated from the trap. Since particles with higher energies are evaporating faster than the ones with lower energies, the process of evaporation leads to the cooling. The temperature obtained in the described process can be of the order of hundreds of nK and allows one to observe the condensate. The most recently developed experimental techniques dropped the temperature to several nK.

In gases, BEC was observed only in 1995, namely, in the vapor alkali gases using the advanced experimental setup [9–12]. I will present the typical experiment parameters based on the two pioneering papers [9, 10]. In the first experiment, BEC was produced in a vapor of rubidium-87 atoms [9] that was confined by magnetic field and evaporatively cooled. Six laser beams intersect in a glass cell creating a magneto-optical trap. The cell was 2.5 cm square by 12 cm long, and the beams were 1.6 cm in diameter. The condensate fraction first appeared near the temperature of 170 nK at a number density of 2.5×10^{12} atoms per cubic centimeter and could be preserved for more than 15 seconds. The s-wave scattering length was about 10^{-6} cm. In another pioneering experiment [10] the BEC was observed in the gas of sodium atoms, which were confined in a novel trap that employed both magnetic and optical forces. Evaporative cooling increased the phase-space density by 6 orders of magnitude within 7 seconds. Condensates contained up to 5×10^5 atoms at densities exceeding 10^{14} cm^{-3}. The critical temperature for the experiment was 2 μK. The trapping volume was of the order of $10^{-8} cm$. The corresponding scattering length of the sodium atoms was 4.9 nm.

The described experimental setups later allowed one to measure directly the number statistics in a Bose gas [13, 14]. It can be done in the following way. For number of order 10^3 or larger, absorption imaging is used yielding spatial and number

information. At lower atom numbers, however, fluorescence imaging is used, because of higher signal-to-noise ratio in this regime. This is accomplished by transferring the atoms into a small magneto-optical trap (MOT). This transfer shows the saturation behavior with MOT beam intensity, indicating that all atoms are captured. The resulting fluorescence signal is detected by a charge-coupled-device (CCD) camera and is properly calibrated. Because of low density during exposure, there is a little possibility for multiple scattering events during detection. Therefore, the measured fluorescence signal from the MOT is proportional to the number of atoms present.

The phenomenon of BEC can be observed not only in a harmonic trap [9–11], but in a box as well [15]. In the latter case the axial motion of the rubidium-87 atoms was confined by optical endcaps, producing the "textbook geometry" of a "particle in a box". The resulting atomic number in this box was generally from 500 to 3500 and was controlled by evaporation timing and spacing of the endcaps. The characteristic size of the box was 18 μm, scattering length was 5.6 nm.

The BEC has a lot of applications. The rapid progress in the quantum-coherent manipulation of mesoscopic cold atom clouds results in the construction of the permanent magnet atom chips. Small-scale magnetic field patterns for atom chips can be made using either microfabricated curent-carrying wires or microscopic structures of permanent magnetization. A long thin BEC can be prepared in a microtrap formed by a videotape atom chip and can be manipulated in the waveguides of the chip [16]. Moreover, the same effects were used to construct the atomic Michelson interferometer [17]. In this case the splitting, reflecting and recombining of condensate was achieved by a standing wave field. The differential phase shift between two arms of the interferometer was introduced either by a magnetic-field gradient or the initial velocity of condensate. The phase coherence effect between two spatially separated BECs on the atomic chip was observed in [18], which showed that it is both promising

and possible to use condensate at high density for interferometry on an atom chip.

The confined BEC in harmonic trap can be also used to realize a quantum gyroscope [19] characterized by two important superfluid effects: a reduced value of the inertia of the sample and a quantization of the angular momentum associated with the vortex. Theoretically proposed gyroscope [19] was characterized by the precession of the symmetry axis of the condensate around the symmetry axis of the confining trap.

Concluding the general introduction, I can state that not only the Einstein's prediction was correct, but also the existence of the new type of matter was discovered, where the quantum effects play the leading role at the macroscopic and mesoscopic scale. This phenomenon has a lot of applications and connections to the different physical effects of quantum and statistical mechanics and thermodynamics.

B. Theoretical models of BEC quantum statistics

In this section I review some existing in the literature approaches to the problem of the BEC fluctuations. Inspired by the series of papers [20, 21], in this dissertation I try to further develop the quantum statistical theory of BEC fluctuations. I mostly focus on the mesoscopic effects, i.e. effects that arise from the fact that the number of atoms in the trap is finite. The mesoscopic effects cannot be described by an infinite thermodynamic limit.

1. Standard theory of BEC and the problem of the mesoscopic effects

The difficulty in the description of the mesoscopic effects is that there is no certain approach for tackling the problem in the standard quantum mechanical theory of the microscopic systems of very few atoms. On the other hand, the standard statistical

mechanics cannot be applied either, because it deals with the macroscopic systems in the thermodynamic limit.

As it was discussed in the previous section, the recent experiments [9-11, 12-15] were obtained for the mesoscopic systems of a finite number of particles (from few hundreds to few millions). Therefore, the manifestation of the mesoscopic effects, which are clearly seen in the region close to the critical temperature of BEC, should add the experimental and theoretical understanding to the problem of transition between few-body systems to macroscopic systems.

The current study of the mesoscopic effects is dealing with the behavior of the quantum fluctuations of the BEC in a box with the periodic boundary conditions. The particle-number constraint, which requires exact conservation of particles in the trap, is essentially the reason of the mesoscopic effects near the critical temperature and is a crucial issue of this work.

Historically the previous efforts were mostly dealing with the mean value $\bar{n}_0$ and variance $\left\langle (n_0 - \bar{n}_0)^2 \right\rangle$ of the condensed atoms. It was assumed that the condensate fluctuations are almost Gaussian, and higher cumulants (semi-invariants) vanish. In fact it is not true even in the thermodynamic limit that was shown in [21].

The many-body Hamiltonian in Eq. (1.19) describes N weakly interacting via the two-body interatomic potential $V(\mathbf{r} - \mathbf{r}')$ bosons confined by an external potential V_{ext}. It also reflects the processes of annihilation and creation of a particle at the position $\mathbf{r}$ by the field operators $\hat{\Psi}(\mathbf{r})$ and $\hat{\Psi}^{\dagger}(\mathbf{r})$, respectively. Starting from this Hamiltonian, one can derive the thermodynamic properties of the system, as well as its ground state energy eigenvalue. The Monte-Carlo path-integral method of calculating the thermodynamic properties of the system interacting within a repulsive "hard-sphere" potential gives an immediate result within statistical errors, but is impractical for the systems with large number of atoms.

Mean-field approaches are commonly developed for interacting systems in order to overcome the problem of solving exactly the full many-body Schroedinger equation. Apart from the convenience of avoiding heavy numerical work, the mean-field theories allow one to understand the behavior of a system in terms of a set of parameters having a clear physical meaning. This is particularly true in the case of trapped bosons. Actually, most of the results reviewed in this work show that the mean-field approach is very effective in providing qualitative predictions for the static, dynamic, and thermodynamic properties of these trapped gases. The basic idea for a mean-field description of a dilute Bose gas was formulated by Bogoliubov [5-8, 22, 23]. The main idea is in separating the condensate contribution to the bosonic field operator. In general, the field operator can be written as $\hat{\Psi}(\mathbf{r}) = \sum_k \Psi_k(\mathbf{r})\hat{a}_k$, where $\Psi_k(\mathbf{r})$ are single-particle wave functions and $\hat{a_k}$ are the corresponding annihilation operators. The bosonic creation and annihilation operators $\hat{a}_k^\dagger$ and $\hat{a}_k$ are defined in the Fock space through the relations:

$$\hat{a}_k^\dagger|n_0, n_1, ..., n_k, ...\rangle = \sqrt{n_k + 1}|n_0, n_1, ..., n_k + 1, ...\rangle,$$

$$\hat{a}_k|n_0, n_1, ..., n_k, ...\rangle = \sqrt{n_k}|n_0, n_1, ..., n_k - 1, ...\rangle, \tag{1.25}$$

where n_k are the eigenvalues of the operator $\hat{n}_k = \hat{a}_k^\dagger\hat{a}_k$ giving the number of atoms in the single-particle state. They obey the usual commutation relationships:

$$[\hat{a}_p, \hat{a}_k^\dagger] = \delta_{p,k}, \qquad [\hat{a}_k, \hat{a}_p] = 0, \qquad [\hat{a}_p^\dagger, \hat{a}_k^\dagger] = 0. \tag{1.26}$$

BEC occurs when the mean number of atoms $\bar{n}_0$ of a particular single-particle state becomes very large: $\bar{n}_0 >> 1$ and the ratio $\bar{n}_0/N$ remains finite in the thermodynamic limit $N \to \infty$. In this limit the states with $\bar{n}_0$ and $\bar{n}_0 \pm 1 \approx \bar{n}_0$ correspond to the same physical configuration and, consequently, the operators $\hat{a}_0$ and $\hat{a}_0^\dagger$ can be treated like

c numbers: $\hat{a}_0 = \hat{a}_0^\dagger = \sqrt{\bar{n}_0}$. Therefore, the Hamiltonian in Eq. (1.19) can be written in the momentum representation as following:

$$H = \sum_{\mathbf{k}} \frac{\hbar^2 \mathbf{k}^2}{2m} \hat{a}_{\mathbf{k}}^\dagger \hat{a}_{\mathbf{k}} + H_{int}, \tag{1.27}$$

where the interaction part of the Hamiltonian in the Bogoliubov approximation is

$$H_{int} = \frac{g}{2V} \left[\hat{n}_0^2 + 2\hat{n}_0 \sum_{\mathbf{k}\neq 0} (\hat{a}_{-\mathbf{k}}^\dagger \hat{a}_{-\mathbf{k}} + \hat{a}_{\mathbf{k}}^\dagger \hat{a}_{\mathbf{k}}) + \hat{n}_0 \sum_{\mathbf{k}\neq 0} (\hat{a}_{\mathbf{k}}^\dagger \hat{a}_{-\mathbf{k}}^\dagger + \hat{a}_{\mathbf{k}} \hat{a}_{-\mathbf{k}}) \right]. \tag{1.28}$$

Here g is the interaction strength in Eq. (1.21). The total number of particles in the system is

$$N = \hat{n}_0 + \frac{1}{2} \sum_{\mathbf{k}\neq 0} (\hat{a}_{-\mathbf{k}}^\dagger \hat{a}_{-\mathbf{k}} + \hat{a}_{\mathbf{k}}^\dagger \hat{a}_{\mathbf{k}}). \tag{1.29}$$

The Bogoliubov canonical transformation of the creation and annihilation operators

$$\hat{a}_{\mathbf{k}} = \frac{1}{\sqrt{1 - A_{\mathbf{k}}^2}} \left(\hat{\alpha}_{\mathbf{k}} + A_{\mathbf{k}} \hat{\alpha}_{-\mathbf{k}}^\dagger \right), \qquad \hat{a}_{\mathbf{k}}^\dagger = \frac{1}{\sqrt{1 - A_{\mathbf{k}}^2}} \left(\hat{\alpha}_{\mathbf{k}}^\dagger + A_{\mathbf{k}} \hat{\alpha}_{-\mathbf{k}} \right) \tag{1.30}$$

diagonalizes the Hamiltonian in Eq. (1.28). In new operator basis $\hat{\alpha}_{\mathbf{k}}$ and $\hat{\alpha}_{\mathbf{k}}^\dagger$, the Hamiltonian looks like:

$$H = E_0 + \sum_{\mathbf{k}\neq 0} \epsilon_{\mathbf{k}} \hat{\alpha}_{\mathbf{k}}^\dagger \hat{\alpha}_{\mathbf{k}}, \tag{1.31}$$

with the modified spectrum

$$\epsilon_{\mathbf{k}} = \sqrt{\left(\frac{\hbar^2 \mathbf{k}^2}{2m} + \frac{U_0 \bar{n}_0}{V} \right)^2 - \left(\frac{U_0 \bar{n}_0}{V} \right)^2}, \tag{1.32}$$

and parameters

$$E_0 = \frac{U_0 N^2}{2V}, \qquad A_{\mathbf{k}} = \frac{V}{U_0 \bar{n}_0} \left(\epsilon_{\mathbf{k}} - \frac{\hbar^2 \mathbf{k}^2}{2m} - \frac{U_0 \bar{n}_0}{V} \right). \tag{1.33}$$

The result of the original Bogoliubov calculation was that only small fraction of the atoms were removed from the condensate at $T = 0$ due to a weak interaction.

Specifically, the mean number of particles in the condensate:

$$\bar{n}_0 = N\left(1 - \frac{8}{2}\left(\frac{a^3 N}{\pi V}\right)^{1/2}\right), \tag{1.34}$$

where a is the s-wave scattering length. For a dilute Bose gas, we have $(N/V)a^3 << 1$. In spite of this small interaction-induced depletion, the Bogoliubov model shows that the interactions in the presence of a condensate lead to an acoustic (or phonon) excitation spectrum at long wavelengths. More precisely, in the limit of small momentum the energy in Eq. (1.32) becomes linear in momentum:

$$\epsilon_{\mathbf{k}} \approx \hbar c k, \tag{1.35}$$

with the phonon velocity $c = (4\pi\hbar^2 a/m(N/mV))^{1/2}$. For the large momentum the Bogoliubov spectrum becomes the free particle spectrum:

$$\epsilon_{\mathbf{k}} \approx \frac{\hbar^2 \mathbf{k}^2}{2m}, \tag{1.36}$$

which agrees with the Landau theory of superfluidity [4].

In the presented above Bogoliubov prescription, the condensate acts like a classical particle reservoir, which the noncondensate atoms can enter and leave via scattering. Thus, the number of atoms is no longer a constant of motion. As an immediate consequence, one needs to include anomalous propagators (Green's functions) representing two particles going into or out of the condensate. This approach forms the basis of the systematic application of the quantum field theory to an interacting system of bosons due to Beliaev [7, 8, 22]. This leads to a generalized Green's function formalism, which builds in the crucial role of the Bose condensate and allows one to determine the general characteristics of the system, such as the excitation spectrum, the momentum distribution of atoms, etc. After this pioneer work, this field of study has been extensively developed and extended (for a review, see Ref. [8]).

In principle, one can calculate the properties of an interacting Bose system, such as thermodynamic potential, specific heat, condensate density, etc. As at $T = 0$, such finite T calculations are complicated by the subtle role of correlations induced by the Bose-broken symmetry. Moreover, even in a dilute gas, the finite T case is difficult because the thermally induced depletion fraction is now large. One has to be careful in treating the condensate and excited atoms in a consistent fashion. Another well-known difficulty is the fact that even for regular repulsive interactions a perturbation theory for Bose-condensed systems diverges at small momenta [8, 22]. That is to say, certain terms in the perturbation series are singular for $\mathbf{k} \to 0$, a result which can be traced back to the fact that the single-particle excitations are phonon-like. These singularities have to be handled with care in order to obtain correct final results. Fortunately, the infrared divergences appear to cancel out in all physical quantities [8].

2. Micro-canonical, canonical and grand-canonical statistics

Specific experimental conditions define which statistics should be applied in a given particular situation. In view of the present experiments on the trapped atoms of dilute gases, dealing with a finite and well defined number of particles, the most important descriptions are due to the micro-canonical and canonical ensembles, since the particle number, even if it is not known exactly, certainly does not fluctuate after the cooling process is over. Magnetic and optical confinement also implies that the system is thermally isolated, which restricts one to the consideration of the micro-canonical ensemble. In the other way of cooling, so called the sympathetic cooling, which takes place in the systems of mixed Bose-Fermi gases or Bose gases with different components, there is an exchange of energy between different species of the gas, and thus the canonical ensemble is appropriate. This description is appropriate also for

the dilute ^{4}He in a porous medium [24–26]. In the canonical ensemble only the total number of particles is constrained to be conserved $\hat{N} = const$, but energy $\hat{H}$ has non-zero fluctuations and only its average value is a constant $\left\langle \hat{H} \right\rangle = \bar{H} = E = const$, determined by a fixed temperature of the system T.

The standard textbooks [4, 5, 22, 23] formulate the BEC statistics problem either in a grand-canonical ensemble, which allows the system to exchange both energy and particles with a reservoir at a given temperature T and chemical potential μ and fixes only the average energy and number of particles, respectively, or in some restricted ensembles. The purpose of the restricted ensemble is to select only those states, which ensure the condensate wave function to have almost fixed phase and amplitude [5]. Although these formulations avoid the difficulties of operator constraints on the total energy and particle number, which are present in the micro-canonical and canonical treatments, they provide effective tools for study of the thermodynamic limit and hydrodynamic properties of the many-body Bose system at the expense of the artificial modification of the condensate statistics. In the grand-canonical ensemble even below the Bose-Einstein condensation temperature, where the ground state mean occupation number is macroscopically large in the sense that $\bar{n}_0 \approx N$, the distribution function

$$\rho_\nu^{GC}(n_\nu) = \frac{1}{1+\bar{n}_\nu}\left(\frac{\bar{n}_\nu}{1+\bar{n}_\nu}\right)^{n_\nu} \tag{1.37}$$

in the ground state $\rho_0^{GC}(n_0)$ becomes very broad and even at $T \to 0$ the variance is anomalously large $\langle (n_0 - \bar{n}_0)^2 \rangle \approx \bar{n}_0^2 \propto N^2$. This prediction contradicts with the basic fact that at low temperatures all particles are expected to occupy the ground state with no fluctuations left. Thus the grand-canonical ensemble could be misleading if not revised properly. The approach that involves fixation of the phase and amplitude of the condensate wave function is not good for the description of the condensate

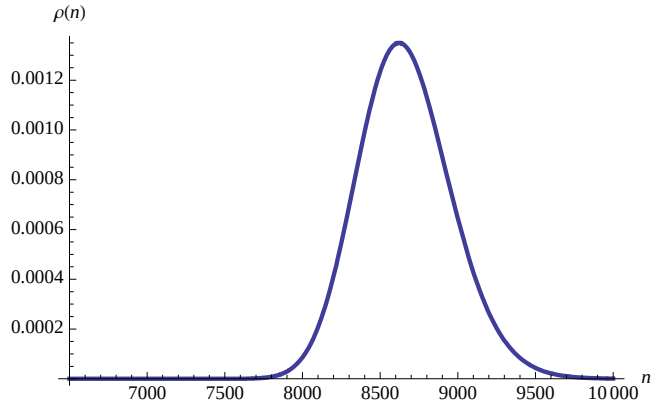

Fig. 1. Negative binomial distribution of the number of noncondensed atoms for an ideal Bose gas in a box with total number of particles $N = 10000$.

formation and fluctuations at all.

It is worthwhile to compare the counting statistics (1.37) with the predictions of other statistics, namely micro-canonical and canonical ensembles [5]. For very high temperatures $T >> T_c$, all three ensembles predict the same behavior. However it is not the same for the low temperature region $T < T_c$. Here the broad grand-canonical distribution function does not agree with the well-peacked canonical and micro-canonical distribution function $\rho_0(n_0)$ around the condensate mean occupation number value. In order to illustrate an actual distribution function, I plot in Fig. 1 the finite negative binomial distribution function of the noncondensate occupation in an ideal Bose gas in the canonical ensemble as is derived within the master-equation approach below in Subsection 4, Eq. (1.53). This is the sharp-peaked statistical distribution, which was naively expected for a Bose statistics.

The micro-canonical and canonical ensemble formalism do not give the same result in all situations. For different traps the agreement requires additional conditions. For example both ensembles have been found to agree in the large-N (almost thermodynamic limit) case for one-dimensional harmonic trap but to differ in the

case of three-dimensional isotropic harmonic trap [21]. In the more general case of d-dimensional σ-power trap, micro-canonical and canonical fluctuations agree in large-N limit when $d/\sigma < 2$ and micro-canonical fluctuations become smaller than the canonical ones in the case of $d/\sigma > 2$.

For large enough particle number $N > 10^5$ the calculation of micro-canonical partition function $\Omega(E, N)$ becomes very time consuming or even impossible. In this case one can employ the approximation technique based on the saddle-point method, which is discussed in details in Chapter V and is widely used in the statistical physics. In this method one starts from the grand-canonical partition function and utilize the saddle-point method for extracting its required canonical and micro-canonical parts. Furthermore, the moments of fluctuations are described by the different order derivatives from the resulting counterparts.

Recently, the new type of ensemble was introduce, so-called Maxwell's demon ensemble [20]. In that approach the overall system is divided into two parts: the condensate part and the excited states, which undergo the particle, not energy, exchange between each other. This ensemble gives an approximate result for the ground state fluctuations both in the micro-canonical and canonical ensembles. This approximation can be understood in the framework of the canonical ensemble quasiparticle approach presented in Chapter II.

3. Exact recursion relation for the statistics of the number of condensed atoms in an ideal Bose gas

It is worth noting that there is one useful reference result in the theory of BEC fluctuations, namely, an exact recursion relation for the statistics of the number of condensed atoms in an ideal Bose gas. Although it does not give any simple analytical answer or physical insight into the problem, it can be used for "exact" numerical

simulations for traps containing a finite number of atoms. It is very useful as a tool to check different approximate analytical solutions. The recursion relation for an ideal Bose gas had been known and used by many authors [20, 21, 23, 27]. In the canonical ensemble, the probability to find n_0 particles occupying the single particle ground state is give by:

$$\rho_0(n_0) = \frac{Z_{N-n_0}(T) - Z_{N-n_o-1}(T)}{Z_N(T)}; \qquad Z_{-1} \equiv 1. \tag{1.38}$$

The recurrence relation for an ideal Bose gas, thus is:

$$Z_N(T) = \frac{1}{N}\sum_{k=1}^{N} Z_1(T/k) Z_{N-k}(T), \qquad Z_1(T) = 1 + \sum_{\nu=0}^{\infty} e^{-\epsilon_\nu/T}, \qquad Z_0(T) = 1, \tag{1.39}$$

which allows one to numerically evaluate the statistics (1.38). Here ν stands for a set of quantum numbers enumerating a given single particle energy levels ϵ_ν, and the ground-state energy assumed to be $\epsilon_0 = 0$ by convention. I will apply the relation (1.39) for evaluation the statistics of an ideal gas in a box in the following sections, in particular, in Chapter II, Section E. An important example is the isotropic, three-dimensional harmonic trap, where one has:

$$Z_1(T) = \sum_{n=0}^{\infty} \frac{1}{2}(n+2)(n+1) e^{-n\hbar\omega/k_B T} = \frac{1}{\left(1 - e^{-\hbar\omega/k_B T}\right)^3}, \tag{1.40}$$

where $(n+2)(n+1)/2$ is the degeneracy of the level $\epsilon_n = n\hbar\omega$.

There is a similar recurrence relation in the micro-canonical ensemble [20]:

$$\Omega(E,N) = \frac{1}{N}\sum_{k=1}^{N}\sum_{\nu=0}^{\infty} \Omega(E - k\epsilon_\nu, N-k), \qquad \Omega(0,N) = 1, \qquad \Omega(E>0,0) = 0, \tag{1.41}$$

where the sum over ν is finite, since for $E < 0$ one has $\Omega(E<0,N) = 0$. Therefore,

the ground state occupation probability in the micro-canonical ensemble is:

$$\rho_0^{MC}(n_0) = \frac{\Omega(E, N - n_0) - \Omega(E, N - n_0 - 1)}{\Omega(E, N)}; \qquad \Omega(E, -1) \equiv 1. \tag{1.42}$$

4. Dynamical master equation approach

Here I outline another approach to the canonical statistics of ideal Bose gases. It was developed in [28] and utilizes a master equation for the condensate in order to find its equilibrium solution. This approach reveals important parallels to the quantum theory of laser and is based on the analogy between a second-order phase transition and laser threshold behavior. The master equation can be simplified in the approximation of detailed balance in the excited states under an assumption that for a given arbitrary number n_0 of atoms in the condensate the remaining $N - n_0$ excited atoms are in an equilibrium state at the prescribed temperature T.

One can consider the cooling of an ideal noninteracting N-atom Bose gas confined inside a trap. The gas is in contact with a thermal reservoir maintained at the temperature T. The most studies have been concerned with the evaluation of the partition function, which is strongly related to the statistics and thermodynamics of the Bose gas. As it was discussed in [28], one can obtain a simple master equation for the density matrix of the Bose gas as it cools towards the ground state via exchanging the heat with a thermal reservoir. The master equation for the distribution function of the condensed bosons p_{n_0} yields

$$\dot{p_{n_0}} = -\kappa\{K_{n_0}(n_0 + 1)p_{n_0} - K_{n_0-1}n_0 p_{n_0-1} + H_{n_0}n_0 p_{n_0} - H_{n_0+1}(n_0 + 1)p_{n_0+1}\}. \tag{1.43}$$

Here κH_{n_0} and κK_{n_0} are the heating and cooling coefficients (which depend upon trap shape, total number of atoms in the trap N and the temperature T) are similar

to the cavity loss and saturated gain parameters in the original laser master equation:

$$K_{n_0} = \sum_{k'>0} (\eta_{k'} + 1)\langle n_{k'} \rangle_{n_0}, \qquad H_{n_0} = \sum_{k'>0} \eta_{k'} (\langle n_{k'} \rangle_{n_0} + 1), \tag{1.44}$$

where

$$\eta_k = \frac{1}{\exp(\epsilon_k / T) - 1}, \qquad \langle n_{k'} \rangle_{n_0} = \sum_{\{n_k\}n_0} n_{k'} \frac{p_{n_0, \{n_k\}_{n_0}}}{p_{n_0}}. \tag{1.45}$$

One can obtain the steady state distribution of the number of atoms condensed to the ground level of the trap from Eq. (1.43), thus the ground state statistics can be determined. The detailed balance condition involving the cooling and the heating coefficients yields the following expression for the number distribution of the condensed atoms:

$$p_{n_0} = p_0 \prod_{i=1}^{n_0} \frac{K_{i-1}}{H_i}, \tag{1.46}$$

where the partition function

$$Z_N = \frac{1}{p_N} = \sum_{n_0=0}^{N} \prod_{i-n_0+1}^{N} \frac{H_i}{K_{i-1}} \tag{1.47}$$

is required to obey the normalization condition $\sum_{n_0=0}^{N} p_{n_0} = 1$. The closed form expression for the coefficients H_{n_0} and K_{n_0} can be achieved under different approximations for a different trap shapes. For example, one can apply the so-called "quasithermal" ansatz [28] that stems the same relative average occupation number in the excited levels of the trap as in the thermal reservoir:

$$\langle n_k \rangle_{n_0} = \eta_k \sum_{k>0} \langle n_k \rangle_{n_0} / \sum_{k'} \eta_{k'} = \frac{(N - \bar{n}_0)}{(\exp(\epsilon_k / T) - 1)\mathcal{H}}. \tag{1.48}$$

As the result, one obtains the heating and cooling coefficients as following:

$$K_{n_0} = (N - n_0)(1 + \eta), \qquad H_{n_0} = \mathcal{H} + (N - n_0)\eta, \tag{1.49}$$

where

$$\mathcal{H} = \sum_{k>0} \eta_k = \sum_{k>0} \frac{1}{\exp(\epsilon_k/T) - 1}, \qquad \eta = \frac{1}{(N - n_0)} \sum_k \langle n_k \rangle_{n_0} \eta_k = \frac{1}{\mathcal{H}} \sum_{k>0} \eta_k^2. \quad (1.50)$$

Thus, the analytical formulas for the distribution function of the condensed bosons and the partition function are:

$$p_{n_0} = \frac{1}{Z_N} \frac{(N - n_0 + \mathcal{H}/\eta - 1)!}{(\mathcal{H}/\eta - 1)!(N - n_0)!} \left(\frac{\eta}{1+\eta} \right)^{N-n_0}, \quad (1.51)$$

$$Z_N = \sum_{n_0=0}^{N} \left(\begin{array}{c} N - n_0 + \mathcal{H}/\eta - 1 \\ N - n_0 \end{array} \right) \left(\frac{\eta}{1+\eta} \right)^{N-n_0}. \quad (1.52)$$

The explicit formula (1.51) obeys the same canonical recursion relation, which was discussed previously in Section 3. One should emphasize the specific behavior of the ground state occupation probability distribution function. It evolves from a quasi-thermal peak edged to zero occupation $n_0 = 0$ at $T \approx T_c$ through a narrow peak centered around some $\bar{n}_0 \neq 0$ at $T \approx T_c/2$ to a δ-function-like peak near $n_0 = N$ for a complete Bose-Einstein condensation at $T << T_c$. It is similar to the evolution of the photon number distribution in a laser mode (from thermal to coherent, lasing).

The probability distribution for the total number of non-condensed atoms, $n = N - n_0$,

$$P_n = p_{N-n} = \frac{1}{Z_N} \left(\begin{array}{c} n + \mathcal{H}/\eta - 1 \\ n \end{array} \right) \left(\frac{\eta}{1+\eta} \right)^{n}, \quad (1.53)$$

is complementary to the probability distribution of the number of condensed atoms $n_0 = N - n$. The distribution (1.53) can be named as *a finite negative binomial distribution*, since it has the form of the well known negative binomial distribution

[29]:

$$P_n = \left(\begin{array}{c} n+M-1 \\ \\ n \end{array} \right) q^n (1-q)^M, \qquad n = 0, 1, 2, ..., \infty, \tag{1.54}$$

that was so named due to a coincidence of the probabilities P_n with the terms in the negative-power binomial formula:

$$\frac{1}{(1-q)^M} = \sum_{n=0}^{\infty} \left(\begin{array}{c} n+M-1 \\ \\ n \end{array} \right) q^n. \tag{1.55}$$

It has similar semantic origin as the well-known binomial distribution,

$$P_n = \left(\begin{array}{c} M \\ \\ n \end{array} \right) (1-q)^n q^{M-n}, \tag{1.56}$$

which was named after the Newton's binomial formula

$$[q + (1-q)]^M = \sum_{n=0}^{M} \left(\begin{array}{c} M \\ \\ n \end{array} \right) (1-q)^n q^{M-n}. \tag{1.57}$$

The finite negative binomial distribution (1.53) tends to the well-known distribution (1.54) only in the limit $N >> (1+\eta)\mathcal{H}$.

The master equation (1.43) for p_{n_0} itself, and the analytic approximate expressions (1.51) and (1.52) for the condensate distribution function p_{n_0} and the partition function Z_N, respectively, are among the main results of the condensate master equation approach. It provides reasonably accurate description of the first two moments of BEC fluctuations in a Bose gas for a large range of parameters and for different trap potentials.

5. Integral representation via the generalized Zeta function

In order to understand relations between various approximate schemes, we formulate a systematic analysis of the equilibrium canonical-ensemble fluctuations of the BEC based on the particle number conserving formalism of Girardeau and Arnowitt [30], the concept of the canonical-ensemble quasiparticles, residue technique and multinomial expansion. This approach will be discussed in details in Chapter II, Section A. In this section I will present an equivalent formulation of the quasiparticle approach in terms of the poles of the generalized Zeta function [31].

Cumulants (semi-invariants) of the BEC fluctuations in an ideal Bose gas can be written in an equivalent form which is quite interesting mathematically [29]. Namely, starting with the cumulant generating function $\ln \Theta_{ex}(\beta, z)$, where $\beta = 1/k_B T$ and $z = e^{\beta\mu}$,

$$\ln \Theta_{ex}(\beta, z) = -\sum_{\nu=1}^{\infty} \ln(1 - z \exp[-\beta(\epsilon_\nu - \epsilon_0)]) = \sum_{\nu=1}^{\infty} \sum_{n=1}^{\infty} \frac{z^n \exp[-n\beta(\epsilon_\nu - \epsilon_0)]}{n}, \quad (1.58)$$

one can use the Mellin-Barnes transform:

$$e^{-a} = \frac{1}{2\pi i} \int_{\tau - i\infty}^{\tau + i\infty} dt \; a^{-t} \Gamma(t) \quad (1.59)$$

to write

$$\ln \Theta_{ex}(\beta, z) = \sum_{\nu=1}^{\infty} \sum_{n=1}^{\infty} \frac{z^n}{n} \frac{1}{2\pi i} \int_{\tau - i\infty}^{\tau + i\infty} dt \Gamma(t) \frac{1}{[n\beta(\epsilon_\nu - \epsilon_0)]^t} =$$

$$= \frac{1}{2\pi i} \int_{\tau - i\infty}^{\tau + i\infty} dt \Gamma(t) \sum_{\nu=1}^{\infty} \frac{1}{[\beta(\epsilon_\nu - \epsilon_0)]^t} \sum_{n=1}^{\infty} \frac{z^n}{n^{t+1}}. \quad (1.60)$$

Recalling the series representation of the Bose functions $g_\alpha(z) = \sum_{n=1}^{\infty} z^n / n^\alpha$ and introducing the generalized, "spectral" Zeta function $Z(\beta, t) = [\beta(\epsilon_\nu - \epsilon_0)]^{-t}$, one

arrives at the convenient (and exact) integral representation:

$$\ln \Theta_{ex}(\beta, z) = \frac{1}{2\pi i} \int_{\tau - i\infty}^{\tau + i\infty} dt \Gamma(t) Z(\beta, t) g_{t+1}(z). \tag{1.61}$$

Applying the well-known relation for the Bose functions

$$z \frac{d}{dz} g_\alpha(z) = g_{\alpha-1}(z) \tag{1.62}$$

and $g_\alpha(1) = \zeta(\alpha)$, where $\zeta(\alpha)$ denotes the original Riemann Zeta function, Eq. (1.61) can be rewritten in terms of the cumulants of the distribution function as:

$$\kappa_k(\beta) = \left(z \frac{\partial}{\partial z} \right)^k \ln \Theta_{ex}(\beta, z)|_{z=1} = \frac{1}{2\pi i} \int_{\tau - i\infty}^{\tau + i\infty} dt \Gamma(t) Z(\beta, t) \zeta(t + 1 - k). \tag{1.63}$$

Thus, by means of the residue theorem, Eq.(1.63) links all cumulants of the canonical distribution function in the condensate regime to the poles of the generalized Zeta function $Z(\beta, t)$, which contains all the system properties, and to the pole of a system-independent Riemann Zeta function, the location of which depends on the order k of the respective cumulant. The formula (1.63) provides a systematic asymptotic expansion of the cumulants $\kappa_k(\beta)$ through the residues of the analytically continued integrands, taken from right to left. The large system behavior extracted from the condensate fluctuations is definitely seen. The details and examples of such analysis can be found in [31].

I would like to emphasize that none of the presented above theories can describe the mesoscopic behavior of the confined Bose gas in the trap without using some approximations, and there is no yet a complete and general theory of the BEC fluctuations.

C. Mesoscopic systems

Successful experimental demonstration and various recent experiments on the Bose-Einstein condensation (BEC) in the magneto-optical traps strongly demand a development of a theory of the BEC phase transition in the actual mesoscopic systems containing a finite number of atoms $N \sim 10^2 - 10^6$ in a finite-size trap (for a review, see e.g. [20] and references therein). One of the most important problems is to find the universal, common to the mesoscopic systems of any size, features in the behaviour of an order parameter, i.e., a mean number of atoms in the condensate $\bar{n}_0$, and its fluctuations as the functions of the number of atoms in the trap and the temperature T in the critical region, $T \sim T_c$ or $N \sim N_c$, as well as above and below it. In the statistical physics until recently most studies were done for the macroscopic systems in the thermodynamic, or bulk, limit when both a volume V and a number of atoms N in the trap tend to infinity [5, 22, 32–34]. An opposite limit of a very few atoms in the trap ($N = 1,\ 2,\ 3,\ $) corresponds to a microscopic system studied by the methods of a standard quantum mechanics.

An intermediate case of a mesoscopic number of atoms is the most difficult for it requires a solution that explicitly depends on the number of atoms in the trap. Besides, for the mesoscopic systems an inapplicability of the standard in the statistical physics approaches, for example, a grand-canonical-ensemble method and a Beliaev-Popov diagram technique [5, 8, 22, 34], becomes especially obvious, in particular, for the analysis of the anomalous fluctuations in the critical region. A simple example is given by a well-known grand-canonical catastrophe of the BEC fluctuations [20, 33, 34]. To get the solution of the BEC phase transition problem right, the most crucial issue is an exact account for a particle-number constraint $\hat{n}_0 + \sum_{\mathbf{k}\neq 0} \hat{n}_{\mathbf{k}} = N = \text{const}$ as an operator equation which is responsible for the very BEC phenomenon and is

equivalent to an infinite set of the c-number constraints. It cannot be replaced by just one condition for the mean values, $N = \bar{n}_0 + \bar{n}$, used in the grand-canonical-ensemble approach to specify an extra parameter, namely, a chemical potential μ. Here $\hat{n}_{\mathbf{k}}$ is an occupation operator for a $\mathbf{k}$-state of an atom in the trap and $\hat{n} = \sum_{\mathbf{k}\neq 0} \hat{n}_{\mathbf{k}}$ is a total occupation of the excited states.

Thus, we have to find an explicit solution to a statistical problem of BEC for a finite number of atoms in the trap in a canonical ensemble. Some results in this direction are known in the literature, however, a clear and full physical picture of the statistics and dynamics of BEC in the mesoscopic systems is absent until now not only in a general case of an interacting gas, but even in the case of an ideal gas (for a review, see e.g. [20, 34] and references therein). In particular, one of the most interesting in the statistical physics of BEC results, namely, a formula for the anomalously large variance of the ground-state occupation, $\langle(\hat{n}_0 - \bar{n}_0)^2\rangle \propto N^{4/3}(T/T_c)^2$, found both for the ideal gas [34] and for the weakly interacting gas [21, 35, 36], is valid only far enough from the critical point, when fluctuations of the order parameter are already relatively small, $\langle(\hat{n}_0 - \bar{n}_0)^2\rangle^{1/2} << \bar{n}_0$. The same is relevant also to a known result on the analytical formula for all higher-order cumulants and moments of the BEC fluctuations, which demonstrates that the BEC fluctuations are essentially non-Gaussian even in the thermodynamic limit [21, 35]. The known results do not provide any clear answers to the questions on the origin, dynamics of a formation, behaviour, and scaling of the order parameter $\bar{n}_0$ and its fluctuations when the mesoscopic system passes through the critical region.

D. Planar Bragg waveguides

A planar periodic Bragg structure is widely used as a resonant element of both classical and quantum laser oscillators. Originally it was introduced for quantum lasers as a way to create a feedback [37, 38]. In recent years distributed feedback lasers are being studied both theoretically and experimentally [39, 40]. In classical relativistic electronics an advantage of using of Bragg resonators formed by the sections of a corrugated waveguide is its compatibility with an electron beam transportation system [41, 42]. In the Bragg resonators two counter-propagating waves are coupled via the corrugation (or periodic variation of dielectric constant). This coupling in an open system leads to an existence of a discrete mode spectrum with different quality factors. Thus, an effective mode selection and control both in quantum laser oscillators and classical Free Electron Laser(FEL) oscillators can be provided.

In the following chapters a similar principle is used to achieve a selective waveguiding. A new scheme of FEL amplifier based on an open planar Bragg waveguide and on an electron beam moving along waveguide axis [43] is offered. To increase effective size of the operating mode one can use a structure with a regular longitudinal corrugation that couples two partial waves propagating at some angle to the axis to the wave propagating directly along the axis. This wave, which is transformed into cutoff modes, is excited by the electrons in moving reference frame.

The discussed above waveguide, in which a wave propagates in the direction transverse to the lattice vector (Fig. 2), can provide high selectivity over the transverse coordinate when its size essentially exceeds a wavelength [43–45]. It is beneficial to use a grating or periodic dielectric media with a defect of periodicity, that results in the existence of a single mode that has low diffraction losses and is located near the defect. This wave is excited by an active medium. Obviously, the Bragg waveg-

uides with a defect of periodicity can be treated as a simple planar realization of photonic band-gap structures [46, 47] that are compatible with an extended planar active medium, including a sheet electron beam. Analysis shows rather high gain of the novel amplification schemes with simultaneous discrimination of parasitic modes.

A photonic-band-gap structure (PBG), which is a periodic array of varying dielectric or metallic structures, was first described by Yablonovitch et al. [47]. In recent years, numerous advances have improved our understanding of the theory of PBG structures. This has led to new applications in passive devices for guiding and confinement of electromagnetic radiation. Their use in both microwave and optical devices has primarily been limited to passive devices such as waveguides and filters, though some applications in active devices have been reported [48]. The results of the investigation of the potential of PBG structures for accelerator cavities are also very promising [46]. For instance, the PBG cavity appears to be very useful in gyrotron oscillator applications at moderate average power levels. At high average power, however, the rods of the PBG structure may not be able to dissipate Ohmic losses as effectively as the smooth walls of conventional cylindrical cavities. This can be mitigated by using thicker rods and by cooling the rods with water flowing through channels in the center of each rod. The PBG structures would be able to handle high peak power levels, and would be particularly well suited to high peak power, moderate average power level amplifiers. They are also very attractive for use as the buncher cavities in amplifiers at any power level. At very high frequencies, where moderate power levels are of interest, the PBG structures also appear to be very attractive.

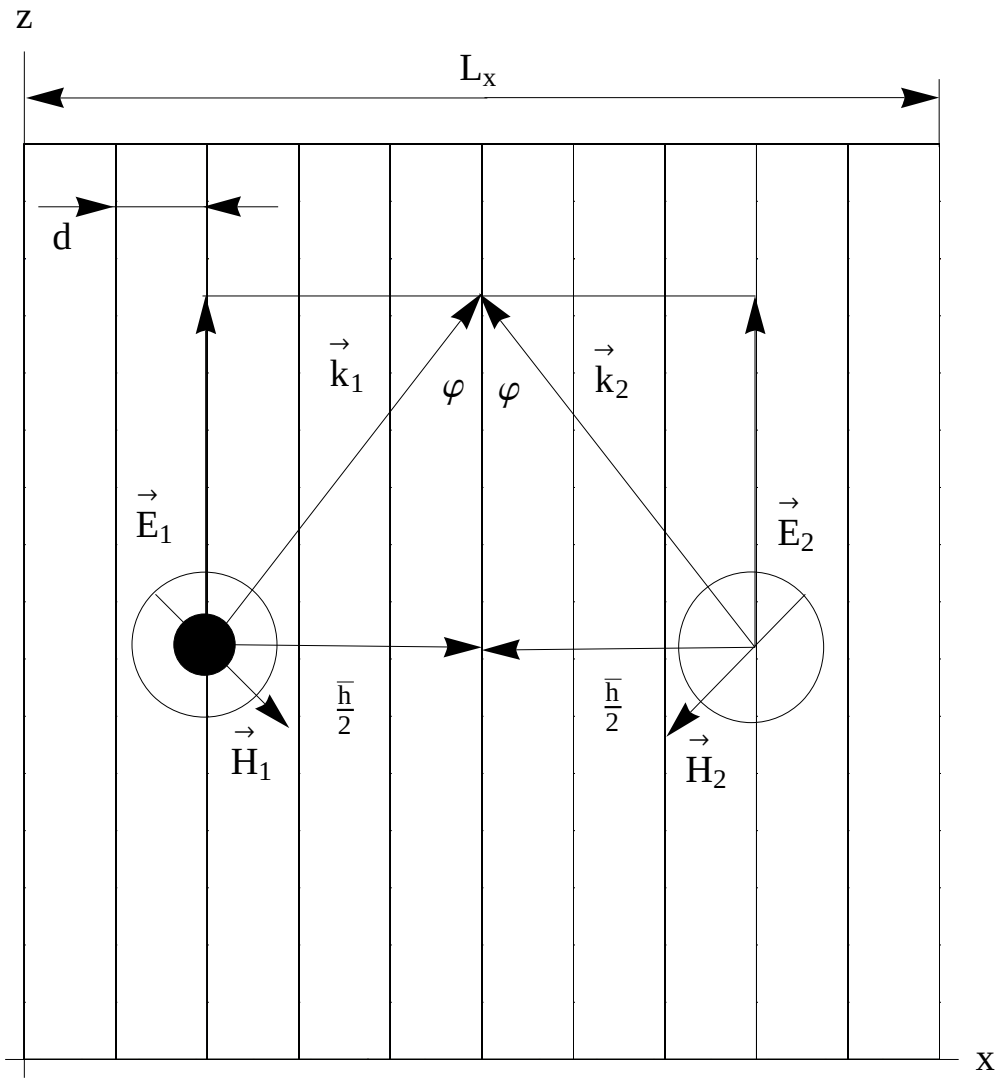

Fig. 2. The scheme of an open Bragg waveguide. Wave propagates in the direction z which is transverse to the lattice vector $\vec{\bar{h}} = \vec{x}^{(0)}\bar{h}$, $\bar{h} = \frac{2\pi}{d}$.

E. Distributed feedback

The two-dimensional distributed feedback (DF) first was introduced for synchronization of the radiation of relativistic electron beams of planar and cylindrical geometry [49–51]. It was assumed to use the radiation of electrons, which oscillate, either in the undulator field (Free Electron Laser (FEL)) or in the uniform magnetic field (Cyclotron). Recent theoretical analysis of the described above systems showed a success of using two-dimensional DF in conditions when one of the transverse dimension of the active media exceeds the radiation wavelength by several orders of magnitude.

Two-dimensional DF is obtained by the use of two-dimensional Bragg resonators of the planar and coaxial geometry. These devices can provide high selectivity in two coordinates, which was proved by the series of simulations and testing experiments.

Initially a mechanism of one-dimensional DF was introduced in quantum electronic devices such as semiconductor lasers. In this chapter I will analyze a generalization of this mechanism in two-dimensional and in principal in three-dimensional geometry. As the result one can obtain synchronization of the radiation of high dimensional active media and increase a space where interaction occurs.

Current experiments are operating with FELs with two-dimensional DF of coaxial (UK [52]) and planar (Novosibirsk [53]) geometries. In Novosibirsk experiment high relativistic electron beams with the power of hundreds of Joules were used. These unique beams have a planar geometry where the transverse dimension of beams can reach 1.5 meters, which means $10^2 - 10^3$ wavelengths in a millimeter range. To construct a coherent amplifier or oscillator one needs to use two-dimensional distributed feedback, which allows synchronizing a radiation in the case of mentioned above oversized space of interaction.

In this work a new scheme of FEL is presented where canalization of radiation

is obtained by use of planar Bragg waveguide. More specifically I will describe a so-called transfer FEL amplifier [54–56], which is a FEL version of a well known in microwave electronic device. In this particular geometry radiation propagates transverse to the particle velocity direction. In the case of rectilinear electron beams such type of interaction can be realized by means of oblique corrugation of slow wave structure [57]. In the case of curvilinear beams the synchronous interaction can be realized in smooth electrodynamical systems [58], which implements to use open oversized waveguides. Unfortunately, well known cylindrical waveguides do not have an appropriate selective properties [58] and a transverse structure of the field is distorted by an action of the electron beam. This problem can be solved by means of using an open waveguides based on Bragg structures [43] that provides high selectivity over the transverse mode index.

These waveguides can be constructed by taking two metal plates with slightly corrugated walls in the direction of group velocity of the electromagnetic wave. Bragg waveguides have very high selective properties in the transverse index. On the other hand, they are compatible with an electron beam transportation systems [41, 42]. But the most non-trivial property of the Bragg waveguides is the possibility of achievement of maximum Doppler frequency up-shift despite the fact that an angle between group velocity of the amplifying wave and velocity of the particles can be quite large.

F. Contents of the BEC studies (Chapters II-V) and brief discussion of the main results

The part dedicated to BEC studies is organized as follows. In Chapter II, Section A I start with the Girardeau-Arnowitt (GA) [30, 59] particle-number conserving operator formalism of the canonical ensemble for analyzing the equilibrium fluctuations of the

partially condensed Bose gas in a box with the periodic boundary conditions. GA operators can be understood as a creation and annihilation operators of particles in the reduced many-body Fock subspace. New quasiparticles are essentially different from the original and allow one to obey the exact N-particle constraint in a very elegant way, taking into account all possible correlations between bosons. In the case of weakly interacting dilute Bose gas I apply the Bogoliubov transformation to the (GA) canonical quasiparticles to formulate the problem in terms of the new, dressed by the condensate, canonical quasiparticles. Moreover, this transformation allows one to consider problems of the gas of atoms with interaction essentially as a problem of ideal gas of dressed quasiparticles in contrast to the gas of atoms and gas of bare quasiparticles. In Chapter II, Section B, I obtain a simple analytical expression for the characteristic function of the ground state fluctuations for both ideal and weakly interacting gas in a box with periodic boundary conditions following the approach of [21].

In Chapter II, Section C I introduce the constrained distribution function through the proper reduction of the many-body Hilbert space. In the present case of the Bose gas in the canonical ensemble, one has to consider as independent only noncondensate Fock states $\left|\{n_{\mathbf{k}},\ \mathbf{k}\neq 0\}\right\rangle$ which uniquely specify the ground-state Fock state $\left|n_0 = N-\sum_{\mathbf{k}\neq 0} n_{\mathbf{k}}\right\rangle$. However, the remaining noncondensate Fock space should be further cut off by the boundary $n_{\mathbf{k}} \leq N$. The latter is equivalent to an introduction of a step-function $\theta(N-\hat{n})$, i.e., 1 if $n \leq N$ or 0 if $n > N$, in all operator equations and under all trace operations. That $\theta(N-\hat{n})$ factor is the constraint nonlinearity that, being accepted, allows one to consider the noncondensate many-body Fock space formally as an unconstrained one. Therefore properly normalized constrained distribution function exactly obeys the well-known recursion relation for an ideal gas and N-particle constraint, by its construction, which makes it truly a solution of the

problem. In Section D of the Chapter II I describe in some details the spectrum of a box trap that is used as a particular example for the numerical simulations in the dissertation.

For the analysis of non-Gaussian properties it is convenient to consider cumulants (semi-invariants) κ_m which are related to the central moments $\mu_m = \langle (n-\bar{n})^m \rangle$ and "generating cumulants" $\tilde{\kappa}_m$ by the following relations:

$$\kappa_1 = \bar{n}, \quad \kappa_2 = \mu_2, \quad \kappa_3 = \mu_3, \quad \kappa_4 = \mu_4 - 3{\mu_2}^2,$$

$$\kappa_5 = \mu_5 - 10\mu_2\mu_3, \quad \kappa_6 = \mu_6 - 15\mu_2\left(\mu_4 - 2\mu_2^2\right), \tag{1.64}$$

$$\kappa_1 = \tilde{\kappa}_1, \quad \kappa_2 = \tilde{\kappa}_2 + \tilde{\kappa}_1,$$

$$\kappa_3 = \tilde{\kappa}_3 + 3\tilde{\kappa}_2 + \tilde{\kappa}_1, \quad \kappa_4 = \tilde{\kappa}_4 + 6\tilde{\kappa}_3 + 7\tilde{\kappa}_2 + \tilde{\kappa}_1, ... \tag{1.65}$$

In Section E of the Chapter II I present the closed-form, analytical expression for the distribution function and its cumulants and obtain the expansion in terms of the multinomial coefficients. In Section F I compare the condensate statistics for the finite system with its thermodynamic limit and present the expressions for the low and high temperature asymptotics for the first few cumulants of ground state statistics for both ideal and weakly interacting Bose gas.

In Chapter III I introduce universal constraint nonlinearity responsible for the phase transition through a reduction of the many-body Hilbert space. I calculate a probability distribution of the number of atoms in the condensate n_0 that is complimentary to the total number of atoms in the excited states (noncondensate) $n = N - n_0$ and explain a remarkable constraint-cut-off mechanism that makes BEC fluctuations strongly non-Gaussian in the critical region (Section A). On this basis I find the universal scaling and structure of the BEC statistical distribution (Section A) as well as of the order parameter (Section B) and all higher-order moments and

cumulants (Section C) of the BEC statistics for any number of atoms trapped in a box with any volume $V = L^3$ and temperature. I prove that these results perfectly match the known values of the statistical moments in the low-temperature region ($T << T_c$), where there is a well-developed condensate, [21, 35] and their known asymptotics in the high-temperature region ($T >> T_c$), where there is no condensate [32–34]. Finally, I demonstrate that the described constraint-cut-off mechanism does yield the strongly non-Gaussian BEC fluctuations, similar to the ones found for the ideal gas in the box, even if one employs a pure Gaussian model for an unconstrained probability distribution of the noncondensate occupation that corresponds to an exactly solvable model of BEC in a degenerate interacting gas (Section D).

In Chapter IV I describe a two-level trap model for the BEC of the ideal gas and its exact solution for the constrained distribution function and its cumulants in the form of the cut-off negative binomial distribution (Section A) and its continuous approximation - cut-off gamma distribution (Section B). In Section C, I compare the results of both models as well as a 3-level trap model against BEC statistics in a real box trap and find an extent of validity of the so-called quasithermal ansatz [21]. The parameters for the 3-level trap are offered in the sense to fix the behavior of the first few cumulants. In the case when the second level coincides with the first excited state of the trap one can observe the perfect agreement between first two and all high order cumulants calculated in the 3-level model with the exact solution for the BEC in the box.

In Chapter V I employ the refined saddle-point approximation to obtain the asymptotic expression for the distribution function of condensed atoms in an ideal gas in a trap. In Section A, following [27], I formulate the method for the case of a harmonic trap and explain why the standard saddle-point approximation does not work for the systems with condensate. Then in Section B I employ this method to

find the condensate distribution function in an ideal gas in a box. In Section C I do numerical simulations and compare the asymptotical results obtained by the refined saddle-point approximation and constraint nonlinearity method in Chapter III for the distribution function. Finally, I shortly discuss still open problem of an applicability of the saddle-point approximation in the BEC statistics.

In Appendices A, B, C I present the detailed derivation of the characteristic function and the initial statistical moments of the ground state occupation as well as the residue technique and derivation of the multinomial expansion for the condensate statistics.

G. Contents of the FEL electrodynamics studies (Chapters VI-VII) and brief discussion of the main results

The part dedicated to FEL electrodynamics studies is organized as follows. In Chapter VI, Section A I study wave propagation in the Bragg waveguide based on a dielectric layer with periodic modulation of a dielectric constant. I present a mode spectrum of this structure and analyze selective characteristics of the mentioned above system. In Subsections 1 and 2 I start with a simplest model of a medium with regular periodicity, where a dispersion relation is presented. In Subsection 3 I consider more appropriate system of a dielectric medium with a step change of a periodicity modulation of a dielectric constant, which demonstrates much higher selective properties. In Subsection 4 I consider more practical regime for realization of radiation systems with high group velocity, which corresponds to the large frequency detuning from the cutoff.

In Chapter VI Section B I present a similar analysis for an open planar metal waveguide with slightly corrugated walls and a defect of periodicity in the middle

of the wall corrugation. This system is more competitive in the case of microwave electronics and particularly it is compatible with electron beam transportation systems. I demonstrate a dispersion relation and present an equation for coupling mode amplitudes. I show that a coupling coefficient, which is a constant in the case of dielectric medium, is a function of an angle between partial waves in the case of metal waveguide.

In Chapter VII, Section A I start with a discussion of a basic FEL amplifier scheme where electron beam moves along waveguide axis [43]. To increase effective size of operating mode one can use a structure with regular longitudinal corrugation that couples two partial waves propagating at some angle to the axis to the wave propagating directly along the axis. This wave, which is transformed into cutoff modes, is excited by the electrons in moving reference frame. I obtain a system of equation describing a process of electromagnetic wave amplification and study a longitudinal coordinate dependence of amplification coefficient.

In Section B I apply a similar theory discussed in Section A to the case of medium with a defect of a periodic modulation of dielectric constant and treat an active medium as a nonlinear negative conductance (an imaginary negative part of dielectric constant). I present a mode excitation equations and a dependence of field amplification on a longitudinal coordinate.

In Section C I consider a transverse current FEL amplifier [54–56] as an alternative geometry of mentioned in Section A device. In this case I obtain a system of equations describing wave amplification and equation of motion for an electron combinational phase, which is discussed in details in Appendix D. I simulate amplification coefficient, full and electron efficiency for this system and show its advantage compare to the case of longitudinal waveguiding described in Section A.

CHAPTER II

QUANTUM STATISTICS OF THE IDEAL AND WEAKLY INTERACTING BOSE GASES IN A BOX IN THE CANONICAL ENSEMBLE

A. Canonical ensemble quasiparticle approach

The standard methods of thermodynamics are not appropriate for the analysis of BEC fluctuations and mesoscopic effects. For example, the most widely known grand-canonical approach suffers from the grand-canonical catastrophe [60]. The restricted ensemble approach, which fixes the amplitude and the phase of the condensate wave function, is unable to analyze the fluctuation problem at all. To study the fluctuations, one should fix only external macroscopical and global, topological parameters of the system such as temperature, pressure, number of particles, super-fluid flow pattern, boundary conditions, etc. Solving the Von Neuman equation with general initial conditions one can get all possible states of the condensate. For the real systems, even with a weak interaction this way is very complicated. The perturbative series involving the initially unperturbed grand-canonical ensemble do not converge [8], thus it is impossible to use them.

One way to handle this problem is to deal with constrained many-body Hilbert space. The possibility of the proper reduction of the Fock space arises from introducing the new canonical ensemble quasiparticles. The usual particle number representation in many-body Hilbert space can be written as a proper combination of creation and annihilation operators $\hat{a}^{\dagger}_{\mathbf{k}}$ and $\hat{a}_{\mathbf{k}}$, which act as following

$$\hat{a}^{\dagger}_{\mathbf{k}}|\psi^{(n)}_{\mathbf{k}}\rangle = \sqrt{n+1}|\psi^{(n)}_{\mathbf{k}}\rangle, \quad \hat{a}_{\mathbf{k}}|\psi^{(n)}_{\mathbf{k}}\rangle = \sqrt{n}|\psi^{(n-1)}_{\mathbf{k}}\rangle, \quad \hat{n}_{\mathbf{k}}|\psi^{(n)}_{\mathbf{k}}\rangle = n|\psi^{(n)}_{\mathbf{k}}\rangle. \tag{2.1}$$

Girardeau and Arnowitt (GA) [30, 59] were the first who introduced the creation and

annihilation operators acting in the canonical ensemble subspace of the Fock space, which takes into account the particle number constraint. These operators obey the usual Bose commutation relations for $\mathbf{k} \neq 0$ in the subspace with $n_0 \neq 0$, namely,

$$\hat{\beta}_{\mathbf{k}}^{\dagger} = \hat{a}_{\mathbf{k}}^{\dagger}\hat{\beta}_0, \quad \hat{\beta}_{\mathbf{k}} = \hat{\beta}_0^{\dagger}\hat{a}_{\mathbf{k}}, \quad \hat{\beta}_0 = (1+\hat{n}_0)^{-1/2}\,\hat{a}_0, \quad \left[\hat{\beta}_{\mathbf{k}}, \hat{\beta}_{\mathbf{k}'}^{\dagger}\right] = \delta_{\mathbf{k},\mathbf{k}'}. \tag{2.2}$$

Since the GA operator subspace excludes states with zero number of the condensed atoms, this approach will be relevant for almost all temperatures $T < T_c$, starting even from a small condensate fraction $\bar{n}_0 << N$. It especially good for the well-peaked ground state occupation number distribution and relatively small variance in comparison with mean occupation number:

$$\langle (n_0 - \bar{n}_0)^2 \rangle^{1/2} << \bar{n}_0. \tag{2.3}$$

Thus, we approximate the exact canonical ensemble H^{CE} subspace by the subspace $H^{\mathrm{CE}}_{n_0 \neq 0}$ with excluded zero condensed fraction states. This means that we are considering the transitions between a condensate state ($\mathbf{k} = 0$) and excited states ($\mathbf{k} \neq 0$). Consequently, one can express all quantum properties of the system using GA operators. For example, the total number of particles is equal to the sum of the number of condensed atoms and excited atoms:

$$\hat{n}_0 = N - \sum_{\mathbf{k} \neq 0} \hat{n}_{\mathbf{k}}, \tag{2.4}$$

where the excited state occupation number is

$$\hat{n}_{\mathbf{k}} = \hat{a}_{\mathbf{k}}^{\dagger}\hat{a}_{\mathbf{k}} = \hat{\beta}_{\mathbf{k}}^{\dagger}\hat{\beta}_{\mathbf{k}}. \tag{2.5}$$

The ground state occupation statistics is very informative part of the BEC fluctuations. Canonical ensemble quasiparticle states can be defined via the bare trap states

as their many-body mixture fixed by the interaction and external conditions. Besides that, there are many other quantities, which can be defined in a similar way, such as occupations of the dressed, excited states, etc.

Let us now consider the case of weakly interacting dilute Bose gas. It can be described by the well-known Hamiltonian [5]

$$H = \sum_{\mathbf{k}} \frac{\hbar^2 \mathbf{k}^2}{2m} \hat{a}^\dagger_{\mathbf{k}} \hat{a}_{\mathbf{k}} + \frac{1}{2V} \sum \langle \mathbf{k_3 k_4} | U | \mathbf{k_1 k_2} \rangle \hat{a}^\dagger_{\mathbf{k_4}} \hat{a}^\dagger_{\mathbf{k_3}} \hat{a}_{\mathbf{k_2}} \hat{a}_{\mathbf{k_1}}, \tag{2.6}$$

where $V = L^3$ is a volume of a box where the gas is confined under a periodic boundary conditions.

The presence of weak interaction implies the Bogoliubov coupling between bare canonical-ensemble quasiparticles $\hat{\beta}_{\mathbf{k}} = \hat{\beta}^\dagger_0 \hat{a}_{\mathbf{k}}$ via the condensate. One can describe it by the quadratic part of the Hamiltonian in Eq. (2.6) as follows:

$$H_B = \frac{N(N-1)U_0}{2V} + \sum_{\mathbf{k}\neq 0} \left(\frac{\hbar^2 \mathbf{k}^2}{2m} + \frac{(\hat{n}_0 + 1/2) U_{\mathbf{k}}}{V} \right) \hat{\beta}^\dagger_{\mathbf{k}} \hat{\beta}_{\mathbf{k}} + \\ \frac{1}{2V} \sum_{\mathbf{k}\neq 0} \left(U_{\mathbf{k}} \sqrt{(1+\hat{n}_0)(2+\hat{n}_0)} \hat{\beta}^\dagger_{\mathbf{k}} \hat{\beta}_{\mathbf{k}} + \text{H.c.} \right). \tag{2.7}$$

Our main assumption is that the ground-state occupation distribution is well peaked (see Eq. (2.3)). Therefore we can use the approximation that $\hat{n}_0 \approx \bar{n}_0 >> 1$. The standard Bogoliubov transformation

$$\hat{\beta}_{\mathbf{k}} = u_{\mathbf{k}} \hat{b}_{\mathbf{k}} + v_{\mathbf{k}} \hat{b}^\dagger_{-\mathbf{k}}; \quad u_{\mathbf{k}} = \frac{1}{\sqrt{1 - A^2_{\mathbf{k}}}}, \quad v_{\mathbf{k}} = \frac{A_{\mathbf{k}}}{\sqrt{1 - A^2_{\mathbf{k}}}}, \\ \hat{\beta}^\dagger_{\mathbf{k}} = u_{\mathbf{k}} \hat{b}^\dagger_{\mathbf{k}} + v_{\mathbf{k}} \hat{b}_{-\mathbf{k}}; \quad A_{\mathbf{k}} = \frac{V}{\bar{n}_0 U_{\mathbf{k}}} \left(\epsilon_{\mathbf{k}} - \frac{\hbar^2 \mathbf{k}^2}{2m} - \frac{\bar{n}_0 U_{\mathbf{k}}}{V} \right), \tag{2.8}$$

determines dressed by condensate canonical-ensemble quasiparticles that fluctuate independently according to approximation in Eq. (2.6). One can rewrite the atom-number-concerving Hamiltonian from Eq. (2.6) in terms of new dressed quasiparticles

in Eq. (2.8) as follows:

$$H_B = E_0 + \sum_{\mathbf{k}\neq 0} \tilde{\epsilon}_{\mathbf{k}} \hat{b}^{\dagger}_{\mathbf{k}} \hat{b}_{\mathbf{k}}, \tag{2.9}$$

where a "gapless" Bogoloubov energy spectrum is

$$\tilde{\epsilon}_{\mathbf{k}} = \sqrt{\left(\frac{\hbar^2 \mathbf{k}^2}{2m} + \frac{\bar{n}_0 U_{\mathbf{k}}}{V}\right)^2 - \left(\frac{\bar{n}_0 U_{\mathbf{k}}}{V}\right)^2}. \tag{2.10}$$

It is now clearly seen that we arrive to the problem of an ideal gas of dressed quasiparticles in contrast to the gas of atoms and gas of bare quasiparticles in Eq. (2.2). Therefore, the analysis of fluctuations can be performed simultaneously in the same fashion in both cases of ideal gas and weakly interacting gas.

B. Characteristic function for the ground state occupation number in an ideal Bose gas

From the construction of the canonical-ensemble quasiparticles outlined in the previous section (see Eq. (2.2)), one concludes, that the occupation numbers $n_{\mathbf{k}}$ can be approximated as an independent stochastic variables and, thus, one can apply an equilibrium distribution to the equilibrium canonical ensemble density matrix:

$$\rho_{\mathbf{k}}\left(n_{\mathbf{k}}\right) = \exp\left(-n_{\mathbf{k}}\epsilon_{\mathbf{k}}/T\right)\left[1 - \exp\left(-\epsilon_{\mathbf{k}}/T\right)\right]. \tag{2.11}$$

The distribution function of the excited atoms according to Eq. (2.4) is just a mirror distribution of the condensed particles:

$$\rho\left(n\right) = \rho_0\left(n_0 = N - n\right). \tag{2.12}$$

In statistical physics there is a useful formalism of describing the density matrix via the characteristic function:

$$\Theta_n(u) = \mathrm{Tr}\{e^{iun}\hat{\rho}\}, \qquad \Theta_n(u=0) = 1. \tag{2.13}$$

Taking the inverse Fourier transformation, one obtains the distribution function

$$\rho(n) = \frac{1}{2\pi}\int_{-\pi}^{\pi} e^{-inu}\Theta_n(u)\,du. \tag{2.14}$$

Very important property of the characteristic function is that the characteristic function for the ensemble of the independent stochastic variables is a product of the individual characteristic functions, thus:

$$\Theta_n(u) = \prod_{\mathbf{k}\neq 0}\Theta_{n_\mathbf{k}}(u), \qquad \ln\Theta_n(u) = \sum_{\mathbf{k}\neq 0}\ln\Theta_{n_\mathbf{k}}(u). \tag{2.15}$$

Each individual characteristic function can be easily calculated from the equilibrium density matrix as following:

$$\Theta_{n_\mathbf{k}}(u) = \mathrm{Tr}\{e^{iu\hat{n}_\mathbf{k}}\hat{\rho}_\mathbf{k}\} = \mathrm{Tr}\{e^{iu\hat{n}_\mathbf{k}}e^{-\epsilon_\mathbf{k}\hat{n}_\mathbf{k}/T}\}\left(1-e^{-\epsilon_\mathbf{k}/T}\right) = \frac{z_\mathbf{k}-1}{z_\mathbf{k}-z}, \tag{2.16}$$

where $z_\mathbf{k} = \exp(\epsilon_\mathbf{k}/T)$ and $z = \exp(iu)$ is a fugacity. Therefore, for an ideal gas in an arbitrary trap, the characteristic function of the number of excited atoms can be written as

$$\Theta_n(u) = \prod_{\mathbf{k}\neq 0}\frac{z_\mathbf{k}-1}{z_\mathbf{k}-e^{iu}}. \tag{2.17}$$

In the case of weakly interacting dilute gas the equilibrium density matrix is not diagonal in the basis of bare atoms, which statistics we want to calculate. It can be written as follows:

$$\hat{\rho} = \prod_{\mathbf{k}\neq 0}\hat{\rho}_\mathbf{k}, \quad \hat{\rho}_\mathbf{k} = e^{-\epsilon_\mathbf{k}\hat{b}^\dagger_\mathbf{k}\hat{b}_\mathbf{k}/T}(1-e^{-\epsilon_\mathbf{k}/T}). \tag{2.18}$$

The mentioned above effect leads to the squeezing of fluctuations effect, which is well known in laser physics. The number of atoms with coupled momenta $\mathbf{k}$ and $-\mathbf{k}$ can be written in terms of Bogoliubov coupling coefficients as follows:

$$\hat{a}^{\dagger}_{\mathbf{k}}\hat{a}_{\mathbf{k}} = \hat{\beta}^{\dagger}_{\mathbf{k}}\hat{\beta}_{\mathbf{k}} + \hat{\beta}^{\dagger}_{-\mathbf{k}}\hat{\beta}_{-\mathbf{k}} =$$

$$= (u^2_{\mathbf{k}} + v^2_{\mathbf{k}})(\hat{b}^{\dagger}_{\mathbf{k}}\hat{b}_{\mathbf{k}} + \hat{b}^{\dagger}_{-\mathbf{k}}\hat{b}_{-\mathbf{k}}) + 2u_{\mathbf{k}}v_{\mathbf{k}}(\hat{b}^{\dagger}_{\mathbf{k}}\hat{b}^{\dagger}_{-\mathbf{k}} + \hat{b}_{\mathbf{k}}\hat{b}_{-\mathbf{k}}) + 2v^2_{\mathbf{k}}. \tag{2.19}$$

The characteristic function for the total number of atoms in the two $\mathbf{k}$ and $-\mathbf{k}$ modes squeezed by Bogoliubov coupling was calculated in [21] as follows:

$$\Theta_{\pm\mathbf{k}}(u) = \mathrm{Tr}\left[e^{iu(\hat{\beta}^{\dagger}_{\mathbf{k}}\hat{\beta}_{\mathbf{k}} + \hat{\beta}^{\dagger}_{-\mathbf{k}}\hat{\beta}_{-\mathbf{k}})}e^{-\epsilon_{\mathbf{k}}(\hat{b}^{\dagger}_{\mathbf{k}}\hat{b}_{\mathbf{k}} + \hat{b}^{\dagger}_{-\mathbf{k}}\hat{b}_{-\mathbf{k}})/T}(1 - e^{-\epsilon_{\mathbf{k}}/T})^2\right] =$$

$$= \frac{[z(A_{\mathbf{k}}) - 1][z(-A_{\mathbf{k}}) - 1]}{[z(A_{\mathbf{k}}) - e^{iu}][z(-A_{\mathbf{k}}) - e^{iu}]}, \tag{2.20}$$

where

$$z(A_{\mathbf{k}}) = \frac{A_{\mathbf{k}} - e^{\epsilon_{\mathbf{k}}/T}}{A_{\mathbf{k}}e^{\epsilon_{\mathbf{k}}/T} - 1}. \tag{2.21}$$

The characteristic function for the total number of the excited atoms is equal to the product of the couple-mode characteristic functions,

$$\Theta_n(u) = \prod_{\mathbf{k}\neq 0, \mathrm{mod}(\pm\mathbf{k})} \Theta_{\pm\mathbf{k}}(u), \tag{2.22}$$

where the product runs over all different pairs of $(\mathbf{k}, -\mathbf{k})$, since these modes are independent to the first approximation (see Eq. (2.6)).

The characteristic function or its logarithm can be expanded as a Taylor series with cumulants (semi-invariants), generating cumulants or initial (noncentered) moments as the coefficients [29]:

$$\Theta_n(u) = \sum_{m=0}^{\infty} \alpha_m \frac{(iu)^m}{m!}, \qquad \alpha_m \equiv \langle n^m \rangle = \frac{d^m}{d(iu)^m}\Theta_n(u)|_{u=0}, \tag{2.23}$$

$$\ln \Theta_n(u) = \sum_{m=1}^{\infty} \kappa_m \frac{(iu)^m}{m!}, \qquad \kappa_m = \frac{d^m}{d(iu)^m} \ln \Theta_n(u)|_{u=0}, \tag{2.24}$$

$$\ln \Theta_n(u) = \sum_{\mathbf{k}\neq 0} \ln \left(\frac{z_{\mathbf{k}} - 1}{z_{\mathbf{k}} - z} \right) = \sum_{m=1}^{\infty} \kappa_m \frac{(iu)^m}{m!} = \sum_{m=1}^{\infty} \tilde{\kappa}_m \frac{\left(e^{iu} - 1\right)^m}{m!}. \tag{2.25}$$

The cumulants κ_m and generating cumulants $\tilde{\kappa}_m$ can be related by the Stirling numbers of the second kind [29]:

$$\sigma_r^{(m)} = \frac{1}{m!} \sum_{k=0}^{m} (-1)^{m-k} \left(\begin{array}{c} m \\ k \end{array} \right) k^r, \qquad \left(e^x - 1\right)^k = k! \sum_{n=k}^{\infty} \sigma_n^{(k)} \frac{x^n}{n!}. \tag{2.26}$$

The useful property is that the cumulant of the sum of independent stochastic variables is equal to a sum of the partial cumulants $\kappa_r = \sum_{\mathbf{k}\neq 0} \kappa_r^{\mathbf{k}}$. This relation follows from the productivity property of the characteristic function (2.15). Also the cumulants can be simply related to the initial (noncentered) and central moments of the distribution by binomial relations [29]:

$$\mu_r = \sum_{k=0}^{r} (-1)^k \left(\begin{array}{c} r \\ k \end{array} \right) \alpha_{r-k} \bar{n}^k, \qquad \alpha_r = \sum_{k=0}^{r} \left(\begin{array}{c} r \\ k \end{array} \right) \mu_{r-k} \bar{n}^k \tag{2.27}$$

$$\bar{n} = \kappa_1, \qquad \left\langle (n - \bar{n})^2 \right\rangle \equiv \mu_2 = \kappa_2, \qquad \left\langle (n - \bar{n})^3 \right\rangle \equiv \mu_3 = \kappa_3,$$

$$\left\langle (n - \bar{n})^4 \right\rangle \equiv \mu_4 = \kappa_4 + 3{\kappa_2}^2,$$

$$\left\langle (n - \bar{n})^5 \right\rangle \equiv \mu_5 = \kappa_5 + 10\kappa_2\kappa_3,$$

$$\left\langle (n - \bar{n})^6 \right\rangle \equiv \mu_6 = \kappa_6 + 15\kappa_2 \left(\kappa_4 + 2\kappa_2^2\right), \tag{2.28}$$

$$\kappa_1 = \tilde{\kappa}_1, \qquad \kappa_2 = \tilde{\kappa}_2 + \tilde{\kappa}_1, \qquad \kappa_3 = \tilde{\kappa}_3 + 3\tilde{\kappa}_2 + \tilde{\kappa}_1,$$

$$\kappa_4 = \tilde{\kappa}_4 + 6\tilde{\kappa}_3 + 7\tilde{\kappa}_2 + \tilde{\kappa}_1, ... \tag{2.29}$$

In the case of low temperatures, far enough from the region near the critical temperature of the Bose condensate, where the properties of the moments except for the

average value do not depend on the total number of atoms in a trap, i.e. the mesoscopic effects are not important, the cumulants of the condensate distribution can be written as:

$$\tilde{\kappa}_m = (m-1)! \sum_{\mathbf{k}\neq 0} (e^{\epsilon_{\mathbf{k}}/T} - 1)^{-m}; \qquad \kappa_r = \sum_{n=k}^{\infty} \sigma_n^{(k)} \tilde{\kappa_m}. \tag{2.30}$$

Similar to Eq. (2.30), in the case of weakly interacting gas, all cumulants can be written as follows

$$\tilde{\kappa}_m = \frac{1}{2}(m-1)! \sum_{\mathbf{k}\neq 0} \left[\frac{1}{[z(A_{\mathbf{k}}) - 1]^m} + \frac{1}{[z(-A_{\mathbf{k}}) - 1]^m} \right]. \tag{2.31}$$

In comparison with the ideal Bose gas in Eq. (2.30), we have a mixture of two species of atom pairs with $z(\pm A_{\mathbf{k}})$ instead of $\exp(\epsilon_{\mathbf{k}}/T)$.

It is worth noting that Eq. (2.31) for $m = 1$ is a non-linear self-consistency equation,

$$N - \bar{n}_0 = \kappa_1(\bar{n}_0) \equiv \sum_{\mathbf{k}\neq 0} \frac{1 + A_{\mathbf{k}}^2 e^{\epsilon_{\mathbf{k}}/T}}{(1 - A_{\mathbf{k}}^2)(e^{\epsilon_{\mathbf{k}}/T} - 1)}, \tag{2.32}$$

for the mean ground state occupation number $\bar{n}_0(T)$, since the Bogoluibov coupling coefficient $A_{\mathbf{k}}$ in Eq. (2.8) and energy spectrum $\epsilon_{\mathbf{k}}$ in Eq. (2.10) are the functions of $\bar{n}_0$. Therefore, the rest of the Eqs. (2.31) for $m \geq 2$, are nothing else but explicit expressions for all cumulants, $m \geq 2$, if one substitutes the solution of the self-consistency Eq. (2.32) for the mean value $\bar{n}_0$.

These formulas are valid in the case of condensate inside the infinite reservoir of the excited atoms. This universal result was found in [21] and is equivalent to the Maxwell's demon ensemble approximation. In particular, this result does not describe many mesoscopic effects and the temperature range near and above critical temperature T_c.

C. Constraint nonlinearity and many-body Fock space cut-off in the canonical ensemble

As it was discussed in previous sections and in [61–64], the only reason for the BEC of atoms on the ground state $\mathbf{k} = 0$ is the conservation of the total number of the Bose particles in the trap, $N = \hat{n}_0 + \hat{n}$. Hence, the occupation operators $\hat{n}_{\mathbf{k}}$ are not independent and the many-body Hilbert space is strongly constrained. A more convenient equivalent formulation of the problem can be given if one introduces constraint nonlinearity in the dynamics and statistics, even for the ideal gas, on the basis of the particle-number constraint. In most previous studies, an actual (e.g., micro-canonical or canonical) quantum ensemble was substituted by an artificial grand-canonical ensemble, where only the mean number of particles is fixed by the appropriate choice of the chemical potential μ and, therefore, most quantum effects in dynamics and statistics of BEC were lost or misunderstood.

Following our general approach [20, 21, 35, 61–64], we solve for the constraint from the very beginning through the proper reduction of the many-body Hilbert space. In the present case of the ideal gas in the canonical ensemble, we have to consider as independent only noncondensate Fock states $\left|\{n_{\mathbf{k}},\ \mathbf{k} \neq 0\}\right\rangle$ which uniquely specify the ground-state Fock state $\left|n_0 = N - \sum_{\mathbf{k}\neq 0} n_{\mathbf{k}}\right\rangle$. However, the remaining noncondensate Fock space should be further cut off by the boundary $n_{\mathbf{k}} \leq N$. The latter is equivalent to an introduction of a step-function $\theta(N - \hat{n})$, i.e., 1 if $n \leq N$ or 0 if $n > N$, in all operator equations and under all trace operations. That $\theta(N - \hat{n})$ factor is the constraint nonlinearity that, being accepted, allows us to consider the noncondensate many-body Fock space formally as an unconstrained one. We adopt this point of view from now on.

Therefore, the BEC fluctuations are described by a mirror image of the proba-

bility distribution of the total number of excited (noncondensed) atoms

$$\rho_n = \rho_{\rm cond}(n_0 = N - n), \qquad \rho_n = \frac{1}{2\pi}\int_{-\pi}^{\pi} e^{-iun}\Theta_n(u)du, \tag{2.33}$$

where

$$\Theta_n(u) = {\rm Tr}\{e^{iun}\hat{\rho}\ \theta(N - \hat{n})\} = \sum_{n=0}^{N} e^{iun}\rho_n \tag{2.34}$$

is a characteristic function for the stochastic variable n, $\hat{\rho} = e^{-H/T}/{\rm Tr}\{e^{-H/T}\theta(N-n)\}$ is an equilibrium density matrix, and the temperature is measured in the energy units, so that the Boltzmann constant is set to be 1. Thus, the actual probability distribution

$$\rho_n = \rho_n^{(\infty)} / \sum_{n=0}^{N} \rho_n^{(\infty)} \tag{2.35}$$

is merely a $\theta(N - n)$ cut off of the unconstrained probability distribution $\rho_n^{(\infty)}$ for an infinite interval of the noncondensate occupations $n \in [0, \infty)$, as is shown in Fig. 3.

The latter distribution $\rho_n^{(\infty)}$ was analytically calculated in [21, 35] (see Section B of this chapter) via all its moments and cumulants for arbitrary trap. Thus, only a straightforward calculation of the moments and cumulants of the cut off probability distribution, given in Eq. (2.35) and depicted as a curve OAN in Fig. 3, remains to fulfill in order to find the actual BEC statistics in the mesoscopic system for all numbers of atoms and temperatures, including a critical region.

D. Properties of the spectrum of the box with the periodic boundary conditions

In this section I explain the subtle points of the momentum summation (product) that occurs in the different statistical quantities in Bose gas in a box with periodic boundary conditions. I will make the analysis for the case of the ideal gas energy spectrum for the simplicity, because it is not essentially a property of the gas or interaction but is the property of the periodic boundary conditions for cartesian

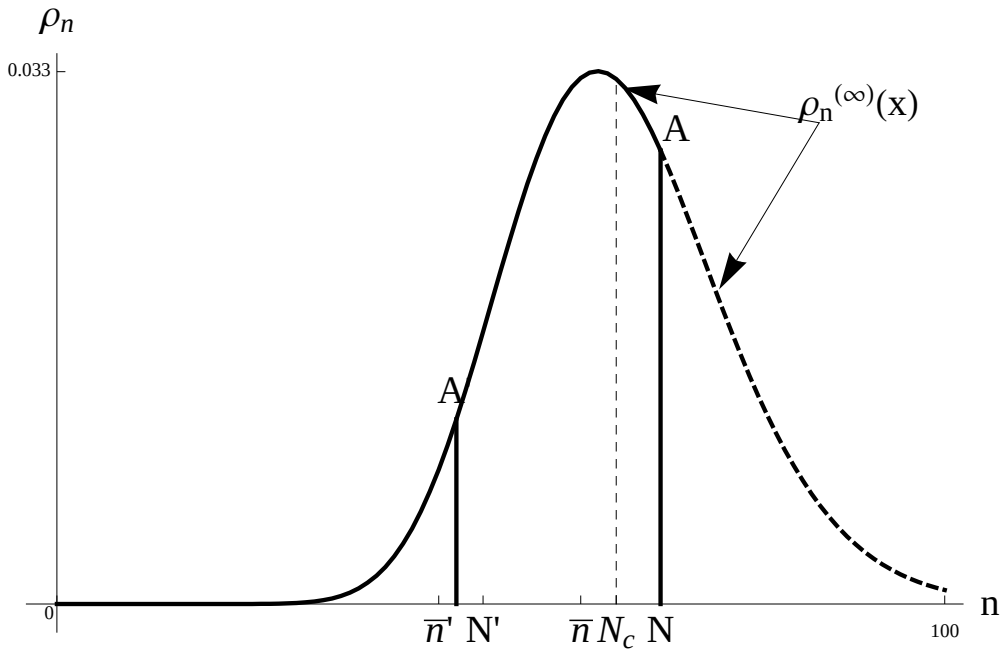

Fig. 3. Unconstrained probability distribution of the number of noncondensed atoms $\rho_n^{(\infty)}$ (dashed line) and its cut offs (solid lines) for a small number of atoms $N' < N_c$ ($OA'N'$, there is no condensate) and for a large number of atoms $N > N_c$ (OAN, there is condensate) for the trap with a given volume and temperature: the trap-size parameter in Eq. (3.2) is $N_v = 100$.

planar boundaries following from the Fourier analysis in the basis of the simplest trigonometric functions. Consider an atomic gas with a mass m in the 3D box of a volume L^3 with periodic boundary conditions, which looks almost like a free particle spectrum, beside the certain quantized momentum $\hbar\mathbf{k}_l$,

$$\epsilon_{\mathbf{k}} = \frac{\hbar^2\mathbf{k}^2}{2m}, \qquad \mathbf{k}_l = \frac{2\pi}{L}\mathbf{l}, \qquad \mathbf{l} = (l_x, l_y, l_z). \tag{2.36}$$

The characteristic quantity $z_{\mathbf{k}} = e^{\epsilon_{\mathbf{k}}/T} = e^{\epsilon_1 \mathbf{l}^2/T}$ has the meaning of the inverse probability of finding particle in the state with energy $\epsilon_{\mathbf{k}}$, and the energy gap parameter is

$$\epsilon_1/T = (2\pi\hbar/L)^2/(2mT). \tag{2.37}$$

It is obvious, that the critical temperature is different for different number of particles, even though the temperature scale is always the critical temperature for the thermodynamic limit of an ideal gas in a box:

$$T_c = \frac{2\pi\hbar^2}{m}\left(\frac{N}{L^3\zeta(3/2)}\right)^{2/3}, \tag{2.38}$$

so that

$$\bar{n}_0 = N - \bar{n} = N - \kappa_1 = N\left[1 - (T/T_c)^{3/2}\right]. \tag{2.39}$$

One can simplify the summation involved in the computation of cumulants and product in characteristic function by applying the symmetry of the boundaries and spectrum. Let us focus on the summation, for instance. One has the sum over all modes beside the mode with zero energy - the excluded zero origin. This summation can be performed over different 3D, 2D, and 1D submanifolds in the momentum space of the box separately. It is obvious that modes with $\mathbf{k}$ and $-\mathbf{k}$ have the same energy. For 3D subspace one has 8 equivalent domains with positive (k_x, k_y, k_z) and 6 ways of rearranging them in the order, for example: $k_x > k_y > k_z$ or $k_x > k_y < k_z$, etc. The total

degeneracy will be $8 \cdot 6 = 48$. Similarly, one can obtain the following degeneracies for 2D submanifold: $4 \cdot 3 = 12$ domains for the pair and 2 ways of rearranging $k_x < k_y$ or $k_x > k_y$, thus the total 2D degeneracy is 24. Note, that 1D submanifold contains three types of subvolumes; namely a domain where for example: $k_x \neq 0, k_y = k_z = 0$ with degeneracy $2 \cdot 3 = 6$, corresponding to the ribs of the cube, $k_x = k_y \neq 0, k_z = 0$ with degeneracy $4 \cdot 3 = 12$, corresponding to the diagonals of each of eight sides of the cube and domain with $k_x = k_y = k_z \neq 0$ with degeneracy 8, as a diagonal in each of eight quadrants of positive or negative k-axis. Thus, one can conclude, that the summation (product) of an arbitrary function $f(\mathbf{k})$ over all momentum space with excluded origin can be written as:

$$\begin{aligned}\sum_{\mathbf{k}\neq 0} f(\mathbf{k}) = \sum_{\mathbf{k}\equiv(k_x,k_y,k_z)\neq 0} f(k_x,k_y,k_z) = 48 \sum_{k_x\geq k_y>k_z>0} f(k_x,k_y,k_z) + \\ 24 \sum_{k_x>k_y>0} f(k_x,k_y,0) + 6 \sum_{k_x>0} f(k_x,0,0) + 12 \sum_{k_x>0} f(k_x,k_x,0) + \\ +8 \sum_{k_x>0} f(k_x,k_x,k_x).\end{aligned} \tag{2.40}$$

For example, the characteristic function (2.17) of the total number of noncondensed particles can be written as:

$$\begin{aligned}\Theta(z) = \prod_{\mathbf{k}\neq 0} \frac{z_{\mathbf{k}} - 1}{z_{\mathbf{k}} - z} = \prod_{k_z=1}^{\infty} \prod_{k_y=k_z+1}^{\infty} \prod_{k_x=k_y}^{\infty} \left(\frac{e^{\epsilon_1(k_x^2+k_y^2+k_z^2)/T} - 1}{e^{\epsilon_1(k_x^2+k_y^2+k_z^2)/T} - z} \right)^{48} \times \\ \times \prod_{k_y=1}^{\infty} \prod_{k_x=k_y+1}^{\infty} \left(\frac{e^{\epsilon_1(k_x^2+k_y^2)/T} - 1}{e^{\epsilon_1(k_x^2+k_y^2)/T} - z} \right)^{24} \prod_{k_x=1}^{\infty} \left(\frac{e^{\epsilon_1(k_x^2)/T} - 1}{e^{\epsilon_1(k_x^2)/T} - z} \right)^{6} \times \\ \times \prod_{k_x=1}^{\infty} \left(\frac{e^{\epsilon_1(2k_x^2)/T} - 1}{e^{\epsilon_1(2k_x^2)/T} - z} \right)^{12} \prod_{k_x=1}^{\infty} \left(\frac{e^{\epsilon_1(3k_x^2)/T} - 1}{e^{\epsilon_1(3k_x^2)/T} - z} \right)^{8}.\end{aligned} \tag{2.41}$$

The difference in summation rule for the case of weakly interacting gas is that the summation is performed on pairs of $(\mathbf{k}, -\mathbf{k})$ which makes the degeneracies to be one half of corresponding degeneracies in the ideal gas: $2\sum_{\mathbf{k}\neq 0,\mathrm{mod}(\mathbf{k},-\mathbf{k})} = \sum_{\mathbf{k}\neq 0}$.

E. Multinomial expansion

The following discussion will be dedicated to the derivation of the closed form expression for the distribution function, its cumulants, as well as the initial and central moments for the ideal and weakly interacting dilute Bose gases using the combinatorial analysis of the multinonial coefficients. The detailed derivation of the following formalism is presented in Appendices A-C.

Let us start with a simpler case of an ideal gas. Consider the characteristic function of the total number of noncondensed atoms given in Eqs. (2.15)-(2.17). It can be written as following:

$$\Theta\left(z\right)=\prod_{\mathbf{k}\neq0}\frac{z_{\mathbf{k}}-1}{z_{\mathbf{k}}-z}=\Theta_{0}\exp\left(-\sum_{\mathbf{k}\neq0}\ln(1-z/z_{\mathbf{k}})\right), \tag{2.42}$$

where $z=e^{iu}$, $\Theta_0\equiv\Theta(z=0)=\prod_{\mathbf{k}\neq0}(z_{\mathbf{k}}-1)/z_{\mathbf{k}}$ is the characteristic function at zero fugacity z. Employing the Taylor expansion of the logarithm under the summation about the point $z=0$ and changing the summation order in the exponent power, one can rewrite (2.42) as following

$$\Theta(z)=\Theta_{0}\exp\left(\sum_{m=1}^{\infty}f_{m}z^{m}\right), \tag{2.43}$$

where coefficients in Taylor expansion above are $f_m\equiv f_m(z=0)$, $f_m(z)=\sum_{\mathbf{k}\neq0}(z-z_{\mathbf{k}})^{-m}$.

Employing the approach discussed in the Appendix A of expressing the condensate statistics as a residues of the characteristic function evaluated at $z=0$ (see Eq. (A.4)) one can conclude, that $\rho(n)$ is nothing else but the Taylor coefficient of the z^n term,

$$\rho(n)=\frac{\Theta_{0}}{n!}\frac{d^{n}}{dz^{n}}\left(\sum_{r=0}^{\infty}\frac{1}{r!}\left(\sum_{m=1}^{\infty}f_{m}z^{m}\right)^{r}\right)\Big|_{z=0}, \tag{2.44}$$

since all the other are zero. Here and in Appendices by $\rho(n)$ I mean an unconstrained

distribution function $\rho_n^{(\infty)}$. One can now employ the wonderful properties of the multinomial coefficients [29]:

$$\left(\sum_{m=1}^{\infty} f_m z^m\right)^r \equiv r! \sum_{n=r}^{\infty} \frac{z^n}{n!} \sum (n; a_1, a_2, a_3..., a_n)^* f_1^{a_1} f_2^{a_2} f_3^{a_3} ... f_n^{a_n}, \tag{2.45}$$

summed over $a_1 + a_2 + a_3 + ... + a_n = r$ and $a_1 + 2a_2 + 3a_3 + .. + na_n = n$, where the multinomial coefficients have the following closed form expression:

$$(n; a_1, a_2, a_3..., a_n)^* = n!/1^{a_1} a_1! 2^{a_2} a_2! 3^{a_3} a_3! ... n^{a_n} n!, \tag{2.46}$$

with the same restricted summation $a_1 + 2a_2 + 3a_3 + .. + na_n = n$. The meaning of these coefficients is the number of permutations of $n = a_1 + 2a_2 + 3a_3 + .. + na_n$ symbols composed of a_k cycles of length k for $k = 1, 2, 3, ..., n$.

Applying the expression (2.45) to obtain the distribution function and changing the summation order as well as employing the fact, that n-th derivative is non zero only for n-th term in the expansion, the result can be written as:

$$\rho(n) = \frac{\Theta_0}{n!} \sum_{m=0}^{n} \sum_{\left(\begin{array}{l} a_1 + a_2 + ... + a_n = m \\ a_1 + 2a_2 + ... + na_n = n \end{array} \right)} (n, a_1, a_2, ..., a_n)^* \prod_{j=1}^{n} f_j^{a_j}. \tag{2.47}$$

This closed form expression for the distribution function is exact and no approximations were implied so far.

The initial moments of the distribution function presented in Eq. (2.47) which can be calculated also via the Taylor expansion of the constrained characteristic function, $\Theta_n(u) = \sum_{m=0}^{N} \alpha_m u^m/m!$ are related to the central moments $\mu_m = \langle (n - \bar{n})^m \rangle$ and to the cumulants κ_m by the following explicit formulas [29]:

$$\alpha_r = \sum_{k=0}^{r} C_r^k \mu_{r-k} \bar{n}^k, \qquad \mu_r = \sum_{k=0}^{r} (-1)^k C_r^k \alpha_{r-k} \bar{n}^k, \tag{2.48}$$

$$\kappa_r = \sum_{m=1}^{r}(-1)^m - 1(m-1)! \sum_{(r,m)} (r; a_1, ..., a_r)' \alpha_1^{a_1} ... \alpha_r^{a_r}, \tag{2.49}$$

$$\alpha_m = \sum_{r=1}^{m} \sum_{(m,r)} (m; a_1, ..., a_m)' \kappa_1^{a_1} ... \kappa_m^{a_m}, \tag{2.50}$$

where $C_r^k = r!/(k!(r-k)!)$, $(m; a_1, ..., a_m)' = m!/((1!)^{a_1} a_1!(2!)^{a_2} a_2! ... (m!)^{a_m} a_m!)$ is a multinomial coefficient, and the sum in Eqs. (2.49)-(2.50) runs over the nonnegative integers $a_1, ..., a_r$ which satisfy the following two conditions: $a_1 + 2a_2 + ... + ra_r = r$ and $a_1 + a_2 + ... + a_r = m$.

We calculate the quantities which are the most important and convenient for the analysis of the BEC statistics, namely, the mean value $\bar{n}$ (which is complimentary for the BEC order parameter $\bar{n}_0 = N - \bar{n}$) as well as the central moments μ_m and cumulants κ_m of the total noncondensate occupation. The point is that the ground-state (condensate) occupation fluctuates complimentary to a sum of many, to large extent independent occupations of the excited states in the noncondensate, conditioned by the particle-number constraint. The central moments of the condensate fluctuations differ from the corresponding central moments of the noncondensate fluctuations only by the sign for the odd orders, $\langle (n_0 - \bar{n}_0)^m \rangle = (-1)^m \langle (n - \bar{n})^m \rangle$.

The centered moments calculated with such a distribution function coincide perfectly with the exact recursion relation of Eq. (1.38):

$$\rho_0(n_0) = \frac{Z_{N-n_0}(T) - Z_{N-n_o-1}(T)}{Z_N(T)}; \qquad Z_{-1} \equiv 1, \tag{2.51}$$

$$Z_N(T) = \frac{1}{N} \sum_{k=1}^{N} Z_1(T/k) Z_{N-k}(T),$$

$$Z_1(T) = 1 + \sum_{\mathbf{k} \neq 0} e^{-\epsilon_{\mathbf{k}}/T}. \tag{2.52}$$

Similar analysis can be performed in the case of weakly interacting gas. Starting from the characteristic function of the total number of noncondensed atoms given in

Eq. (2.20) one can express it in the following form:

$$\Theta_n(z) = \prod_{\mathbf{k}\neq 0,\mathrm{mod}(\pm\mathbf{k})} = \frac{[z(A_\mathbf{k})-1][z(-A_\mathbf{k})-1]}{[z(A_\mathbf{k})-z][z(-A_\mathbf{k})-z]} =$$

$$= \Theta_0 \exp\left(-\frac{1}{2}\sum_{\mathbf{k}\neq 0}\ln[1-z/z(A_\mathbf{k})] - \frac{1}{2}\sum_{\mathbf{k}\neq 0}\ln[1-z/z(-A_\mathbf{k})]\right), \tag{2.53}$$

where $\Theta_0 \equiv \Theta(z=0) = \prod_{\mathbf{k}\neq 0,\mathrm{mod}(\pm\mathbf{k})}[z(A_\mathbf{k})-1][z(-A_\mathbf{k})-1]/[z(A_\mathbf{k})z(-A_\mathbf{k})]$ is a characteristic function at zero fugacity z. It is obvious that one has two similar contributions from both $z(\pm A_\mathbf{k})$ in the exponent compare to the case of the ideal gas, where one has one term with $z_\mathbf{k}$. The factor $1/2$ in front of these two terms is following from the summation rule discussed in the previous section, in particular: $\sum_{\mathbf{k}\neq 0,\mathrm{mod}(\mathbf{k},-\mathbf{k})}\Theta_\mathbf{k} = (1/2)\sum_{\mathbf{k}\neq 0}\Theta_\mathbf{k}$. Performing calculation similar to the case of the ideal gas one arrives to essentially the same Eq. (2.47) but with different coefficients f_m. In the case of weakly interacting gas these coefficients also have two additive terms: $f_m \equiv f_m(z=0)$, $f_m(z) = (1/2)\sum_{\mathbf{k}\neq 0}[(z-z(A_\mathbf{k}))^{-m} + (z-z(-A_\mathbf{k}))^{-m}]$. The existence of two additive contributions to the different quantities in the presence of interaction modifies also a single particle partition function. In contrast with the ideal gas one need to rewrite Eq. (2.52) as follows:

$$Z_1(T) = 1 + \frac{1}{2}\sum_{\mathbf{k}\neq 0}\left(z(A_\mathbf{k})^{-1} + z(-A_\mathbf{k})^{-1}\right). \tag{2.54}$$

Beside the presented above modification of single-particle partition function, the recursion relation in Eq. (2.51) remains unchanged. Therefore, one can compare the condensate statistics obtained from the multinomial expansion and by means of recursion relation in both cases of the ideal and weakly interacting gas. The perfect match can be observed by numerical simulations. The resulting temperature scaled first four central moments of the ground state occupation fluctuations for an ideal

gas in a box, calculated from the Eqs. (2.50) and (2.48) for $N = 100$ using the multinomial expansion formalism in Eq. (2.47) and exact recursion relation for both cases of the ideal and weakly interacting gas in Eq. (2.51) are presented in figures on pages 55-58.

F. Mesoscopic effects versus the thermodynamic limit

In this section, I summarize the results obtained in the previous section for the mesoscopic condensate statistics and compare it to the thermodynamic limit statistics, obtained in [21] for both ideal and weakly interacting Bose gas in a box. The first four central moments of the distribution function in the mesoscopic system can be found by plugging in the distribution function (2.47) into the expressions for the initial moments (2.50) and for the central moments (2.48). The expressions for the first four central moments in the thermodynamic limit are obtained through the cumulants (2.30) for the case of ideal gas and (2.31) in the case of weakly interacting gas, generating cumulants (2.29), and their connection to the central moments (2.28). For the particular case of an ideal Bose gas in a box it can be written as follows:

$$\tilde{\kappa}_m = (m-1)! \sum_{\mathbf{l}=\{l_x,l_y,l_z\}\neq 0} (e^{\epsilon_1 \mathbf{l}^2/T} - 1)^{-m}; \qquad \kappa_r = \sum_{n=k}^{\infty} \sigma_n^{(k)} \tilde{\kappa}_m, \tag{2.55}$$

where the energy gap parameter ϵ_1 is defined in Eq. (2.37).

$$\bar{n} = \kappa_1, \qquad \left\langle (n-\bar{n})^2 \right\rangle \equiv \mu_2 = \kappa_2, \qquad \left\langle (n-\bar{n})^3 \right\rangle \equiv \mu_3 = \kappa_3,$$

$$\left\langle (n-\bar{n})^4 \right\rangle \equiv \mu_4 = \kappa_4 + 3{\kappa_2}^2. \tag{2.56}$$

If the temperature is much smaller than the energy gap $T << \epsilon_1$, all cumulants and moments become the same, starting with the variance

$$\mu_m \approx \kappa_m \approx \kappa_1 \approx f_1 \propto \left(\frac{T}{T_c}\right)^{3/2} N, \qquad m \geq 2, \tag{2.57}$$

since all $f_m << f_1$ are exponentially small for $m \geq 2$ as follows:

$$\tilde{\kappa}_m \approx f_m \approx 6(m-1)! e^{-m\epsilon_1/T}. \tag{2.58}$$

Thus, the low temperature distribution of the number of noncondensed atoms is Poissonian, and therefore, the condensed atoms are distributed as a "mirror" image (non-Poissonian) as $n_0 = N - n$. This result agrees with the previous calculations [21] for the low temperature behavior in the thermodynamic limit. It can be simply performed, expanding formula (2.47) at low temperature. This consistency is not surprising, since in the low temperature region, the finite number of particles does not play an important role in the evaluation. High temperature asymptotics differ much from the previous calculations. It can be seen from the expressions in Eq. (2.30) for the cumulants, that all the moments are anomalously large and the lowest-energy-modes dominate, i.e., formally infrared divergent. One can expand $\exp(\epsilon_1 \mathbf{l}^2/T) - 1 \approx \epsilon_1 \mathbf{l}^2/T$, so that

$$\kappa_m \approx \tilde{\kappa}_m \propto T^m \propto N^{2m/3}, \qquad m \geq 2. \tag{2.59}$$

In this case even the variance should be calculated from the Eq. (2.30) as a discrete sum:

$$\mu_2 = \kappa_2 N^{4/3} \left(\frac{T}{T_c}\right)^2 \frac{s_4}{\pi^2 [\zeta(3/2)]^{4/3}}, \tag{2.60}$$

where ζ is the zeta function of Riemann,

$$s_4 = \sum_{\mathbf{l} \neq \mathbf{0}} \frac{1}{\mathbf{l}^4}, \tag{2.61}$$

and T_c is the standard critical temperature in the thermodynamic limit, which was defined in Eq. (2.38). It is worth noting that an excess coefficient, i.e. the fourth cumulant normalized by the variance to the second power,

$$\gamma_2 \equiv \frac{\kappa_4}{\kappa_2^2} \rightarrow const \neq 0, \tag{2.62}$$

remains finite in the thermodynamic limit $N \rightarrow \infty$. Therefore, it is clear that the condensate fluctuations are not Gaussian in the thermodynamic limit.

The multinomial approach corrects the high temperature dependence of the cumulants. The resulting expression exhibits a decay at high temperatures that is consistent with the grand canonical result for an ideal gas, a result, which is physically reasonable, since at high temperature the condensate fraction is almost zero and the gas behaves like classical ideal gas. In this case both ideal and weakly interacting gas give the same answer, since at high temperature, where the condensate fraction is small, Bogoliubov spectrum becomes essentially free particle spectrum (see Eq. (2.10)):

$$\kappa_m \approx \tilde{\kappa}_m \propto (T/T_c)^{-3/2}. \tag{2.63}$$

The grand-canonical approach gives, for instance, the mean ground state occupation number $\bar{n}_0$ satisfying the self-consistent equation:

$$N - \bar{n}_0 = \sum_{\mathbf{k}\neq 0} \frac{1}{\left(1 + \frac{1}{\bar{n}_0}\right) e^{\epsilon_{\mathbf{k}}/T} - 1}. \tag{2.64}$$

In the case when $T >> T_c$ the condensate fraction is small $\bar{n}_0 << 1$, and therefore one can expand the right hand side of Eq. (2.64). Combining the terms with $\bar{n}_0$, one can obtain the following result:

$$\bar{n}_0 \approx \frac{N}{1 + \sum_{\mathbf{k}\neq 0} e^{\epsilon_{\mathbf{k}}/T}}. \tag{2.65}$$

The summation in the denominator can be performed in the continuum limit, neglecting the excluded point of zero energy, since we are considering an ideal gas model that yields:

$$\bar{n}_0 \approx \zeta\left(\frac{3}{2}\right)\left(\frac{T}{T_c}\right)^{-3/2}, \tag{2.66}$$

which confirms the analytical asymptotics of the formula (2.63) at high enough temperatures.

There are essential differences between the weakly interacting and ideal gases. First, the energy gap is increased by the interaction, that is

$$\tilde{\epsilon}_1 = \sqrt{\epsilon_1^2 + 2\epsilon_1 \bar{n}_0(T)U_0/V} > \epsilon_1 = \left(\frac{2\pi\hbar}{L}\right)^2 \frac{1}{2m}, \tag{2.67}$$

so that the border T $\tilde{\epsilon}_1$ between the moderate temperature and very low temperature regimes is shifted to higher temperatures. Another important effect of the weak interaction is a suppression of all condensate-fluctuation cumulants by a factor of 1/2, compared with the ideal gas (see Eq. (2.31)), for the moderate temperatures $\tilde{\epsilon}_1 << T < T_c$ when a strong coupling ($A_{\mathbf{k}} \approx -1$) contribution dominates in Eq. (2.31). The factor 1/2 comes from the fact that, according to Eq. (2.21),

$$z(A_{\mathbf{k}} = -1) = 1, \quad z(-A_{\mathbf{k}} = 1) = -1 \tag{2.68}$$

so that the first term in Eq. (2.31) is resonantly large but the second term is relatively small. In this case, the effective energy spectrum, which can be introduced for the purpose of comparison with the ideal gas formula in Eq. (2.30),

$$\epsilon_{\mathbf{k}}^{\text{eff}} = T\ln[z(A_{\mathbf{k}})] \approx \frac{1}{2}(1 + A_{\mathbf{k}})\epsilon_{\mathbf{k}} \approx \frac{1}{2}\epsilon_{\mathbf{k}}^2 V/U_0\bar{n}_0 \approx \frac{\mathbf{k}^2}{2m}. \tag{2.69}$$

That is, the occupation of a pair of strongly coupled modes in the weakly interacting gas can be characterized by the same effective energy spectrum as that of a free atom.

This remarkable property explains why the ground-state occupation fluctuations in the interacting gas in this case are anomalously large to the same extent as in the noninteracting gas except factor of 1/2 suppression in the cumulants of all orders. These facts were considered in [36] to be an accidental coincidence. We see now that, roughly speaking, this is so because the atoms are coupled in strongly correlated pairs such that the number of independent stochastic occupation variables ("degrees of freedom") contributing to the fluctuations of the total number of excited atoms is only 1/2 the atom number N.

As follows from Eq. (2.31), the interaction essentially modifies condensate fluctuations also at very low temperatures, $T << \tilde{\epsilon}_1$ (see Figs. 4-7). Namely, in the Bogoliubov Bose gas a temperature-independent quantum noise, $\tilde{\kappa}_m \to \tilde{\kappa}_m(T=0) \neq 0$, $m \geq 2$, additional to the ideal Bose gas (IBG) noise, $\tilde{\kappa}_m^{\mathrm{IBG}}(T \to 0)$, $m \geq 0$ appears due to quantum fluctuations of the excited atoms that are forced by the interaction to occupy the excited levels even at $T = 0$, so that $\bar{n}_{\mathbf{k}}(T=0) \neq 0$.

The effect of suppression of the condensate fluctuations at low temperatures ($T << T_c$) can be deduced from the asymptotic expansion of the properly normalized first four cumulants of the ground state occupation statistics via the solution of the non-linear self-consistency equation for the mean ground state occupation number. These asymptotics are close to that, obtained from the cumulant analysis in [21] similar to the formulas for an ideal gas in Eq. (2.30). The expressions presented below were obtained in the framework of the multinomial expansion (see Chapter II, Section E), taking into account modifications originated from the effect of weak interaction via the Bogoliubov spectrum and squeezed states and the first order exponential corrections in the temperature dependences. Thus, using explicitly the particle conserving formalism I found the following formulas for the mean value $\bar{n}_0$ and all the generating cumulants $\tilde{\kappa}_m$:

$$\bar{n}_0 = N - (a_0 + a_1 e^{-\epsilon_1/T}) \tag{2.70}$$

$$\tilde{\kappa}_m = b_{0_m} + b_{1_m} e^{-\epsilon_1/T}, \tag{2.71}$$

where

$$a_0 = \sum_{\mathbf{k}\neq 0} \frac{A_{\mathbf{k}}}{1 - A_{\mathbf{k}}^2},$$

$$a_1 = (1 - A_1^2)^{-1} \left[1 + A_1^2 + 2\frac{a_0}{N} A_1 (A_1^2 + 2) \sum_{\mathbf{k}\neq 0} \left(1 - \frac{\mathbf{k}^2}{\sqrt{\mathbf{k}^4 + 2\alpha\mathbf{k}^2}} - A_{\mathbf{k}} \right) \right], \tag{2.72}$$

$$b_{0_m} = \frac{1}{2}(m-1)! \sum_{\mathbf{k}\neq 0} \left[\left(-1 - \frac{1}{A_{\mathbf{k}}} \right)^{-m} + \left(-1 + \frac{1}{A_{\mathbf{k}}} \right)^{-m} \right] +$$

$$+ \frac{1}{2} m! \sum_{\mathbf{k}\neq 0} \left[\left(1 - \frac{1}{A_{\mathbf{k}}} \right) \left(-1 - \frac{1}{A_{\mathbf{k}}} \right)^{-m} - \left(1 + \frac{1}{A_{\mathbf{k}}} \right) \left(-1 + \frac{1}{A_{\mathbf{k}}} \right)^{-m} \right] +$$

$$+ a_0 \sum_{\mathbf{k}\neq 0} \left(1 - \frac{\mathbf{k}^2}{\sqrt{\mathbf{k}^4 + 2\alpha\mathbf{k}^2}} + A_{\mathbf{k}} \right) \sum_{\mathbf{k}\neq 0} b_{2_m}(\mathbf{k}), \tag{2.73}$$

$$b_{1_m} = 2 b_{2_m}(1) a_0 - a_1 \sum_{\mathbf{k}\neq 0} \left(1 - \frac{\mathbf{k}^2}{\sqrt{\mathbf{k}^4 + 2\alpha\mathbf{k}^2}} + A_{\mathbf{k}} \right) \sum_{\mathbf{k}\neq 0} b_{2_m}(\mathbf{k}), \tag{2.74}$$

$$b_{2_m}(\mathbf{k}) = \frac{1}{2A_{\mathbf{k}}^2} m! \left[\left(-1 - \frac{1}{A_{\mathbf{k}}} \right)^{-m-1} + \left(-1 + \frac{1}{A_{\mathbf{k}}} \right)^{-m-1} \right], \tag{2.75}$$

where $A_{\mathbf{k}}$ in Eqs. (2.72)-(2.75) is a solution of self-consistent equation $A_{\mathbf{k}} \approx A_{\mathbf{k}}(\bar{n}_0 = N) = (\sqrt{\mathbf{k}^4 + 2\alpha\mathbf{k}^2} - \mathbf{k}^2)/\alpha - 1$, $\alpha = U_0 N/(\epsilon_1 L^3)$, $U_0 = 4\pi\hbar^2 a/m$ is an interaction strength, proportional to the s-wave scattering length a. The results in Eqs. (2.70) and (2.71) are valid when $T << \epsilon_1$.

The above described temperature scaling of the condensate fluctuations (cumulants) is depicted in Figs. 4-7 both for the weakly interacting and ideal gases. One can also obtain the crossover between fluctuations in an ideal and weakly interacting Bose gases. This crossover is observed at moderate-high temperatures where the grand-canonical approximation is not yet applicable. The relations written below are

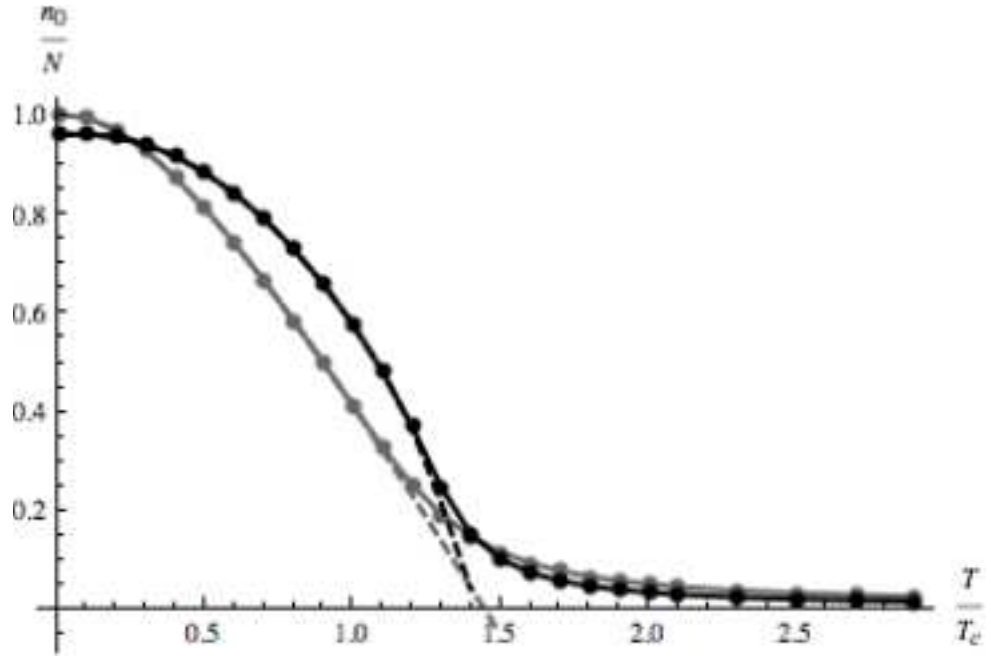

Fig. 4. Temperature scaling of the mean value of the ground state occupation fluctuations for an ideal Bose gas (grey lines) and weakly interacting Bose gas (black lines) for $N = 100$ obtained from thermodynamic limit expression in Eqs. (2.30) - (2.31) (dashed lines) compared with the multinomial expansion in Eq. (2.47) (dots) and with the exact recursion relation for an ideal gas in Eq. (2.51) (solid lines). The multinomial expansion result is almost indistinguishable from the recursion relation as it is clearly seen in graphs.

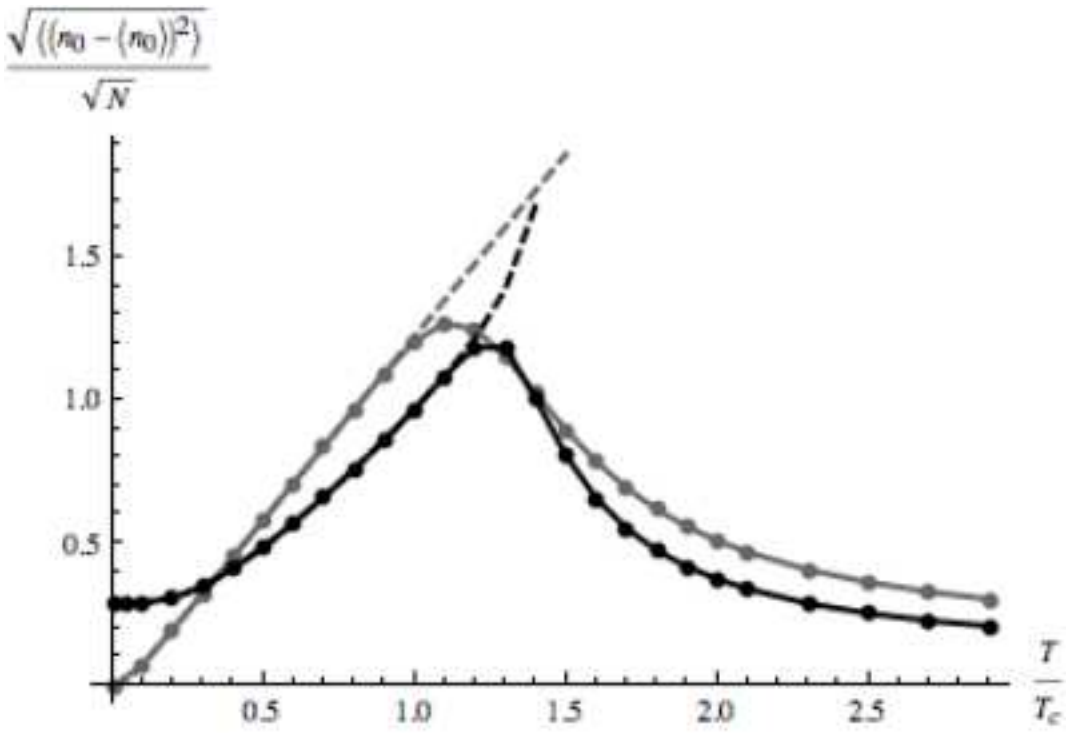

Fig. 5. Temperature scaling of the variance of the ground state occupation fluctuations for an ideal Bose gas (grey lines) and weakly interacting Bose gas (black lines) for $N = 100$ according to Eqs. (2.30) - (2.31) (dashed lines), Eq. (2.47) (dots), and Eq. (2.51) (solid lines).

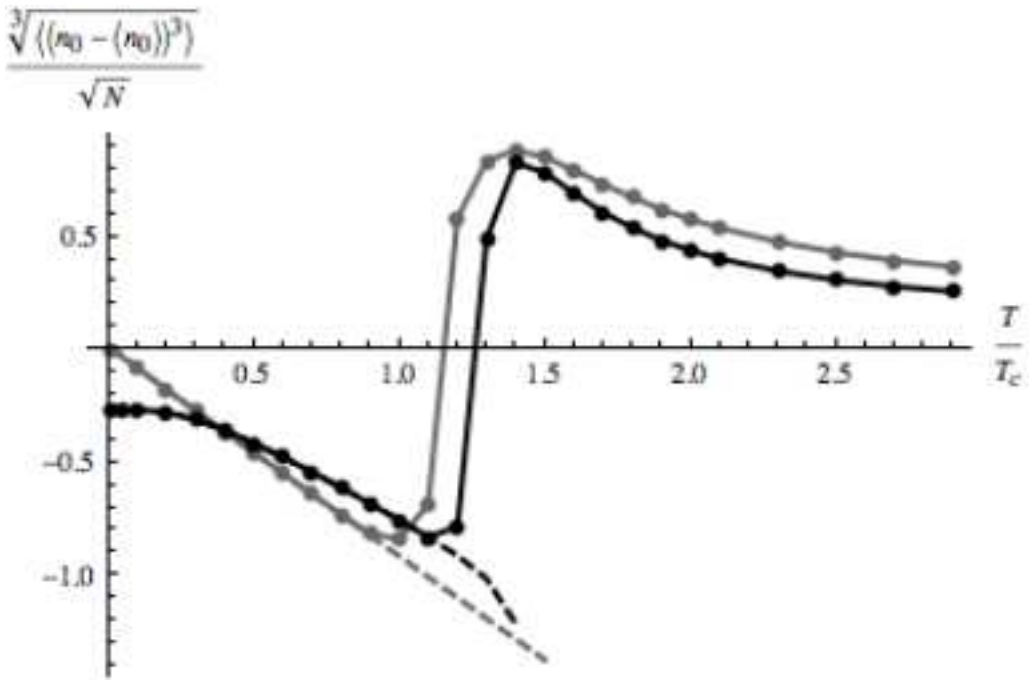

Fig. 6. Temperature scaling of the third central moment μ_3 of the ground state occupation fluctuations for an ideal Bose gas (grey lines) and weakly interacting Bose gas (black lines) for $N = 100$ according to Eqs. (2.30) - (2.31) (dashed lines), Eq. (2.47) (dots), and Eq. (2.51) (solid lines).

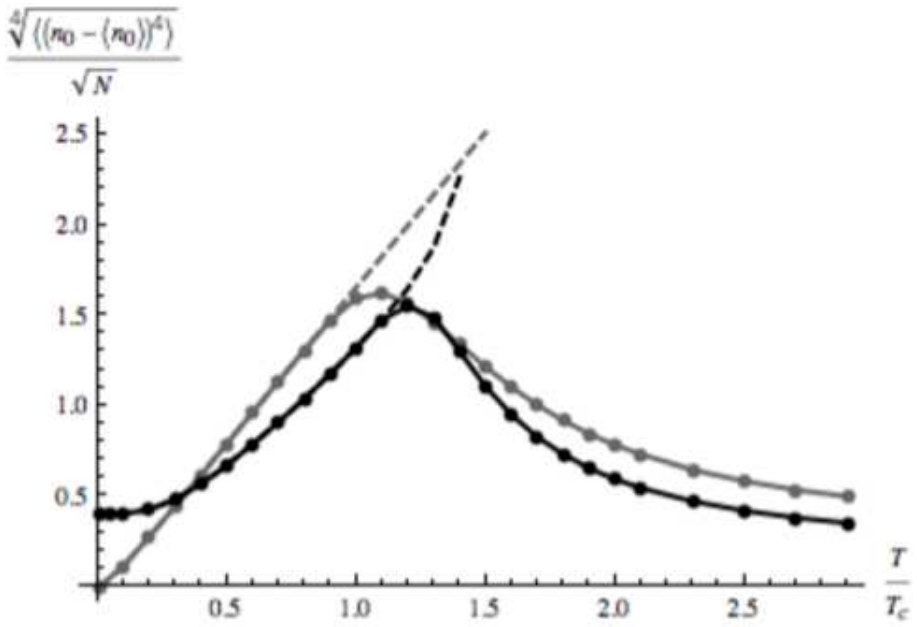

Fig. 7. Temperature scaling of the fourth central moment μ_4 of the ground state occupation fluctuations for an ideal Bose gas (grey lines) and weakly interacting Bose gas (black lines) for $N = 100$ according to Eqs. (2.30) - (2.31) (dashed lines), Eq. (2.47) (dots), and Eq. (2.51) (solid lines).

connecting the asymptotical behavior of the condensate statistics in weakly interacting gas at moderate temperatures in terms of the statistics of the BEC fluctuations of the ideal gas. I present these formulas in term of relations between the condensate fluctuations in the weakly interacting Bose gas (left-hand-side with "int" subscript) to the condensate fluctuations in an ideal Bose gas (right-hand-side, without subscripts). The solution of the nonlinear self-consistency equation for the mean ground state occupation number is:

$$\langle n_{0_{int}} \rangle = \frac{\langle n_0 \rangle}{1 - \xi \left(\frac{\langle n^2 \rangle - \langle n \rangle \langle n_T \rangle}{N} + \langle n_T \rangle - \langle n \rangle \right)}. \tag{2.76}$$

The initial (noncentered) moments of the number of the noncondensed atoms are:

$$\langle n_{int}^p \rangle = \frac{1 - \xi \left(\frac{\langle n^2 \rangle}{N} - \langle n \rangle + \frac{\langle n^{p+1} \rangle}{\langle n^p \rangle} \langle \frac{n_0}{N} \rangle \right)}{1 - \xi \frac{\langle (n - \langle n \rangle)^2 \rangle}{N}} \langle n^p \rangle, \tag{2.77}$$

where $\langle n_T \rangle = \sum_{\mathbf{k} \neq 0} \left(\exp(\epsilon_{\mathbf{k}}/T) - 1 \right)^{-1}$ is the usual Bose-Einstein occupation number and $\xi = \epsilon_1 \alpha / T$. It is easy to check that in the limiting case of vanishing interaction strength the fluctuations become the same as they were in an ideal gas. The condition of an applicability of the presented above high temperature asymptotical expansions is

$$\frac{T}{T_c} >> 2 \frac{a}{L} (\zeta(3/2))^{2/3} N^{1/3} \bar{n}_0, \tag{2.78}$$

where I explicitly used the expression for the interaction strength in term of the s-wave scattering length, $U_0 = 4\pi\hbar^2 a/m$. Depending on the interaction strength one can analyze the asymptotical behavior of the fluctuations at temperatures of the order of T_c. This condition is satisfied for a wide range of parameters in real experiments [12–14] and thus can be used to illuminate the crossover between the fluctuations in the ideal and weakly interacting Bose gases. I would like to emphasize that the above crossover relations, i.e. the high temperature asymptotics, were derived using

the particle-number constraint, the canonical ensemble quasiparticle formalism, and the multinomial expansion.

Concluding the whole chapter, I briefly emphasize its main points. First, I constructed the set of canonical ensemble quasiparticles (GA operators), which take into account the particle number constraint. Using the outlined method I analyzed the structure of the characteristic function of the total number of noncondensed atoms in both ideal and weakly interacting Bose gas. The latter case was analyzed in the framework of Bogoliubov dressed quasiparticles. Then I introduced the new properly normalized distribution function, which correctly describes the behavior of the ground-state fluctuations in any temperature regime, which was constructed from the simple physical reasons. I obtained the numerical dependences for the fluctuations for the mesoscopic system of an ideal and weakly interacting Bose gas in a box with periodic boundary conditions as the functions of temperature. All the listed calculations are valid for the whole temperature range from zero to infinity. I considered the asymptotic expressions for the fluctuations for both low and high temperatures and compared them with the well know grand canonical formalism for high temperatures, where both ideal and weakly interacting gas give the same answer. For the low temperature the dressed condensate fluctuations for the interacting gas are depleted compare the bare fluctuations in the ideal gas. For the moderate temperatures I found a crossover relations between fluctuations of weakly interacting gas and ideal gas.

In the next chapter I will discuss another approach in analyzing these fluctuations, in the vicinity of the critical temperature.

CHAPTER III

UNIVERSAL SCALING AND ORIGIN OF NON-GAUSSIAN BOSE-EINSTEIN CONDENSATE STATISTICS IN A MESOSCOPIC IDEAL GAS

A. Constraint-cut-off mechanism of strong non-Gaussian BEC fluctuations. Universal structure and cut-off of the condensate occupation probability distribution

The best way to analyze BEC statistics in the mesoscopic systems is to study the central moments and cumulants of the noncondensate occupation as functions of the number of atoms in the trap since these functions are more physically instructive and more directly related to the intrinsic quantum statistics in a finite system than less transparent temperature dependences. The maximum number of the noncondensed atoms $\bar{n}^{(\infty)} = N_c$ is achieved in the limit of an infinite number of atoms loaded in the trap, $N \to \infty$, and is given by a discrete sum [21, 35]

$$N_c = \sum_{\mathbf{k}\neq 0} (e^{\epsilon_{\mathbf{k}}/T} - 1)^{-1}. \tag{3.1}$$

In the standard analysis in the thermodynamic limit this sum is approximated by a continuous integral that yields a little bit larger number:

$$N_v = \zeta(3/2) \left(\frac{mT}{2\pi\hbar^2} \right)^{3/2} V, \tag{3.2}$$

where ζ is the zeta function of Riemann, $\zeta(3/2) \approx 2.612$. Let us note also that a ratio of an energy scale for the box trap to the temperature is determined by precisely the same trap-size parameter N_v, namely, for the energy of the first excited state one has $\epsilon_1/T = \pi[\zeta(3/2)/N_v]^{2/3}$. Hence, the sum in Eq. (3.1) over the energy spectrum of the trap as well as all other similar sums, like the one in Eq. (3.3) below, actually depend only on a single combination of the trap parameters given by Eq. (3.2). Thus, the

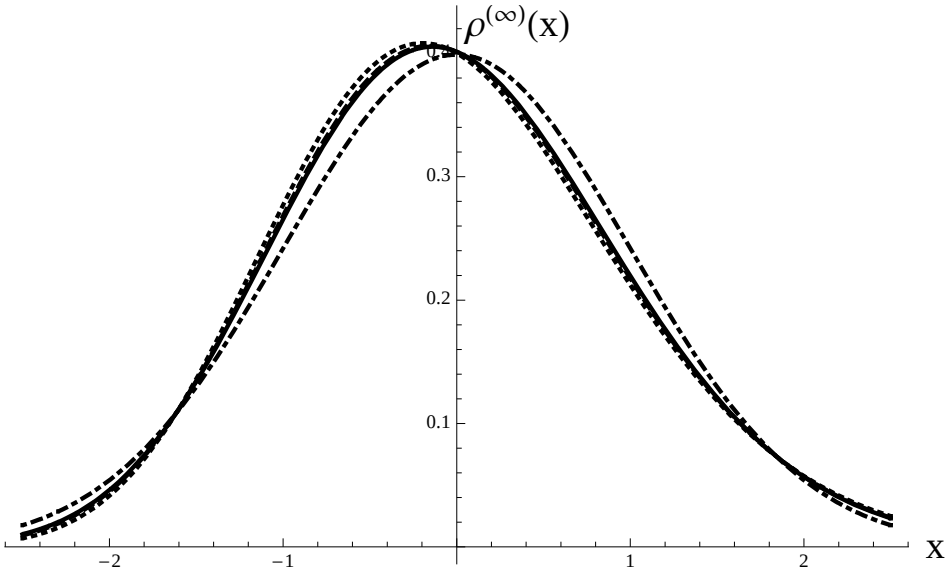

Fig. 8. Scaled unconstrained probability distribution of the stochastic variable $x = n - N_c/\sigma^{(\infty)}$ for the different finite traps: $N_v = 10^2$ (dotted line), $N_v = 10^3$ (dashed line), $N_v = 10^4$ (solid line). The Gaussian distribution $\exp(-x^2/2)/(2\pi)^{1/2}$ is depicted by a dotted-dashed line.

mesoscopic system of the ideal gas atoms in the finite box is completely specified by two parameters, N_v and N. It is convenient to study a development of the BEC phase transition with an increase of the number of atoms N assuming that the volume and the temperature of the mesoscopic system are fixed, that is the trap-size parameter N_v given by Eq. (3.2) is fixed. The critical number of the loaded in the trap atoms is equal to the close to N_v number N_c given by Eq. (3.1). Thus, when we change the number of atoms from $N < N_c$ to $N > N_c$ the system undergoes the same BEC phase transition phenomenon as the one observed when we change the temperature around the critical temperature T_c from $T > T_c$ to $T < T_c$.

Following the approach formulated in the Section C and Fig. 3, we find that

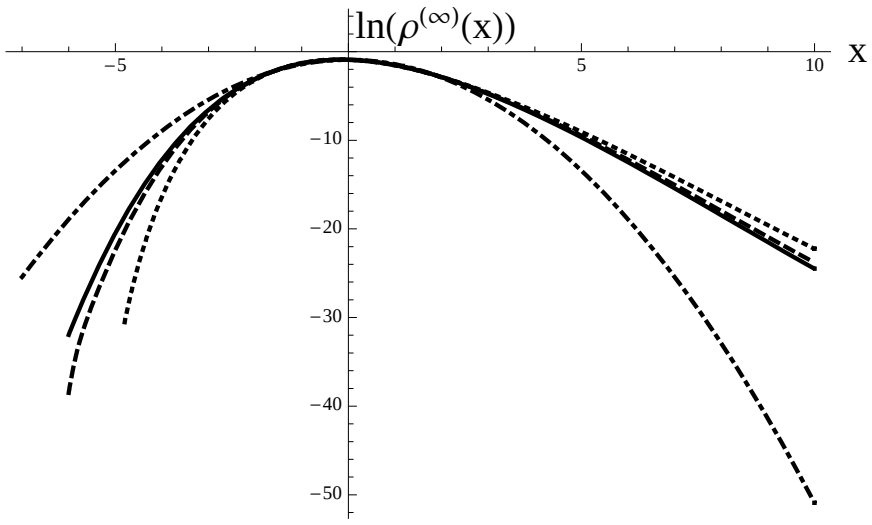

Fig. 9. Logarithm of the scaled unconstrained probability distribution of the stochastic variable $x = n - N_c/\sigma^{(\infty)}$ for the different finite traps: $N_v = 10^2$ (dotted line), $N_v = 10^3$ (dashed line), $N_v = 10^4$ (solid line). The Gaussian distribution $\exp(-x^2/2)/(2\pi)^{1/2}$ is depicted by a dotted-dashed line.

the analytically calculated in [21, 35] unconstrained probability distributions $\rho_n^{(\infty)}$for different sizes and temperatures of the trap tend, with an increase of the trap-size parameter N_v, to a universal function if they are considered for the scaled stochastic variable $x = (n - N_c)/\sigma^{(\infty)}$ (see Figs. 8 and 9). Here the dispersion of the BEC fluctuations $\sigma^{(\infty)}$ is an independent on the number of atoms N quantity calculated for the unconstrained probability distribution ($N \to \infty$) in [21, 35] as function of the trap-size parameter N_v,

$$\sigma^{(\infty)} \equiv [\kappa_2^{(\infty)}(N_v)]^{1/2} = \left[\sum_{\mathbf{k}\neq 0}(e^{\epsilon_{\mathbf{k}}/T} - 1)^{-2} + N_c\right]^{1/2}. \tag{3.3}$$

In the thermodynamic limit the discrete sum can be approximated as an integral and

$$\sigma^{(\infty)} \approx \frac{s_4^{1/2} N_n^{2/3}}{\pi[\zeta(3/2)]^{2/3}}, \qquad s_4 = \sum_{\mathbf{q}\neq 0}\frac{1}{q^4} \approx 16.53. \tag{3.4}$$

The dispersion of the BEC fluctuations (Eqs. (3.3) and (3.4)) is anomalously large and scales as $\sigma^{(\infty)} \sim N_v^{2/3}$, contrary to a much smaller value $N_v^{1/2}$, which one could naively expect from a standard analysis based on the grand-canonical or thermodynamic fluctuations.

This remarkable universality could be expected in the relatively narrow vicinity of the maximum of the distribution, $|n - N_c| \leq \sigma^{(\infty)}$, where a Gaussian approximation always works well. However, we find that for much wider part of the right tail (at least, up to $n - N_c \sim 8\sigma^{(\infty)}$ for $N_v = 10^3$ and up to $n - N_c \sim 10\sigma^{(\infty)}$ for $N_v = 10^4$) and also for the left tail (of course, except of the close to $n \approx 0$ part, where the system contains only a few atoms and is not a mesoscopic system anymore) the actual mesoscopic probability distribution becomes very close to the universal, thermodynamic-limit probability distribution already starting from very moderate values of the trap-size parameter $N_v \sim 10^2 \div 10^3$. This result is clearly shown in Fig. 8 as well as in Fig. 9,

where a logarithmic scale allows us to see the behaviour of the tails in more details. The universal probability distribution has very fat and long right tail of the large occupation fluctuations, $n - N_c >> \sigma^{(\infty)}$, whereas the left tail of small occupation fluctuations, $N_c - n >> \sigma^{(\infty)}$, is strongly suppressed as compared to the Gaussian distribution.

The most crucial point is that the universal probability distribution does not collapse to a kind of δ-function or a pure Gaussian distribution but remains finite, smooth, and nontrivial in the thermodynamic limit, so that an intrinsic critical structure of the BEC phase transition clearly reveals itself in the already quite small mesoscopic systems with the critical number of atoms $N_c \sim 10^2$. We find a polynomial approximation for the

$$\ln[\rho^{(\infty)}(x)] = a_0 + a_2(x + \Delta x)^2/2! + a_3(x + \Delta x)^3/3! + a_4(x + \Delta x)^4/4! + ... \,. \quad (3.5)$$

It contains very essential third ($a_3 \approx 0.3$) and forth ($a_4 \approx -0.06$) order terms which provide the same or larger contributions at the tails as compared to that of the Gaussian, quadratic part having a coefficient $a_2 \approx 1$. There is also a small shift $\Delta x \approx 0.13$ of the maximum of the probability distribution to the left of the mean value due to the discussed above asymmetric tails.

All numerical graphs presented in this paper were obtained by direct calculation of the characteristic function in Eq. (2.33) for the mesoscopic ideal gas using the analytical formulas [21, 35] and then the probability distribution in Eq. (2.33) by means of a Fast Fourier Transform technique (FFT):

$$\rho(n) = \frac{1}{2\pi}\int_{-\pi}^{\pi} e^{-inu}\Theta_n(u)\,du \equiv \frac{1}{m}\sum_{r=1}^{m}\left(e^{-2\pi isr/m}\Theta_n\left(\frac{r}{m}\right)e^{-2\pi i(r-1)(n-1)/m}\right). \quad (3.6)$$

It easily allows us to calculate the BEC statistics in the mesoscopic systems with the critical number of atoms $N_c < 10^5$ using a standard PC.

Let us apply now the remarkable universality and general constraint-cut-off approach to the analysis of various effects of BEC in the mesoscopic systems with a finite number of atoms in the trap in the critical region as well as below and above the critical region. To this end, we have to introduce a finite number of atoms $N \sim N_c$, $N < N_c$, and $N > N_c$, respectively, and to perform a cut off of the probability distribution $\rho_n^{(\infty)}$ dictated by the particle-number constraint as was formulated in the Section C. An immediate result is that the actual, cut off probability distribution (OAN or $OA'N'$ in Fig. 3) is strongly asymmetric and peculiar for all $N < N_c$ and $N \sim N_c$, including the critical region. We find that the outlined constraint-cut-off mechanism is responsible for all unusual critical phenomena of the BEC phase transition in the ideal gas and, in particular, makes the BEC statistics strongly non-Gaussian. In the deep condensate region, $n - N_c >> \sigma^{(\infty)}$, the non-Gaussian behaviour is less pronounced but remains finite even in the thermodynamic limit due to the discussed above non-Gaussian asymmetric tails found in [21, 35].

B. Universal scaling and structure of the BEC order parameter

In accord with the constraint-cut-off mechanism, depicted in Fig. 3, the mean non-condensate occupation $\bar{n}$ almost linearly follows the cut-off value N of the number of loaded in the trap atoms until the value of $\bar{n}$ saturates at the critical level N_c, when N passes through the critical value N_c by an amount about $2\sigma^{(\infty)}$ (Fig. 10). The complimentary, mean condensate occupation, i.e. the BEC order parameter, has a similar, but upside-down pattern that, with an increase of trap-size parameter N_v, becomes a degenerate straight-line angle OCB, which represents the BEC behaviour before and after the phase transition as it is approximated by the standard Landau mean-field theory in the thermodynamic limit. A universal structure of the BEC

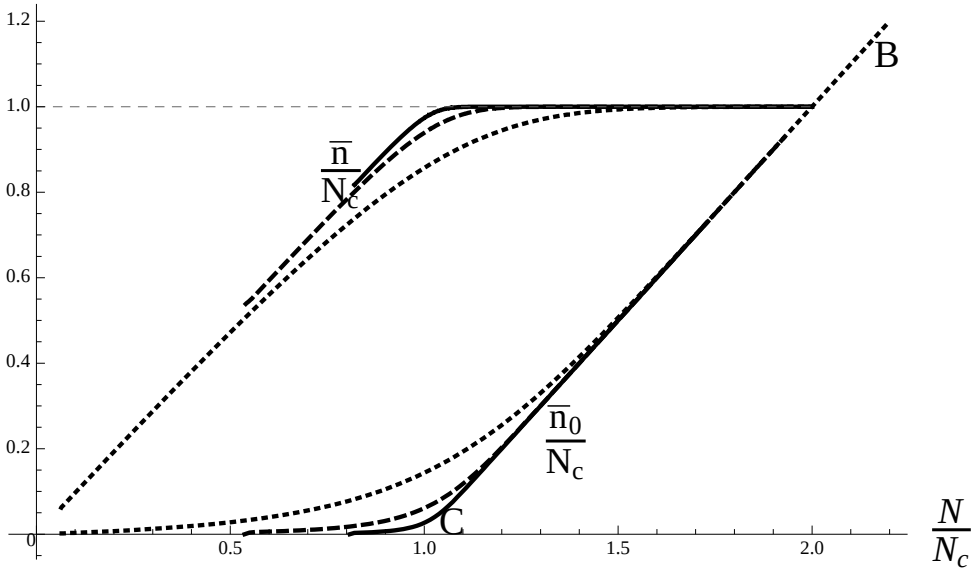

Fig. 10. The mean occupations of the noncondensate, $\bar{n}/N_c$, and the condensate, $\bar{n}_0/N_c$, as functions of the number of atoms, N/N_c, loaded in the trap; all quantities are normalized by the critical number of atoms N_c from Eq. (3.1): $N_v = 10^2$ - dotted line, $N_v = 10^3$ - dashed line, $N_v = 10^4$ - solid line.

phase transition is missing.

To unveil and resolve the universal scaling and structure of the BEC order parameter near a critical point we divide both the function and the argument by the dispersion of the BEC fluctuations $\sigma^{(\infty)}$ and calculate a scaled condensate occupation $\bar{n}_0' = \bar{n}_0/\sigma^{(\infty)}$ as function of a scaled deviation from the critical point $\eta = (N - N_c)/\sigma^{(\infty)}$. We find that with an increase of the trap-size parameter N_v the function $\bar{n}_0'(\eta)$ quickly merges some universal smooth function $F_0(\eta)$ which describes the universal structure of the BEC order parameter in the critical region in the thermodynamic limit $N_v \to \infty$, as is shown in Fig. 11. It is very different from the prediction of the Landau mean-field theory (broken line ABC in Fig. 11). We can

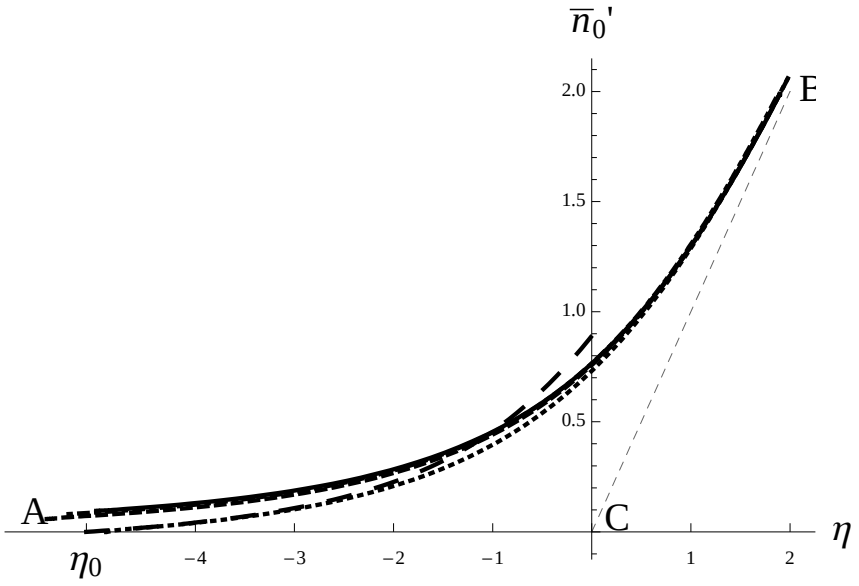

Fig. 11. Universal structure of the scaled order parameter $\bar{n}_0'(\eta) = \bar{n}_0/\sigma^{(\infty)}$ as function of $\eta = (N - N_c)/\sigma^{(\infty)}$ in the critical region: the dashed-dotted line is an analytical approximation of the universal function $F_0(\eta)$ in Eq. (3.7), the solid line is the function $\bar{n}_0'(\eta)$ for the mesoscopic system with the trap-size parameter $N_v = 10^4$, the dashed line for $N_v = 10^3$, the dotted line for $N_v = 10^2$. The long-dashed line represents the result within the grand-canonical-ensemble approximation in Eq. (3.10) for $N_v = 10^2$. The angle ACB represents the prediction of the standard Landau mean-field theory.

immediately conclude that even for the small mesoscopic systems with $N_v \sim 10^2$ the difference between the universal order-parameter and the mesoscopic order-parameter functions is relatively small, $|F_0(\eta)\sigma^{(\infty)} - \bar{n}_0'(\eta)| << \bar{n}_0'(\eta)$. This statement is true everywhere except of the very beginning of the curve $\bar{n}_0'(\eta)$, where the system is not mesoscopic anymore, there are only a few atoms in the trap $N \leq 10$, and, obviously, the number of atoms in the condensate should become exactly zero, $\bar{n}_0 = 0$, at the point $\eta_0(N_v) = -N_c/\sigma^{(\infty)} \approx N_v^{1/3}$ where there are no atoms in the trap, $N = 0$, as is seen in Fig. 11 at $\eta_0 = -5.1$ for $N_v = 10^2$. We find that the universal dependence, presented in Fig. 11, can be approximated in the whole critical region $|\eta| \leq 6$ with the accuracy $\sim 1\%$ by means of the elementary functions if we consider an inverse function $\eta = g_0(y)$, where $y = \bar{n}_0/(2^{1/2}\sigma^{(\infty)})$ is a scaled condensate occupation. Namely, we have

$$\eta = g_0(y) \approx 2^{1/2}\left(1 - \frac{e^{-5y/3}}{y^{3/2}}\right) y. \tag{3.7}$$

A tiny difference between the universal and actual order-parameter curves for the finite mesoscopic system with the trap-size parameter $N_v = 10^4$ even cannot be seen in Fig. 11.

The same universal order parameter structure can be analyzed also as a somewhat inverse dependence of the ratio $(N - N_c)/\bar{n}_0$ on the scaled condensate occupation $y = \bar{n}_0/(2^{1/2}\sigma^{(\infty)})$. It is depicted in Fig. 12 for the different values of the trap-size parameter $N_v = 10^2,\ 10^3,\ 10^4$. The analytical approximation in Eq. (3.7) yields a function

$$(N - N_c)/\bar{n}_0 \approx 1 - e^{-5y/3}/y^{3/2}, \tag{3.8}$$

which is very close to the mesoscopic order-parameter curve for all values $N_v = 10^2,\ 10^3,\ 10^4$. Their difference is enlarged in the insert in Fig. 12. At the critical point, where the number of atoms in the trap is $N = N_c$, we find $y \approx 0.52$, that

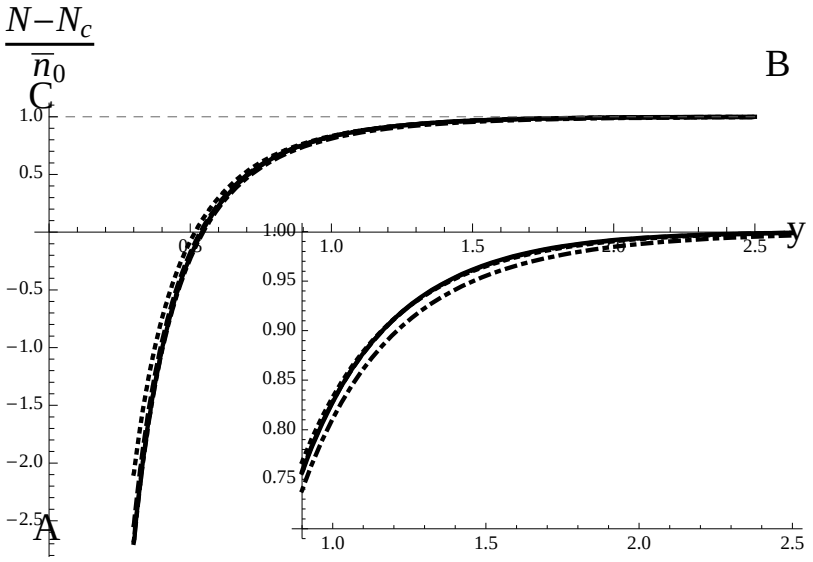

Fig. 12. Universal dependence of the ratio $(N - N_c)/\bar{n}_0$ on the scaled order parameter $y = \bar{n}_0/(2^{1/2}\sigma^{(\infty)}$ in the critical region: the dashed-dotted line is an analytical approximation of the universal function in Eq. (3.8), the solid line is the function $\eta/\bar{n}_0'(\eta)$ for the mesoscopic system with the trap-size parameter $N_v = 10^4$, the dashed line for $N_v = 10^3$, the dotted line for $N_v = 10^2$. The angle ACB represents the prediction of the standard Landau mean-field theory. Insert: A closer look at the same dependences in the region of a fully developed condensate.

is $\bar{n}_0 \approx \sigma^{(\infty)}$). The standard Landau mean-field theory does not resolve the smooth universal structure in Fig. 12 at all and predicts $(N - N_c)/\bar{n}_0$ in the form of a degenerate right angle ACB.

C. Universal scaling and sructure of all higher-order moments and cumulants of the BEC fluctuations

As a direct consequence of the universality of the noncondensate occupation probability distribution formulated in the Section A, we find that all higher-order moments and cumulants of the BEC fluctuations also have the universal scaling and smooth nontrivial structure. The analysis is similar to the one developed in the Section B for the order parameter and is based on the calculation of the scaled central moments $\mu'_m = \mu_m/(\sigma^{(\infty)})^m$ and scaled cumulants $\kappa'_m = \kappa_m/(\sigma^{(\infty)})^m$ as functions of the scaled deviation from the critical point, $\eta = (N - N_c)/\sigma^{(\infty)}$. We find that with an increase of the trap-size parameter N_v the functions $\mu'_m(\eta)$ and $\kappa'_m(\eta)$ quickly merge some universal functions $M_m(\eta)$ and $C_m(\eta)$, respectively, which describe the universal structure of the BEC critical fluctuations in the thermodynamic limit $N_v \to \infty$, as is shown in Fig. 13 for the second, third, and forth moments and cumulants of the noncondensate occupation. In Fig. 13, the thermodynamic-limit universal functions $M_m(\eta)$ and $C_m(\eta)$ practically coincide with the corresponding functions for the mesoscopic system with the trap-size parameter $N_v = 10^4$. The universal behaviour is clearly observed starting from very small mesoscopic systems with a typical number of atoms $Nv \sim 10 \div 100$.

An essential deviation from the universal curves takes place only at the very beginning of each curve at $\eta = \eta_0(N_v) = -N_c/\sigma^{(\infty)}$, where the number of atoms in the trap is zero and, hence, all fluctuations $\mu'_m(\eta)$ and $\kappa'_m(\eta)$ should be exactly zero,

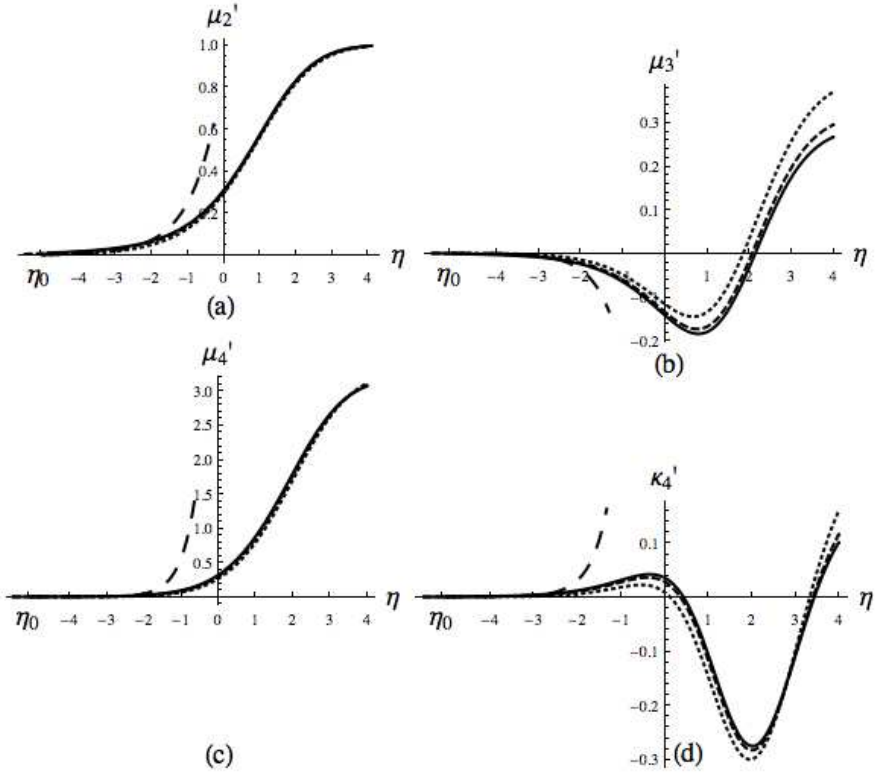

Fig. 13. Universal structures of the scaled central moments and cumulants (a) $\mu_2' \equiv \kappa_2' = \mu_2/(\sigma^{(\infty)})^2$, (b) $\mu_3' \equiv \kappa_3' = \mu_3/(\sigma^{(\infty)})^3$, (c) $\mu_4' = \mu_4/(\sigma^{(\infty)})^4$, and (d) $\kappa_4' = \mu_4' - 3(\mu_2')^2$ of the total noncondensate occupation in the critical region calculated as functions of $\eta = (N - N_c)/\sigma^{(\infty)}$ for the mesoscopic system with the trap-size parameter $N_v = 10^2$ (dotted line), $N_v = 10^3$ (dashed line), $N_v = 10^4$ (solid line). The long-dashed line represents the result within the grand-canonical-ensemble approximation in Eq. (3.10) for $N_v = 10^2$.

as is seen in Fig. 13 at $\eta_0 = -5.1$ for $N_v = 10^2$. In this limit the system loses its mesoscopic status and can be studied quantum mechanically as a microscopic system of a few atoms $N = 1,\ 2,\ 3,\ \ldots$.

Qualitatively, behaviour of the moments and cumulants, depicted in Fig. 13, can be immediately predicted on the basis of the constrain-cut-off mechanism using Fig. 3. The variance $\mu_2 = \kappa_2$ has to grow monotonically with increasing N and to have a maximum derivative at $N \approx N_c$ because the width of the cut-off probability distribution OAN increases when the cut-off boundary AN moves to the right and the maximum widths derivative is achieved at the center of the critical region. That behaviour, indeed, is found in our numerical simulations depicted in Fig. 13a.

The third central moment, or the third cumulant, $\mu_3 = \kappa_3 = \langle (n - \bar{n})^3 \rangle$, is the main characteristic of an asymmetry of the probability distribution relative to the mean value $\bar{n}$. For small enough numbers of atoms in the trap N, when the probability distribution has a strongly asymmetric, curved-triangle shape $OA'N'$ in Fig. 3, the value of the asymmetry μ_3 is negative due to a large contribution from the left tail and increases in magnitude with increasing N until some maximum-in-magnitude negative value is reached. When the number of atoms N enters the central part of the critical region, the absolute value of the asymmetry μ_3 decreases and after passing through the critical point $N = N_c$ approaches zero, since the shape of the cut-off probability distribution OAN in Fig. 3 becomes more and more symmetric. Finally, the asymmetry coefficient $\mu_3' = \mu_3/(\sigma^{(\infty)})^3$ changes the sign and tends to a finite positive value $\mu_3'^{(\infty)} = 0.41,\ 0.32,\ 0.29$ for the values of $N_v = 10^2,\ 10^3,\ 10^4$, respectively, that is a characteristic feature of the unconstrained probability distribution $\rho_n^{(\infty)}$ due to a large positive contribution of the fat and wide right tail, discussed in the Section A and Figs. 8 and 9 . The predicted behavior of the asymmetry $\mu_3 = \kappa_3$ is precisely revealed in the simulations presented in Fig. 13b.

In a similar way, one can explain the depicted in Figs. 13c and 13d behaviour of the fourth moment μ_4 and the fourth cumulant, the excess κ_4. The latter, in general, characterizes a positive excess (if $\kappa_4 > 0$) or a negative excess (if $\kappa_4 < 0$) of the flatness of the "plateau" of the probability distribution relative to the flatness of the plateau of the Gaussian distribution. Again, one has to take into account that the unconstrained probability distribution $\rho_n^{(\infty)}$, according to Figs. 8 and 9, is more flat than the Gaussian distribution, that is it has a positive excess coefficient $\kappa_4'^{(\infty)} \approx 0.29,\ 0.22$, and 0.19 for the values of $N_v = 10^2,\ 10^3$, and 10^4, respectively.

The limit of the small number of atoms N, namely, $N_v - N >> \sigma^{(\infty)}$, corresponds to a high-temperature regime of a classical gas without condensate and is well studied in the grand-canonical-ensemble approximation [5, 20, 22, 32–34]. In that approximation the occupations of all states, both in the condensate, n_0, and in the noncondensate, $n_{\mathbf{k}}$, are treated as the independent stochastic variables with the probability distributions

$$\rho_{n_{\mathbf{k}}} = \exp[-(\epsilon_{\mathbf{k}} - \mu)/T]/\{1 - \exp[-(\epsilon_{\mathbf{k}} - \mu)/T]\}, \tag{3.9}$$

and the particle-number constraint is satisfied only on average, $N = \bar{n}_0 + \sum_{\mathbf{k}\neq 0} \bar{n}_{\mathbf{k}}$. This is achieved by introducing an extra term in the Hamiltonian $H = \sum_{\mathbf{k}=0}^{\infty}(\epsilon_{\mathbf{k}} - \mu)\hat{n}_{\mathbf{k}}$ and by choosing the chemical potential μ as a solution of the mean particle-number constraint $\sum_{\mathbf{k}=0}^{\infty}(e^{(\epsilon_{\mathbf{k}}-\mu)/T} - 1)^{-1} = N$. The chemical potential is negative, $\mu < 0$, and is directly related to the ground-state ($\epsilon_{\mathbf{k}=0} = 0$) occupation $\bar{n}_0 = (e^{-\mu/T} - 1)^{-1}$. The condensate occupation distribution in Eq. (3.9), $\rho_{n_0} \approx e^{\mu n_0/T}/(1 - e^{\mu/T})$, implies a pure exponential approximation,

$$\rho_n \approx e^{-\mu n/T} e^{\mu N/T}/(1 - e^{\mu/T}), \qquad n \leq N, \qquad N_v - N >> \sigma^{(\infty)} \tag{3.10}$$

for the related to this case cut-off probability distribution ρ_n, represented by the

curve $OA'N'$ in Fig. 3. Although we know from the Section A that the left tail of the unconstrained probability distribution $\rho_n^{(\infty)}$ in Figs. 3, 8-9 is not purely exponential, the grand-canonical-ensemble approximation is reasonable since the main contribution to the condensate statistics comes in this case from a relatively narrow (with a width of the order of a few dispersions) region, adjacent to the left of the point A in Fig. 3. Obviously, the smaller is the interval of the allowed noncondensate occupations $[0,\ N]$, i.e., the smaller is the number of atoms in the trap, the better is the grand-canonical-ensemble approximation in Eq. (3.10). Besides, all calculations, utilizing the pure exponential distribution in Eq. (3.10), are elementary [20, 32]. The result is the explicit asymptotics for the average condensate occupation, $\bar{n}_0$, and all central moments, μ_m, and cumulants, κ_m, of the total noncondensate occupation, which are depicted in Figs. 11 and 13 by the long-dashed lines for the mesoscopic system with the trap-size parameter $N_v = 10^2$. An agreement with the exact numerical simulations for the same values of N_v in the region of application of this approximation, $N_v - N >> \sigma^{(\infty)}$, is very good. However, of course, in the critical region, $|N_v - N| \leq 2\sigma^{(\infty)}$, and for the region of the well-developed BEC, $N_v - N >> 2\sigma^{(\infty)}$, the grand-canonical-ensemble approximation fails.

The other limit, opposite to the high-temperature case, is the limit when the number of atoms is large, $N_v - N >> 2\sigma^{(\infty)}$. It corresponds to a low-temperature regime of the fully developed condensate. In this limit, the cut-off part of the probability distribution in Fig. 3 contains only an unimportant end piece of the right tail. Thus, the mean value as well as all moments and cumulants of the noncondensate occupation should tend to the constants, which are precisely their unconstrained values analytically calculated in [21, 35]. We find that this is indeed true, as is clearly seen from Figs. 10-13.

D. Exactly solvable Gaussian model of BEC statistics in a degenerate interacting gas demonstrating strongly non-Gaussian condensate fluctuations

In the critical region, the universal scaling and structure of the BEC statistics found in the Sections A-C can be qualitatively explained within a pure Gaussian model for the unconstrained probability distribution of the total noncondensate occupation

$$\rho_n^{(\infty)} = \exp\left[-\frac{(n-N_c)^2}{2\sigma^2}\right] \Big/ \sum_{m=0}^{\infty} \exp\left[-\frac{(n-N_c)^2}{2\sigma^2}\right], \qquad n \in [0,\infty). \tag{3.11}$$

It is depicted in Figs. 8 and 9. That model correspond to a degenerate interacting gas of N trapped atoms with a very degenerate interaction between only excited atoms in the noncondensate and a complimentary number of the ground-state ($\epsilon_{\mathbf{k}=0} = 0$), condensed atoms $n_0 = N - n$, described by the Hamiltonian:

$$H = \left(\sum_{\mathbf{k}\neq 0} \hat{n}_{\mathbf{k}} - N_c\right)^2 T/(2\sigma^2)$$

and the equilibrium density matrix $\hat{\rho} = e^{-H/T}/\mathrm{Tr}\{e^{-H/T}\theta(N-\hat{n})\}$.

The two parameters of the model, σ and N_c, correspond, respectively, to the dispersion $\sigma^{(\infty)}$ and the critical number of atoms in the trap N_c, used for the ideal gas in the box in the previous sections. In order to compare the results for the Gaussian model with the results for the ideal gas in the box, we assume, following Eqs. (3.3) and (3.4), that, $\sigma = \sigma^{(\infty)} \approx (s_4^{1/2}/\pi)[N_v/\zeta(3/2)]^{2/3}$, where N_v depends on N_c in accord with Eq. (3.1).

The mean value and all moments and cumulants of the noncondensate occupation within the Gaussian model can be calculated exactly. We find their universal structures in the thermodynamic limit, $N_c \to \infty$, analytically in terms of the error function $\mathrm{erf}(x)$ and the related special functions, since the probability distribution of the scaled variable $x = (n - N_c)/\sigma$ becomes a standard continuous unrestricted Gaussian distri-

bution $\rho^{(\infty)}(x) = \exp(-x^2/2)/(2\pi)^{1/2}$, $x \in (-\infty, \infty)$ and a continuous approximation of the discrete sums by the integrals is applied. All cumulants of the unconstrained Gaussian distribution $\rho^{(\infty)}(x)$ are zero, except of variance $\kappa_2'^{(\infty)} = \mu_2'^{(\infty)} = 1$, that is $\kappa_m'^{(\infty)} = 0$ for $m \neq 2$.

However, the actual physical system of N atoms in the trap is described by the constraint-cut-off probability distribution

$$\rho(x) = \exp(-x^2/2)\theta(\eta - x) / \int_{-\infty}^{\eta} \exp(-x^2/2)dx, \qquad \eta = \frac{N - N_c}{\sigma}, \tag{3.12}$$

as is discussed in the Section C and Fig. 3. This actual distribution, in a general case, is essentially non-Gaussian and, hence, all cumulants are nonzero, $\kappa_m'^{(\infty)} \neq 0$ for $m \geq 2$. Nevertheless, to find the mean value and all moments is easy, in particular, $\bar{x} = -(2/\pi)^{1/2}\{\exp(-\eta^2/2)/[1 + \mathrm{erf}(\eta/2^{1/2})]\}$. Thus, the universal structure of the order parameter $\bar{n}_0 = N - \bar{n}$ in the Gaussian model is given by the following analytical formula

$$\frac{\bar{n}_0}{\sigma} = \eta + \left(\frac{2}{\pi}\right)^{1/2} \frac{\exp(-\eta^2/2)}{1 + \mathrm{erf}(\eta/2^{1/2})} \tag{3.13}$$

Following a tradition of the previous sections, we skip all elementary derivations and present the results directly in the form of the graphs similar to Figs. 11-13.

In the whole critical region, as is clearly seen in Figs. 14 and 15, the result for the universal structure of the scaled order parameter $\bar{n}_0'(\eta) = \bar{n}_0/\sigma^{(\infty)}$ in the Gaussian model, given by the exact analytical solution in Eq. (3.13), is very close to the universal structure of the order parameter in the ideal gas in the box, plotted in Figs. 14 and 15 both as the numerical simulations for the large enough mesoscopic system ($N_v = 10^4$) and as the analytical approximation in Eq. (3.7) or Eq. (3.8), respectively.

Comparison of the universal structures of the higher-order moments and cumu-

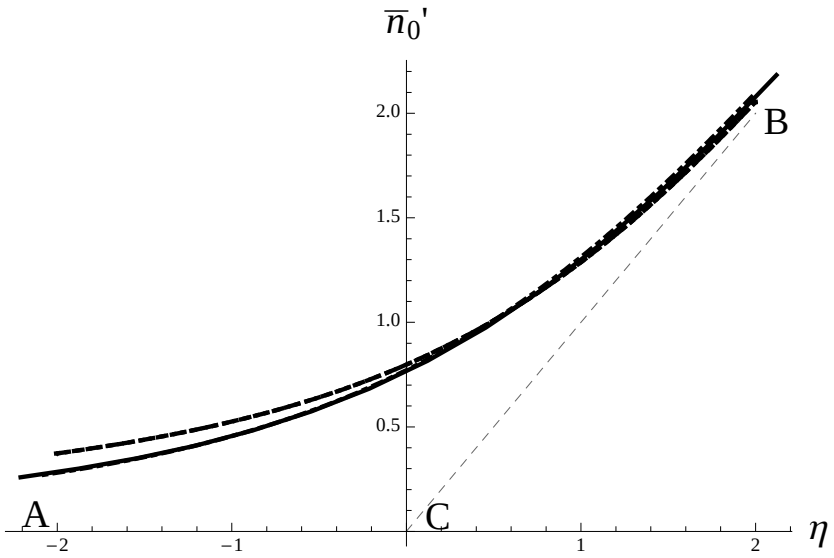

Fig. 14. Universal structure of the scaled order parameter $\bar{n}_0'(\eta) = \bar{n}_0/\sigma^{(\infty)}$ as function of $\eta = (N - N_c)/\sigma^{(\infty)}$ in the critical region for the Gaussian model in the thermodynamic limit given by Eq. (3.13) (the dashed line) and for the ideal gas in the box (the dashed-dotted line and the solid line are the plots for the analytical approximation in Eq. (3.7) and for the mesoscopic system with the trap-size parameter $N_v = 10^4$, respectively). The angle ACB represents the prediction of the standard Landau mean-field theory.

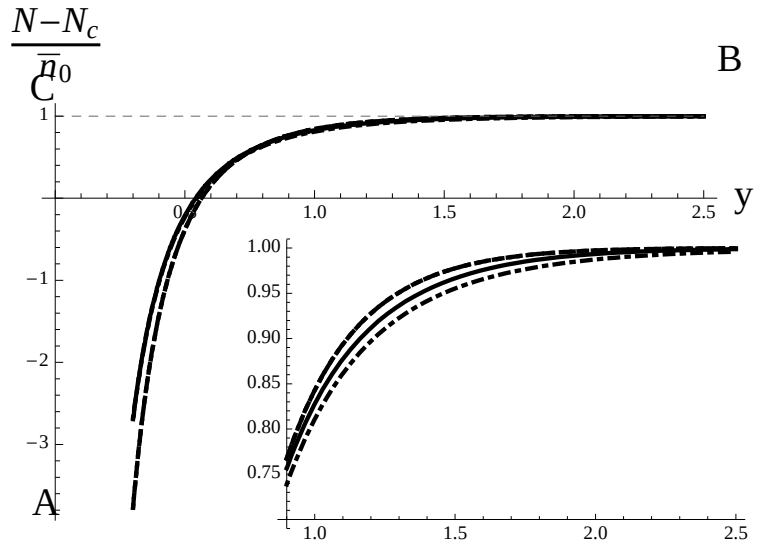

Fig. 15. Universal dependence of the ratio $(N - N_c)/\bar{n}_0$ on the scaled order parameter $y = \bar{n}_0/(2^{1/2}\sigma^{(\infty)}$ in the critical region for the Gaussian model in the thermodynamic limit given by Eq. (3.13) (the dashed line) and for the ideal gas in the box (the dashed-dotted line and the solid line are the plots for the analytical approximation in Eq. (3.8) and for the mesoscopic system with the trap-size parameter $N_v = 10^4$, respectively). The angle ACB represents the prediction of the standard Landau mean-field theory. Insert: A closer look at the same dependences in the region of a fully developed condensate.

lants (the variance κ_2, the asymmetry κ_3, and the excess κ_4) of the Gaussian model with the corresponding functions of the ideal gas in the box, presented in Fig. 16, proves that in the whole critical region they have qualitatively similar structures, which are governed by the universal constrain-cut-off mechanism as it is explained in the Sections A and C. Of course, the details of these structures, especially far from the critical region, are different since the tails of the unconstrained probability distribution $\rho_n^{(\infty)}$ in the ideal gas are essentially non-Gaussian and asymmetric. The latter fact is the reason why all cumulants κ_m, except of variance κ_2, vanish in the deep condensate region, $N \to \infty$ in the Gaussian model and remain finite, even in the thermodynamic limit, in the ideal gas in the box.

A remarkable general conclusion is that in the whole critical region all cumulants are essentially nonzero (i.e., the BEC statistics is essentially non-Gaussian) for the mesoscopic systems of any size as well as for the macroscopic systems in the thermodynamic limit, both for the pure Gaussian model and for the ideal gas in the trap.

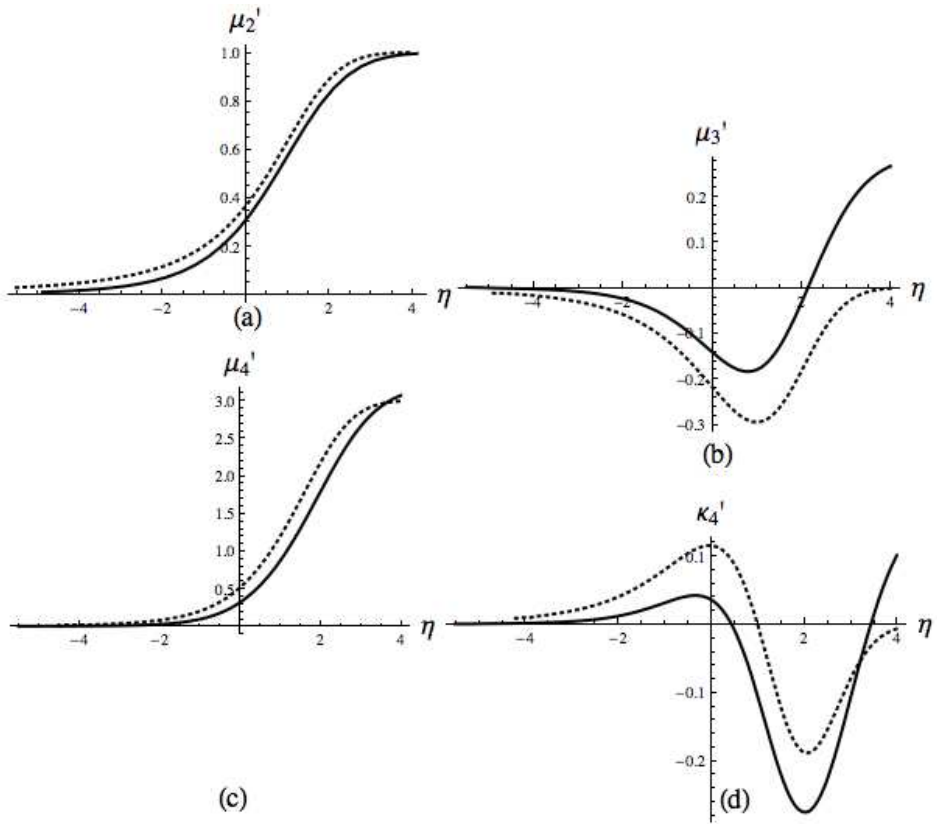

Fig. 16. Universal structures of the scaled central moments and cumulants (a) $\mu_2' \equiv \kappa_2' = \mu_2/(\sigma^{(\infty)})^2$, (b) $\mu_3' \equiv \kappa_3' = \mu_3/(\sigma^{(\infty)})^3$, (c) $\mu_4' = \mu_4/(\sigma^{(\infty)})^4$, and (d) $\kappa_4' = \mu_4' - 3(\mu_2')^2$ of the total noncondensate occupation in the critical region calculated as functions of $\eta = (N - N_c)/\sigma^{(\infty)}$ for the mesoscopic system with the trap-size parameter $N_v = 10^4$ for the Gaussian model (dotted lines) and for the ideal gas in the box (solid lines).

CHAPTER IV

MESOSCOPIC BOSE-EINSTEIN CONDENSATION OF AN IDEAL GAS IN A TWO-LEVEL TRAP

In this chapter we introduce a two-level trap model of BEC [65] that can be used as a basic block in the theory of BEC and has an analogy with a very successful two-level atom model in quantum optics. Namely, we consider a two-energy-level trap with arbitrary degeneracy of an upper level and find an analytical solution for the condensate statistics in a mesoscopic ideal gas with arbitrary number of atoms and any temperature, including a critical region. The solution is a cut-off negative binomial distribution that tends to a cut-off gamma distribution in the thermodynamic limit. We identify a universal constraint-cut-off mechanism that makes BEC fluctuations strongly non-Gaussian. We find that a quasithermal ansatz, suggested in [21], is a solution for effective two-level trap and explain why and to what extent it is so good for real traps. We show how to model BEC in real traps by BEC in the two-level or three-level traps.

A. Exact solution for BEC in a two-level trap: cut-off negative binomial distribution

Let us consider N atoms in a trap with just two energy levels, the ground level $\epsilon_0 = 0$ and one excited level $\epsilon > 0$. The excited level contains $g \geq 0$ degenerate states. Our idea behind this model is to isolate and study a contribution from a subset of closely spaced levels in the trap. It is similar to modeling of an inhomogeneously broaden optical transition in quantum optics by a homogeneously broaden two-level atoms. We find the unconstrained probability mass function and characteristic function of the

total noncondensate occupation as a superposition of g identical random variables,

$$\rho_n^{(2)(\infty)} = \frac{(g-1+n)!}{n!(g-1)!}(1-q)^g q^n, \quad \Theta^{(2)(\infty)}(u) = \left(\frac{1-q}{1-zq}\right)^g, \quad z = e^{iu}, \quad q = e^{-\epsilon/T}. \tag{4.1}$$

It is a well-known negative binomial distribution [29] with $\tilde{\kappa}_m^{(2)(\infty)} = g[q/(1-q)]^m(m-1)!$. Its cumulative mass function $\sum_{n=0}^{N} \equiv \langle\theta(N-n)\rangle^{(2)(\infty)} = I_{1-q}(g, N+1)$ is given by the incomplete beta function and yields, via Eq. (2.35), the explicit formulas for the cut-off negative binomial distribution as well as its characteristic function and cumulants:

$$\rho_n^{(2)} = \frac{\Gamma(n+g)(1-q)^g q^n}{\Gamma(g)\Gamma(n+1)I_{1-q}(g, N+1)}, \tag{4.2}$$

$$\Theta^{(2)} = \left(\frac{1-q}{1-zq}\right)^g \frac{I_{1-qz}(g, N+1)}{I_{1-q}(g, N+1)}, \tag{4.3}$$

$$\frac{\tilde{\kappa}_{m+1}^{(2)}}{q^{m+1}} = \frac{d^m}{dq^m}\frac{\tilde{\kappa}_1^{(2)}}{q}, \quad \tilde{\kappa}_1^{(2)} \equiv \bar{n} = \frac{qg}{1-q} - Q, \quad \tilde{\kappa}_2^{(2)} = \frac{gq}{(1-q)^2} + \left[\frac{g-1}{1-q} - N - g - Q\right], \tag{4.4}$$

where

$$Q = \frac{(1-q)^{g-1}q^{N+1}}{B(g, N+1)I_{1-q}(g, N+1)}, \tag{4.5}$$

$B(a,b) = \Gamma(a)\Gamma(b)/\Gamma(a+b)$ is the beta function, $\Gamma(a)$ is the gamma function.

B. Continuous approximation: cut-off gamma distribution

The most interesting is a case $\epsilon << T$, that implies $N_c \equiv \tilde{\kappa}_1^{(\infty)} = gq/(1-q) >> g$ and $1-q << 1$. Then, in the whole interesting for BEC region $n >> g$, $N >> g$, we can neglect a discreteness of the distribution in Eq. (4.1) and replace it with a continuous gamma distribution

$$\rho_n^{(\Gamma)(\infty)} = \frac{\epsilon[\epsilon(n+g-1)/T]^{g-1}}{T\Gamma(g)\exp[\epsilon(n+g-1)/T]}, \tag{4.6}$$

$$\Theta^{(\Gamma)(\infty)}(t) = \int_{1-g}^{\infty} e^{itn} \rho_n^{(\Gamma)(\infty)} dn = e^{-i(g-1)t} \left(1 - \frac{itT}{\epsilon}\right)^{-g}, \tag{4.7}$$

for which the mean value $\langle n \rangle^{(\Gamma)(\infty)} = gT/\epsilon - g + 1$ and all cumulants of orders $m \geq 2$, $\kappa_m^{(\Gamma)(\infty)} = g[T/\epsilon]^m (m-1)!$, are equal to the corresponding generating cumulants of the distribution in Eq. (4.1). We derive Eq. (4.6) from Eq. (4.1) using the Stirling formula $n! \approx \sqrt{2\pi} n^{n+1/2} e^{-n}$ and an approximation $\sqrt{(n+g-1)/n} \approx 1$. The cumulative distribution function of the distribution in Eq. (4.6), $\langle \theta(N-n) \rangle^{(\Gamma)(\infty)} = \gamma(g, (N+g-1)\epsilon/T)/\Gamma(g)$, is given by the incomplete gamma function $\gamma(a,x) = \int_0^x t^{a-1} e^{-t} dt$ and yields the explicit formulas for the probability density function of the cut-off gamma distribution and all its initial moments ($m = 1,\ 2,$) [65]

$$\rho_n^{(\Gamma)} = \frac{\epsilon (E_n)^{g-1}}{T \gamma(g, E_N) \exp(E_n)}, \quad \langle (n+g-1)^m \rangle^{(\Gamma)} = \left(\frac{T}{\epsilon}\right)^m \frac{\gamma(g+m, E_N)}{\gamma(g, E_N)}, \tag{4.8}$$

where $E_n = \epsilon(n+g-1)/T$.

The cut-off gamma distribution in Eq. (4.8) approximates the discrete distribution in Eq. (4.2) so good that any differences between the two distributions as well as between their cumulants cannot be even seen in Figs. 17-18 and, thus, the same solid lines represent the results for both distributions in Eqs. (4.2) and (4.8). (Of course, in Fig. 17 the properly renormalized function $\rho_n^{(\Gamma)(\infty)} \int_0^\infty \rho_n^{(\infty)} dn \approx q \rho_n^{(\Gamma)(\infty)}$ is compared against $\rho_n^{(\infty)}$, not the function $\rho_n^{(\Gamma)(\infty)}$ itself.)

C. Modeling BEC in a real trap by BEC in a two-level trap

BEC statistics in a real trap is essentially the constraint-cut-off statistics of a sum of the populations of all excited states with inhomogeneously broaden spectrum of energies $\epsilon_{\mathbf{k}}$ ranging from the first level ϵ_1 through all levels with energies $\sim T$. We can describe it analytically by using the exact solution for the two-level trap as a building block. In fact, we need just to find the unconstrained distribution of the total

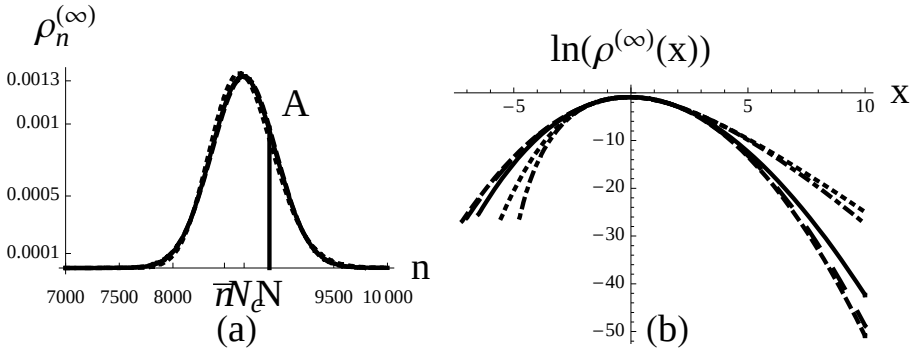

Fig. 17. (a) Unconstrained probability mass function $\rho_n^{(\infty)}$ of the noncondensate occupation n with a constraint cut-off at $n = N$ and (b) the logarithm of the same distribution $\rho^{(\infty)}$as a function of scaled noncondensate occupation $x = (n - N_c)/\sigma^{(\infty)}$ in the cases of the two-level trap (solid line), Gaussian model (dashed line), and box trap (dotted line) for the values of the critical number of atoms N_c and dispersion $\sigma^{(\infty)}$ corresponding to the box-trap parameter $N_v = 10^4$. The dashed-dotted and long-dashed lines represent the case of the two-level trap for $N_v = 10^2$ and $N_v = 10^6$, respectively.

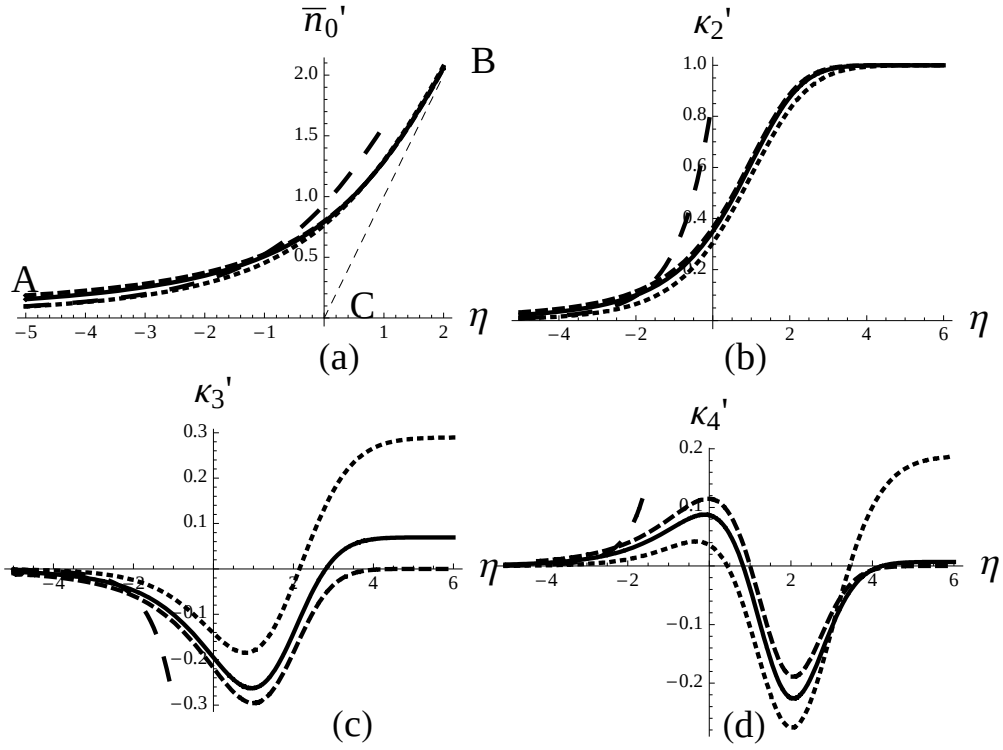

Fig. 18. Scaled order parameter $\bar{n}_0' = \bar{n}_0/\sigma^{(\infty)}$, (a), and cumulants $\kappa_m' = \kappa_m/(\sigma^{(\infty)})^m$, (b) $m = 2$, (c) $m = 3$, (d) $m = 4$, in the critical region as the functions of $\eta = (N - N_c)/\sigma^{(\infty)}$ for the box trap with $N_v = 10^4$ (dotted lines) as well as for the corresponding two-level trap (solid lines) and Gaussian model (dashed lines). The long-dashed line represents the result within the grand-canonical-ensemble approximation. Straight lines ACB represent the mean-field theory result.

noncondensate occupation, that is the sum of the independent random occupations of excited states, and then to cut off it as it is explained in Chapter III. There are different ways to implement this approach.

First of all, we can model the whole energy spectrum of a trap $\epsilon_{\mathbf{k}}$ by means of just one effective energy level ϵ with the degeneracy g and choose the two parameters ϵ and g to ensure matching of the first two cumulants of the model with their corresponding values in the real trap, $\kappa_1^{(\infty)} \equiv \tilde{\kappa}_1^{(\infty)} = N_c$, $\kappa_2^{(\infty)} \equiv \tilde{\kappa}_2^{(\infty)} + \tilde{\kappa}_1^{(\infty)} = \sigma^{(\infty)2}$. According to the negative binomial distribution in Eq. (4.1), we find $g = N_c^2/[\sigma^{(\infty)2} - N_c]$ and $q = 1 - N_c/\sigma^{(\infty)2}$, that is $\epsilon/T = g/N_c$ if $\epsilon << T$. The result is given by the cut-off negative binomial distribution in Eq. (4.2) and exactly coincides with the well-known quasithermal ansatz, which we suggested in [21]. Thus, the quasithermal ansatz is not only a good guess anymore, but also a rigorously justified effective two-level trap model of BEC statistics.

This fact explains why the quasithermal ansatz was so successful and close to the BEC statistics in the real mesoscopic traps for the low order moments and, at the same time, reveals its main drawback. Namely, in the thermodynamic limit, $N \to \infty$, for the box trap one has $g \approx cN_v^{2/3}$ and $\epsilon/T \approx c/N_v^{1/3} >> \epsilon_1/T = \pi(\zeta(3/2)/N_v)^{2/3}$, where $c = \pi^2(\zeta(3/2))^{4/3}/s_4$, $s_4 = \sum_{\mathbf{q}\neq 0} \mathbf{q}^{-4} \approx 16.53$. So, all higher order cumulants $\tilde{\kappa}_m = (m-1)! \sum_{\mathbf{k}\neq 0} (e^{\epsilon_{\mathbf{k}}/T} - 1)^{-m} \approx (m-1)!6(e^{\epsilon_1/T} - 1)^{-m}$, $m \geq 3$, which are dominated in the box trap by the most long-wavelength 6-fold-degenerate first excited state with the energy ϵ_1 and wavenumber $k = 2\pi/L$, are modeled incorrectly. That means that the quasithermal ansatz does not describe the long-ranged correlations and anomalies in the BEC statistics [35] in the deep condensed regime ($N >> N_c$) and, in particular, predicts vanishing non-Gaussian coefficients $\tilde{\kappa}_m^{(\infty)}/\tilde{\kappa}_2^{(\infty)m/2} \approx (m-1)!/g^{m/2-1} \propto N_v^{-(m+2)/3} \to 0$. This fact is clearly seen in Fig. 17 where the distribution in Eq. (4.1) for the effective two-level trap tends to the

pure Gaussian distribution with increasing trap parameter N_v and does not coincide with the dotted line of the real box trap. In the real box trap all non-Gaussian coefficients remain nonzero and do not depend on N_v in the thermodynamic limit: $\tilde{\kappa}_m^{(\infty)}/\tilde{\kappa}_2^{(\infty)m/2} \approx (m-1)!/6^{m/2-1}$. Thus, the formulated above choice for the parameters of the effective two-level trap model and, hence, the quasithermal ansatz [21] fail to give correct higher order cumulants in the condensed phase outside the critical region. However in the most interesting, critical region, this effective two-level trap model yields all cumulants and all universal, strongly non-Gaussian functions of the constraint-cut-off BEC statistics [66] qualitatively right, namely, similar to the cut-off Gaussian model in Eq. (3.12), as is shown in Fig. 18. The grand-canonical-ensemble approximation, shown in Fig. 18 by a long-dashed line, is not correct at all both in the critical as well as condensed regions.

In order to describe correctly all higher order cumulants, one has to take into account exactly a dominant contribution from the lowest energy level. For the box trap, it could be done by setting $\epsilon = \epsilon_1$ and $g = g_1 = 6$ in the two-level trap model since the lowest level is 6-fold degenerate. However, that model would not give the correct values for the first two cumulants (the mean value and variance), which are mainly determined by the contributions from the higher energy levels. A natural way out of this problem is to adopt a three-level trap model where the total noncondensate occupation is a sum of occupations of two excited levels, $n = n_1 + n_2$, and the first level with parameters ϵ_1 and g_1 is responsible for the long-range BEC correlations (higher order cumulants), while the second level with parameters ϵ_2 and g_2 takes care of the correct mean value and variance. The unconstrained distribution $\rho_n^{(3)(\infty)}$ for that three-level trap model is just a superposition of two two-level trap models. In

the continuous approximation (see Eq. (4.6)), we find [65]

$$\rho_n^{(3)(\infty)} = \frac{\left(\frac{\epsilon_1}{T}\right)^{g_1}\left(\frac{\epsilon_2}{T}\right)^{g_2}(n+g_1+g_2-2)^{g_1+g_2-1}M\left(g_1,g_1+g_2,(n+g_1+g_2-2)\frac{\epsilon_2-\epsilon_1}{T}\right)}{\Gamma(g_1+g_2)\exp[\epsilon_2(n+g_1+g_2-2)/T]}, \tag{4.9}$$

$M(a,b,z) = [\Gamma(b)/(\Gamma(b-a)\Gamma(a))]\int_0^1 e^{zt}t^{a-1}(1-t)^{b-a-1}dt$ is the degenerate hypergeometric function [29], $g_2T/\epsilon_2+g_1T/\epsilon_1 = N_c+g_1+g_2-2$, $g_2(T/\epsilon_2)^2+g_1(T/\epsilon_1)^2 = \sigma^{(\infty)2}$. Another choice for the parameters $\epsilon_1,\ g_1,\ \epsilon_2,\ g_2$ is to match the first four cumulants to their box-trap values at $N \to \infty$ and do not match exactly the higher-orders cumulants. Remarkably, the result in Eq. (4.9) is so good that in Fig. 17(a) (and in Figs. 17(b) and 18 for the second choice of parameters) it cannot be discerned from the exact numerical curve (dotted line) for the real box trap. For the first choice of parameters, the result in Eq. (4.9) shows small deviations ($\sim$10%) from the exact curves for the box trap only at the very left tail in Fig. 17(b) and at the right part of Figs. 18(c),(d), but all higher-order cumulants match perfectly. So, we do not plot the curves for the result in Eq. (4.9) to avoid figures overloading.

CHAPTER V

SADDLE-POINT METHOD FOR CONDENSED BOSE GASES

A. Review of the saddle-point method for a condensed Bose gas in a harmonic trap

The saddle-point method is a very powerful technique in statistical physics, but its canonical form is not applicable in the case of systems with condensate. As it is discussed in Appendices, the characteristic function has an infinite number of poles on the real positive half of z axis. The lowest order pole is at the point $z_1 = e^{\epsilon_1/T}$. We are integrating over the unit circle in the complex plane and the distance between the saddle point and the lowest pole can be infinitesimal. However, the traditional Gaussian approximation requires the vicinity of the saddle point to have no singularities. Following the approach introduced by Holthaus and Kalinowski [20, 27], I will give a solution to this problem by exempting the minimal energy contribution from the characteristic function treating it explicitly, and performing the Gauss integration as usual. As result, I will obtain an expression in terms of the hypergeometric functions, which leads to the parabolic cylinder functions. First, I will apply this technique to the problem of an ideal Bose gas in a harmonic trap, reviewing the solution in thermodynamic limit. I start with the grand-canonical partition function:

$$\Xi(\beta, z) = \prod_{\nu=0}^{\infty} \frac{1}{1 - z\exp(-\beta\epsilon_\nu)}, \tag{5.1}$$

where ϵ_ν are single-particle energies, $\beta = 1/T$ (T is expressed in energy units) and $z = \exp(\beta\mu)$. The grand-canonical partition function $\Xi(\beta, z)$ generates the canonical partition function $Z_N(\beta)$ by means of the expansion:

$$\Xi(\beta, z) = \sum_{N=0}^{\infty} z^N Z_N(\beta). \tag{5.2}$$

Then one can treat z as a complex variable and express $Z_N(\beta)$ as a contour integral using the Cauchy's theorem:

$$Z_N(\beta) = \frac{1}{2\pi i}\oint dz \frac{\Xi(\beta, z)}{z^{N+1}} = \frac{1}{2\pi i}\oint dz \exp(-F(z)), \tag{5.3}$$

where the path of integration encircles the origin counterclockwise, and

$$F(z) = (N+1)\ln(z) + \ln \Xi(\beta, z) = (N+1)\ln(z) + \sum_{\nu=0}^{\infty} \ln\left(1 - z\exp(-\beta\epsilon_\nu)\right). \tag{5.4}$$

The usual definition for the saddle point ($z = z^*$) requires the first derivative to be zero in this point

$$\frac{dF}{dz}\Big|_{z=z^*} = 0, \tag{5.5}$$

which gives the following equation for z^*

$$N + 1 = \sum_{\nu=0}^{\infty} \frac{1}{\exp(\beta\epsilon_\nu/z^*(N)) - 1}. \tag{5.6}$$

This is almost the grand-canonical relation between particle number $N+1$ and the fugacity z_0. In the case of a harmonic trap (linear spectrum) [27] this equation can be solved in the continuum limit, which leads to the dilogarithm functions. In the canonical saddle-point method the Taylor expansion of the function $F(z)$ yields

$$F(z) \approx F(z^*) + \frac{1}{2}F''(z^*)(z - z^*)^2. \tag{5.7}$$

Thus, performing the Gaussian integral, one can obtain:

$$Z_N(\beta) \approx \frac{\exp(-F(z^*(N)))}{\sqrt{-2\pi F''(z^*(N))}}. \tag{5.8}$$

The canonical occupation number of the ground state, and its mean-square fluctuations, are obtained by differentiating the canonical partition function:

$$\bar{n}_0 = \frac{\partial Z_N(\beta)}{\partial(-\beta\epsilon_0)} = \frac{1}{Z_N(\beta)}\frac{1}{2\pi i}\oint dz \frac{\partial \Xi(\beta, z)}{\partial(-\beta\epsilon_0)}, \tag{5.9}$$

$$\Delta n_0 = \frac{\partial^2 Z_N(\beta)}{\partial(-\beta\epsilon_0)^2} = -\bar{n}_0^2 + \frac{1}{Z_N(\beta)}\frac{1}{2\pi i}\oint dz \frac{\partial^2 \Xi(\beta, z)}{\partial(-\beta\epsilon_0)^2}. \tag{5.10}$$

The saddle-point approximation is then applied to the integrands of Eqs. (5.9) and (5.10). In the condensate region there is a substantial deviation of the saddle-point expressions from the "exact" numerical answer obtained from the exact recursion relation (1.38).

The reason of this inaccuracy is that in the condensate region, the saddle-point z_0 lies close to the singular point $z = e^{\beta\epsilon_0}$ of the function $F(z)$. As result, the approximation in Eq. (5.8) becomes invalid in the condensate region. To improve this method, it was proposed in Ref. [27] to treat the potentially dangerous term in (5.4) as it is, and represent $Z_N(\beta)$ as:

$$Z_N(\beta) = \frac{1}{2\pi i}\oint dz \frac{\exp(-F_1(z))}{1 - z\exp(-\beta\epsilon_0)}, \tag{5.11}$$

where

$$F_1(z) = (N+1)\ln(z) + \sum_{\nu=1}^{\infty} \ln\left(1 - z\exp(-\beta\epsilon_\nu)\right) \tag{5.12}$$

has no singularity at $z = e^{\beta\epsilon_0}$. If the point of singularity exists, it is shifted now to the next available pole, i.e. $z = e^{\beta\epsilon_1}$. Since $z^* < e^{\beta\epsilon_0}$, the saddle point is far away from the singularity point by the distance $e^{\beta\epsilon_1} - e^{\beta\epsilon_0} \approx \hbar\omega/T$, which makes the expansion (5.12) valid and safe for sufficiently large number of particles N. One can use the following expression for the integral in Eq. (5.11):

$$\frac{1}{2\pi i}\oint dz \frac{\exp\left[-f_1(z) - (\xi-1)\beta\epsilon_0\right]}{\left(1 - z\exp(-\beta\epsilon_0)\right)^{\xi}} \approx$$

$$\approx \frac{1}{\sqrt{2\pi}}\left(-f_1''(z^*)\right)^{(\xi-1)/2} \exp\left(\beta\epsilon_0 - f_1(z^*) - \xi + \eta^2/2 - \eta_1^2/4\right) D_{-\xi}(\eta_1), \tag{5.13}$$

where $\eta = (\exp(\beta\epsilon_0) - z^*)\sqrt{-f_1''(z^*)}$, $\eta_1 = \eta - \xi/\eta$, z^* is a saddle point of the

function,

$$f(z) = f_1(z) + (\xi - 1)\beta\epsilon_0 + \xi \ln(1 - z\exp(-\beta\epsilon_0)), \tag{5.14}$$

and $D_{-\xi}(z)$ is a parabolic cylinder function. This function can be further written as a combination of the hypergeometric functions as

$$D_s(z) = 2^{s/2}e^{-z^2/4}\sqrt{\pi}\left[\frac{{}_1F_1(-s/2, 1/2, z^2/2)}{\Gamma[(1-s)/2]} - \frac{\sqrt{2}z \cdot {}_1F_1((1-s)/2, 3/2, z^2/2)}{\Gamma[-s/2]}\right]. \tag{5.15}$$

Thus, the integration in Eq. (5.11) yields:

$$Z_N(\beta) = \frac{1}{2}\exp\left(\beta\epsilon_0 - F_1(z^*) - 1 + \eta^2/2\right)\mathrm{erfc}\left(\frac{\eta_1}{\sqrt{2}}\right), \tag{5.16}$$

where $\mathrm{erfc}(z) = 2/\sqrt{2}\int_z^\infty \exp(-t^2)dt$ is the complementary error function,

$$\eta = (\exp(\beta\epsilon_0) - z^*)\sqrt{-F_1''(z^*)}, \qquad \eta_1 = \eta - 1/\eta, \tag{5.17}$$

since in the case of a harmonic trap $\xi = 1$. Calculations of the occupation number, variance, and higher moments deal with the integrals from derivatives of $\Xi(\beta, z)$ with respect to $-\beta\epsilon_0$. The refined saddle-point expressions for the first four central moments or cumulants are in remarkable agreement with the numerical results obtained from the exact recursion relation for an ideal gas in a harmonic trap.

B. The development of the saddle-point method for a condensed Bose gas in a box

I express the characteristic function as the contour integral over the unit circle in the complex z-plane using the Cauchy's theorem for $z = e^{iu}$:

$$\rho(n) = \frac{1}{2\pi}\int_{-\pi}^{\pi} e^{-inu}\Theta_n(u)\,du = \frac{\Theta_0}{2\pi i}\oint_{|z|=1} dz\frac{\tilde{\Theta}(z)}{z^{n+1}} = \frac{1}{2\pi i}\oint_{|z|=1} dz\exp(-F(z)), \tag{5.18}$$

where the path of integration encircles the origin counterclockwise, and in the case of a box:

$$\Theta_0 = \prod_{\mathbf{k}\neq 0} \left(1 - 1/z_{\mathbf{k}}\right), \qquad \tilde{\Theta}(z) = \prod_{\mathbf{k}\neq 0} \frac{1}{1 - z/z_{\mathbf{k}}}, \tag{5.19}$$

$$F(z) = (n+1)\ln(z) + \ln\Theta(z) = (n+1)\ln(z) + \sum_{\mathbf{k}\neq 0} \ln\left(1 - z/z_{\mathbf{k}}\right). \tag{5.20}$$

The equation for the saddle point z^* is:

$$n + 1 = \sum_{\mathbf{k}\neq 0} \frac{1}{z_{\mathbf{k}}/z^*(n) - 1}. \tag{5.21}$$

As result, for the standard saddle-point approximation one can obtain

$$\rho(n) \approx \frac{\exp(-F(z^*(n)))}{\sqrt{-2\pi F''(z^*(n))}}. \tag{5.22}$$

In fact, the deviation from the exact solution in the canonical saddle-point method for a box can only be seen in the condensate regime, and thus, for our purposes (in the critical region), the approximation in Eq. (5.22) gives precise enough estimate. Nevertheless, the refined saddle-point method gives a much better accuracy. Hence, one should express the distribution function in the following way:

$$\rho\left(n\right) = \frac{\Theta_0}{2\pi i} \oint_{|z|=1} dz \frac{\exp(-F_1(z))}{1 - z/z_1}, \tag{5.23}$$

where the function

$$F_1(z) = (n+1)\ln(z) + \sum_{\mathbf{k}\neq 0,1} \ln\left(1 - z/z_{\mathbf{k}}\right), \tag{5.24}$$

has no singularity at $z = e^{\epsilon_1/T}$. If the point of singularity exists, it is shifted now to the next available pole, i.e. $z = e^{2\epsilon_1/T}$. Since $z^* < e^{\epsilon_1/T}$, the saddle point is far away from the singularity point by the distance $e^{2\epsilon_1/T} - e^{\epsilon_1/T} \approx N\epsilon_1/T$, which makes the expansion in Eq. (5.24) valid for sufficiently large number of particles N. Now I

employ the expression obtained in the previous section for the integral in Eq. (5.13). The corresponding degeneracy is $g_1 = \xi = 6$ and, thus, one can express the resulting distribution function as:

$$\rho(n) = \frac{1}{\sqrt{2\pi}} \left(-F_1^{''}(z^*(n))\right)^{5/2} \times$$

$$\times \exp\left(\epsilon_1/T - F_1(z^*(n)) - 6 + \eta^2(n)/2 - \eta_1^2(n)/4\right) D_{-6}(\eta_1(n)). \tag{5.25}$$

Using the above result, one can analyze the asymptotical behavior of the distribution function and estimate the leading term in the expansion. I return to the Eq. (5.21) for the saddle point definition. Let us consider a small n, so that $n << N$. The particular choice of the estimate is obvious. I would like to analyze the behavior far from the maximum value of the function, where it can be approximated by Gaussian function. In this case, expanding the right-hand-side of the Eq. (5.21) and implying that $z^*(n=0) \approx 0$, $\delta z = z^* - 0 \approx (n+1)/f_1(0)$, where:

$$f_m(z) = \sum_{\mathbf{k}\neq 0} (z - z_{\mathbf{k}})^{-m}, \tag{5.26}$$

the saddle-point approximation yields the following result $\rho(n)|_{n<<N} \approx n^{-n}$, or more accurately:

$$\rho(n)|_{n<<N} \propto n^{-n} e^{(\ln f_1(0)+1)n - 1/2 \ln n}. \tag{5.27}$$

Here all n's are properly normalized by the variance. Eq. (5.27) is nothing but a Stirling approximation of the $n!$ in the exponent ($n! \approx (2\pi n)^{1/2}(n/e)^n$) which essentially makes distribution function of noncondensed atoms Poissonian for small n and was known before (see [21]). Going further, one can obtain that the dependence in the vicinity of the maximal value is truly gaussian with the parameters N_c and $\sigma^{(\infty)}$ defined in Eqs (3.1) and (3.3), respectively. In this case $\delta z = z^* - z_c =$

$z_c\sigma^{(\infty)}n/(z_c^2 f_2(z_c)+N_c)$. Thus, performing the integration, one can obtain:

$$\rho(n\approx N_c)\propto e^{-\frac{(n-N_c)^2}{f_2(z_c)z_c^2+N_c}}\approx e^{-\frac{(n-N_c)^2}{\sigma^{(\infty)2}}}, \tag{5.28}$$

where $z_c = z(N_c)$. At large n, of the order of one or several N_v, the value $z(N)$ is close to the pole at $z = e^{2\epsilon_1/T}$, which means, that the Gaussian function should decay fast enough from its maximum value. In other words, the width of the Gaussian function should be much smaller than the distance between the saddle point itself and the closest pole: $z(N)-z(n) << e^{2\epsilon_1/T}-z(N)$. Therefore, the allowed region for n is $N-n << \sigma^{(\infty)}$. In this case, one can expect the linear-exponentially decaying behavior, i. e.,

$\delta z = z(N)-z(n)\approx z(N)\sigma^{(\infty)}n/(z^2(N)f_2(z(N))+N)$, and finally

$$\rho(n\approx N)\propto e^{-\ln(z(N_v))(N-n)}\propto e^{-3(N-n)/\sigma^{(\infty)}} \tag{5.29}$$

I intentionally dropped the pre-exponential factors, which depends on n, since I am considering the leading order asymptotical behavior of the distribution function. The universality of the asymptotics is really surprising, since the proper scaled distribution functions for the different size of the traps have not only the same shape, but are almost identical, which means, that there are only two real macroscopical scales of the distibution function. First scale is its maximum value at thermal mean occupation number $\bar{n}_{\max} = N_c$. The second one is the characteristic width scale, which is essentially the variance, calculated in the thermal approximation $\sigma^{(\infty)}$. Those similarities imply the universality in the description of the statistical moments, the same way it was done for the distribution function in Chapter III.

Unfortunately, the agreement in behavior of the distribution function in the condensed region ($N > N_c$) obtained by a saddle-point method and actual FFT calculation is more or less a coincidence, because of the following reasons. If one

wants to calculate corrections from the neighborhood of the saddle point for finite N_v, then a naive perturbation up to first order yields a wrong sign of the shift for the critical temperature. A detailed analysis shows that a nonanalyticity occurs at the saddle-point near the critical point and infinitely many orders in the saddle-point expansion must be calculated and resummed to find the correct result. This fact has been discussed in the literature, for instance, in [34] for the box potential near the critical point, and the problem is still open.

C. Comparison with the numerical results

In this section, I present the comparison of the obtained results with the numerical simulations. I will compare the refined saddle-point approximation results for the asymptotical behavior of the distribution function and the result of applying the FFT technique in Eq. (3.6). It is worth noting that I am not using the saddle-point approximation for calculation of the condensate fluctuations, like it was done in the case of a harmonic trap because of the reasons discussed in the last part of the previous section and the certain properties of the box spectrum. According to the asymptotic formulas in Eqs. (5.27)-(5.29), one can separate the whole region of the distribution function by three parts.

The contribution around the maximum mean occupation number of the condensate N_c is Gaussian, with a relatively good accuracy (see Eq. (5.28) and Fig. 19). It has a little shift in its maximum value due to the asymmetry of the actual distribution function compare to Gaussian distribution discussed in details in Chapter III.

A similar analysis can be performed in the evaluation of the contributions at the wings. I found that, in the lower-N region, the behavior is Poissonian, which was confirmed in [21] (see Eq. (5.27) and Fig. 20). It follows from the fact that $\log(n)$

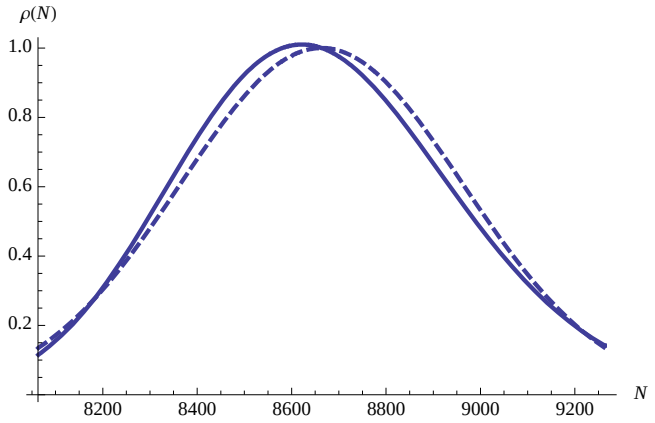

Fig. 19. Canonical ensemble distribution function in the vicinity of its maximum as a function of the number of noncondensed particles in a box with $N = 10000$ atoms. Dashed and solid lines are obtained by the numerical calculation of discrete Fourier summation in Eq. (3.6) for an ideal gas and refined saddle–point method in Eq. (5.28), respectively.

term in the exponent is a smooth function, almost a constant if the argument N is varying slowly. The distribution function for the small N is plotted in the inverse direction from large N to small N, starting from $4\sigma^{(\infty)}$ distance from the maximum value N_c.

I am not presenting a behavior of the distribution function for large N, because it was shown in [34] that saddle-point method does not work in any order of perturbation theory for this case. That is why even though the calculation for the particular box trap gives a simple answer in Eq. (5.29), I am not interpreting this as a physical result.

In spite of the fact that the saddle-point method, is truly very powerful approximation method in theoretical physics, which leads to the simple analytical formulas for the BEC fluctuations in some regions of the parameters, the question of applicability and physical reasoning of this method in the problem of BEC is still open.

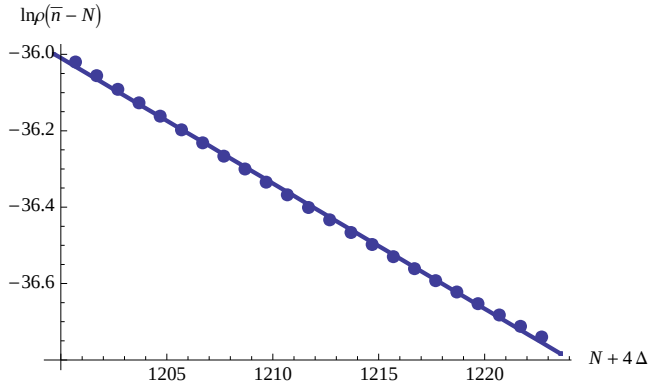

Fig. 20. Logarithm of the canonical ensemble distribution function in the region of small n as a function of a number of noncondensed particles in a box with $N = 10000$ atoms. Dashed and solid lines are obtained by the numerical calculation of discrete Fourier summation in Eq. (3.6) for an ideal gas and refined saddle-point method in Eq. (5.27), respectively.

CHAPTER VI

ELECTROMAGNETIC MODES OF OPEN PLANAR BRAGG STRUCTURES

A. Dielectic layer with periodic modulation of dielectric constant

1. Dispersion relation

The simplest model of a Bragg waveguide is a dielectric layer with a periodic modulation of a dielectric constant. This model is used in the analysis of the photonic crystal structures and is simpler than a model of a Bragg waveguide formed by two corrugated metal plates. Let us consider a two-dimensional open planar waveguide of a width a_0 filled with dielectric with a small ($\tilde{\alpha} << 1$) periodic modulation of the dielectric constant:

$$\epsilon(x) = 1 + \tilde{\alpha}\cos(\bar{h}x), \tag{6.1}$$

where $\bar{h} = 2\pi/d$. Consider for simplicity a mode with an electric field perpendicular to the direction of a gradient of the dielectric constant (see Fig. 2). One can describe a monochromatic electromagnetic field which is uniform on y coordinate by use of a vector potential:

$$\vec{A} = \mathrm{Re}\left(\vec{y}^{(0)} A(x,z) e^{i\omega t}\right), \qquad \vec{H} = \vec{\nabla} \times \vec{A}, \qquad \vec{E} = -ik\vec{A}. \tag{6.2}$$

The scalar Helmholtz equation for the vector potential has the following form:

$$\Delta A + k^2(1 + \tilde{\alpha}\cos(\bar{h}x))A = 0, \tag{6.3}$$

where $k = \omega/c$. One can seek a solution of Eq. (6.3) as a combination of two waves coupled on a lattice (see Fig. 2):

$$A(x,z) = \left[A_1(x)e^{i\frac{\bar{h}}{2}x} + A_2(x)e^{-i\frac{\bar{h}}{2}x}\right] e^{-ihz}, \tag{6.4}$$

where $A_{1,2}(x)$ are slowly varying functions of their arguments in a wavelength scale. After averaging of Eq. (6.3) it leads to the following equations for amplitudes:

$$\frac{\bar{h}}{2k}\frac{dA_{1,2}}{dx} \pm i\Gamma A_{1,2} \mp i\alpha A_{2,1} = 0, \tag{6.5}$$

where $\alpha = k\tilde{\alpha}/4$, $\Gamma = \frac{1}{2k}\left(k^2 - h^2 - \bar{h}^2/4\right)$. For a solution of Eq. (6.5) in the form $A_{1,2}e^{igx}$, the dispersion relation for unbounded in x coordinate media can be written as follows:

$$\left(\frac{\bar{h}}{2}g\right)^2 = (k\Gamma)^2 - (k\alpha)^2, \tag{6.6}$$

where $g << \bar{h}/2$.

2. Eigenmodes

We assume the following boundary conditions for the radiation on the edges of a waveguide ($x = 0, l_x$):

$$A_1(0) = A_2(l_x) = 0. \tag{6.7}$$

The dispersion relation for the modes in Eq. (6.5) with the boundary conditions in Eq. (6.7) can be easily found as follows:

$$e^{2igl_x} = \frac{2k\Gamma + \bar{h}g}{2k\Gamma - \bar{h}g}. \tag{6.8}$$

The latter equation has the form of a well-known characteristic equation for eigenmodes for a Bragg resonator [37, 41]. In the assumption of a strong coupling ($\alpha l_x >> 1$) the solution of Eq. (6.8) can be written as follows:

$$g_n = \frac{\pi n}{l_x} + i\frac{1}{2}\frac{\pi n}{\alpha l_x^2}\frac{\bar{h}}{2k},\ \mathrm{Re}\Gamma_n = \alpha\frac{n}{|n|}\left(1 + \frac{1}{2}\left(\frac{\pi n}{\alpha l_x}\frac{\bar{h}}{2k}\right)^2\right),\ \mathrm{Im}\Gamma_n = \alpha\frac{1}{2}\frac{(\pi n)^2}{(\alpha l_x)^3}\left(\frac{\bar{h}}{2k}\right)^3, \tag{6.9}$$

where $n = \pm 1, \pm 2, \pm 3...$ are the mode indices.

The longitudinal wavenumber is given by $h_n^2 = k^2 - \bar{h}^2/4 - 2k\Gamma_n$. Therefore, the

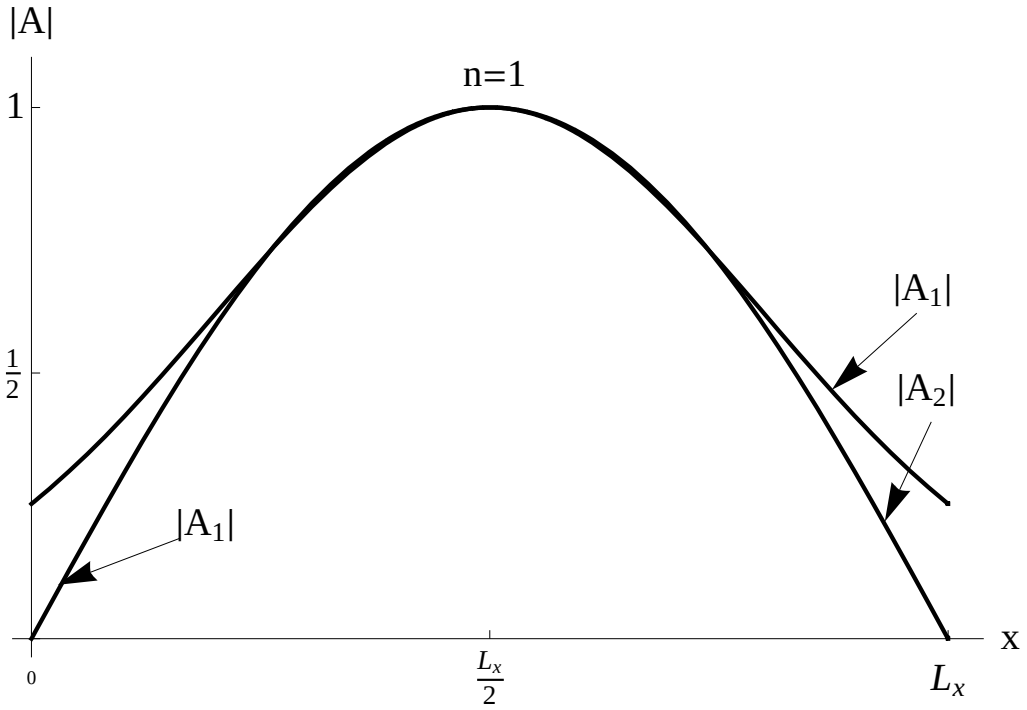

Fig. 21. The transverse structure of a waveguide mode with $n = \pm 1$ for a Bragg structure with regular periodicity.

full set of wavenumbers is given by:

$$\begin{cases} \mathrm{Re}h_n = \left[\frac{1}{2}\left(R_n + \sqrt{R_n^2 + I_n^2}\right)\right]^{1/2}, \\ \mathrm{Im}h_n = \left[\frac{1}{2}\left(-R_n + \sqrt{R_n^2 + I_n^2}\right)\right]^{1/2}, \end{cases} \tag{6.10}$$

where $R_n = \mathrm{Re}h_n^2 = k^2 - \bar{h}^2/4 - 2k\mathrm{Re}\Gamma_n$, $I_n = \mathrm{Im}h_n^2 = -2k\mathrm{Im}\Gamma_n$.

The transverse structure of the n-th mode is given by:

$$A_n(x,z) = A\left[\sin(g_n x)e^{i\frac{\bar{h}}{2}x} + \sin(g_n(x-l_x))e^{-i\frac{\bar{h}}{2}x - ig_n l_x}\right]e^{-ih_n z}, \tag{6.11}$$

and is essentially a distribution close to a standing wave with a sine wave envelope having $|N|$ half-periods on the length l_x (see Fig. 21).

Figs. 22-23 show the dependences of a real part of longitudinal wavenumber

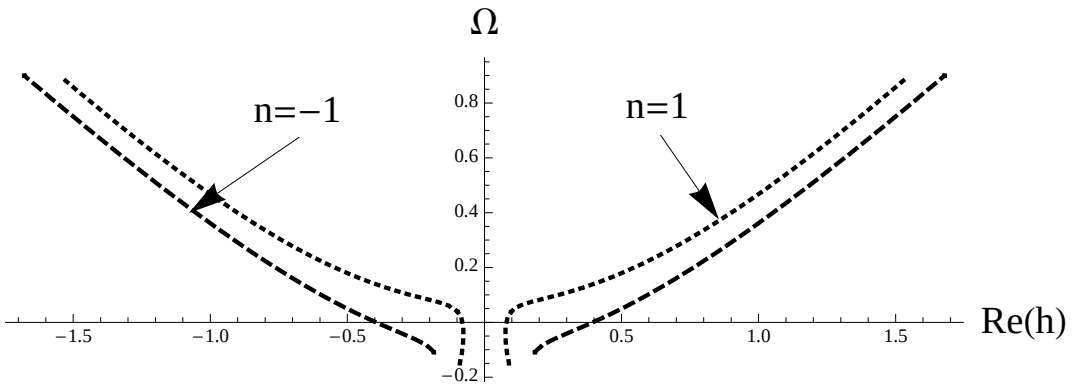

Fig. 22. The dispersion diagram of an open planar Bragg waveguide with regular periodicity for $n = \pm 1$. Real part of the longitudinal wavenumber Reh as a function of the frequency shift from the cutoff $\Omega = 2k/\bar{h} - 1$.

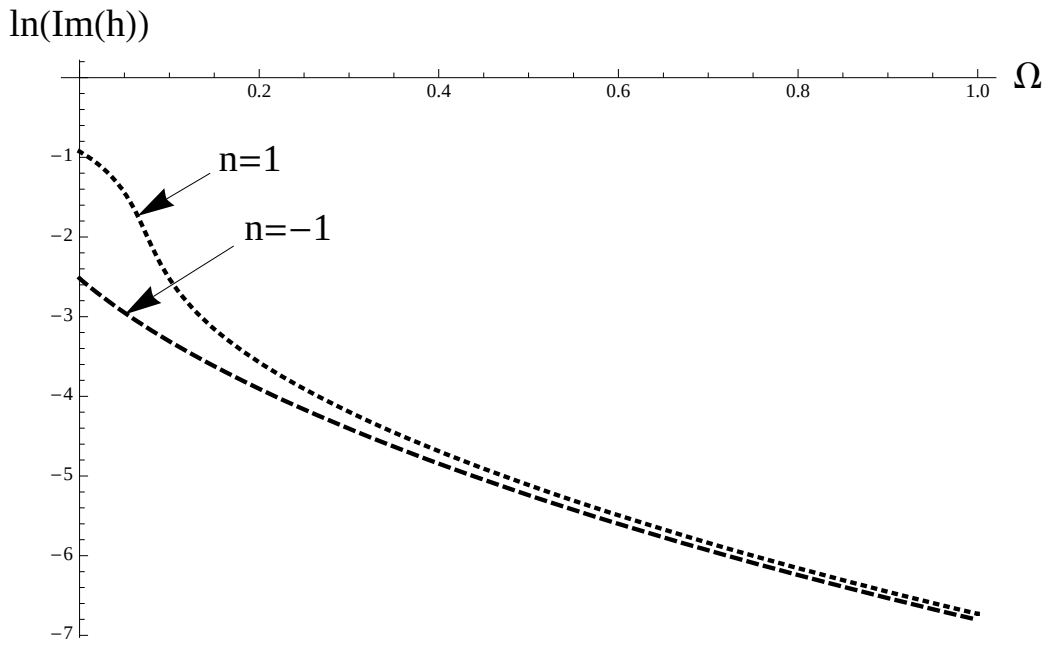

Fig. 23. The dispersion diagram of an open planar Bragg waveguide with regular periodicity for $n = \pm 1$. Diffraction losses ln(Imh) as a function of the frequency shift from the cutoff $\Omega = 2k/\bar{h} - 1$.

(Reh_n) and diffraction losses on a frequency detuning from the resonance frequency $\Omega = 2k/\bar{h} - 1$. Close to the cut-off frequency a longitudinal wavenumber does not reach zero. This fact is consistent with the energy flow through an open waveguide side surfaces (see Eq. (6.7)). The distance between branches for the neighboring modes is proportional to $\alpha/(\alpha l_x)^2 << 1$, while the diffraction losses decay with a growth of the waveguide width slowly as $1/l_x^3$. As a result, the structures with a strict periodicity have limited filtration. As in the case of Bragg resonators one can significantly increase selective properties of a waveguide by introducing a defect of periodicity.

3. Bragg waveguide with a defect of periodicity

Let us consider a step phase change in a modulation part of dielectric constant $\epsilon(x)$ by π in the transverse cross section of a waveguide. In this case a coupling becomes coordinate dependent: $\tilde{\alpha}(x) = \tilde{\alpha}\mathrm{sqn}(x - l_x/2)$. The idea is that it should lead to existence of a mode with small diffraction losses, which is localized in the vicinity of a defect. Similarly to the case of Bragg resonators, a dispersion relation analogies to Eq. (6.8) has the form:

$$2\alpha^2 = \left[\Gamma^2 - \Gamma\left(g\frac{\bar{h}}{2k}\right)\right]\exp(igl_x) + \left[\Gamma^2 + \Gamma\left(g\frac{\bar{h}}{2k}\right)\right]\exp(-igl_x). \qquad (6.12)$$

Eq. (6.12) has a solution at exact Bragg resonance (Re$\Gamma = 0$), which corresponds to a small diffraction losses coefficient (Imh). The wave envelope for this mode (I will set zeroth index for this fundamental mode) exponentially decays from the center of a waveguide to the edge as $\exp(-|\alpha l_x|)$ (See Fig. 24). The expressions for the transverse and longitudinal wavenumbers of the fundamental mode can be written as

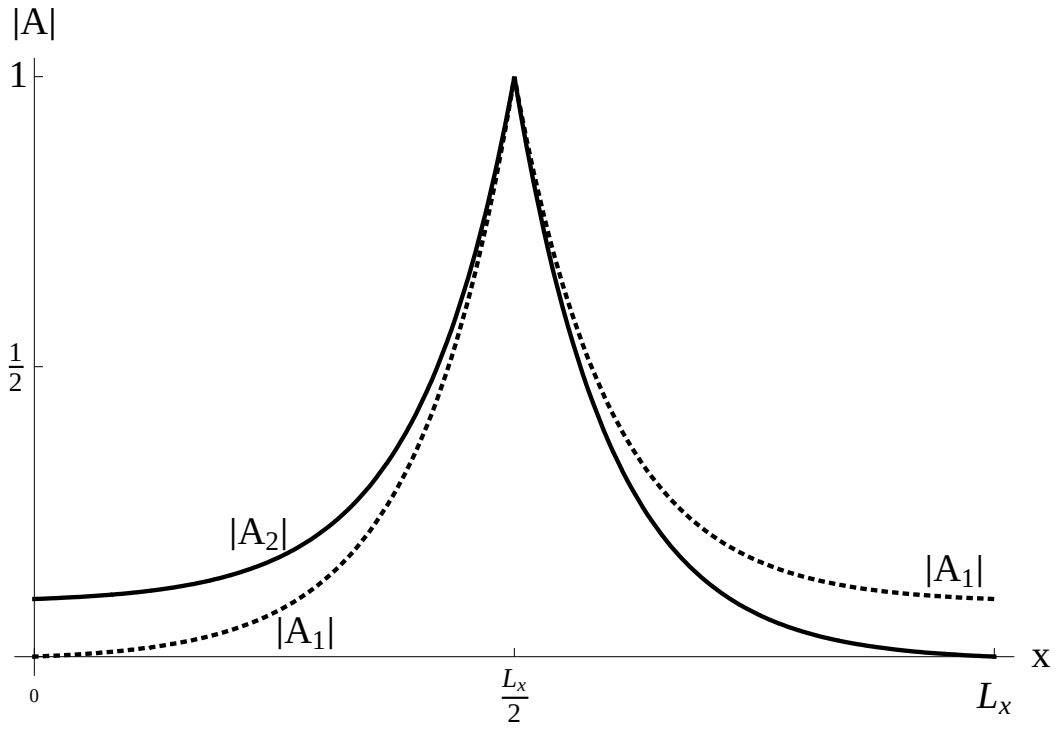

Fig. 24. The transverse structure of the fundamental mode with $n = 0$ localized in the vicinity of the defect.

follows:

$$g_0 = \pm i\alpha\frac{2k}{\bar{h}}, \quad \mathrm{Re}\Gamma_0 = 0, \quad \mathrm{Im}\Gamma_0 = -2\alpha\frac{k}{h}\exp\left(-\alpha\frac{2k}{\bar{h}}l_x\right). \tag{6.13}$$

For the large enough width of a structure l_x, modes of the higher order (parasitic modes) have significantly larger decay rates, since they decrease as $1/l_x^3$ as far as the decrement of the fundamental mode decreases exponentially as $\exp\left(-\alpha(2k/\bar{h})l_x\right)$. The wavenumbers of parasitic modes are given by:

$$g_n = 2\frac{\pi n}{l_x} - 2i\frac{\pi n}{\alpha l_x^2}\frac{\bar{h}}{2k},\ \mathrm{Re}\Gamma_n = \alpha\frac{n}{|n|}\left(1 + 2\left(\frac{\pi n}{\alpha l_x}\frac{\bar{h}}{2k}\right)^2\right),\ \mathrm{Im}\Gamma_n = -\alpha 4\frac{(\pi n)^2}{(\alpha l_x)^3}\left(\frac{\bar{h}}{2k}\right)^3. \tag{6.14}$$

Corresponding dependences of dispersion curves as well as transverse structure of

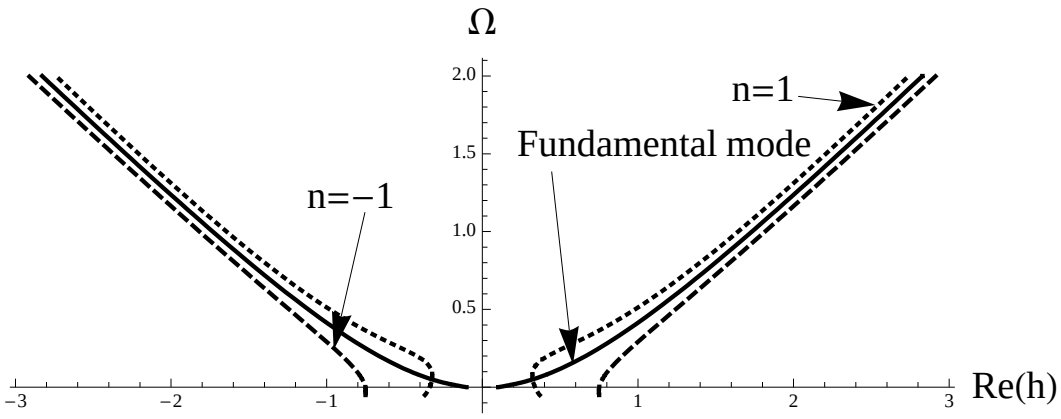

Fig. 25. The dispersion diagram of an open planar Bragg waveguide with a defect of periodicity for fundamental mode with $n = 0$ and modes with $n = \pm 1$. Real part of longitudinal wavenumber Reh as a function of the frequency shift form the cutoff $\Omega = 2k/\bar{h} - 1$.

parasitic modes with lowest indices $n = \pm 1$ are depicted in Figs. 25 - 26 and Fig. 27, respectively. It is worth noting that mode filtration becomes better as frequency increases. A dependence of corresponding filtration coefficient (ratio of decrements of higher order modes to decrement of the fundamental mode) on a frequency is depicted on Fig. 28.

4. Large detuning from the cut-off frequency

For a practical use of a Bragg waveguides it is more convenient to consider regimes with large enough group velocity, which can be realized in the case of large radiation frequency detuning from the cut-off frequency (Bragg frequency). In this case one can simplify Eq. (6.10) expanding it with respect to small parameter α:

$$\mathrm{Re}h_n = h_0 - \frac{k}{h_0}\mathrm{Re}\Gamma_n, \quad \mathrm{Im}h_n = -\frac{k}{h_0}\mathrm{Im}\Gamma_n, \tag{6.15}$$

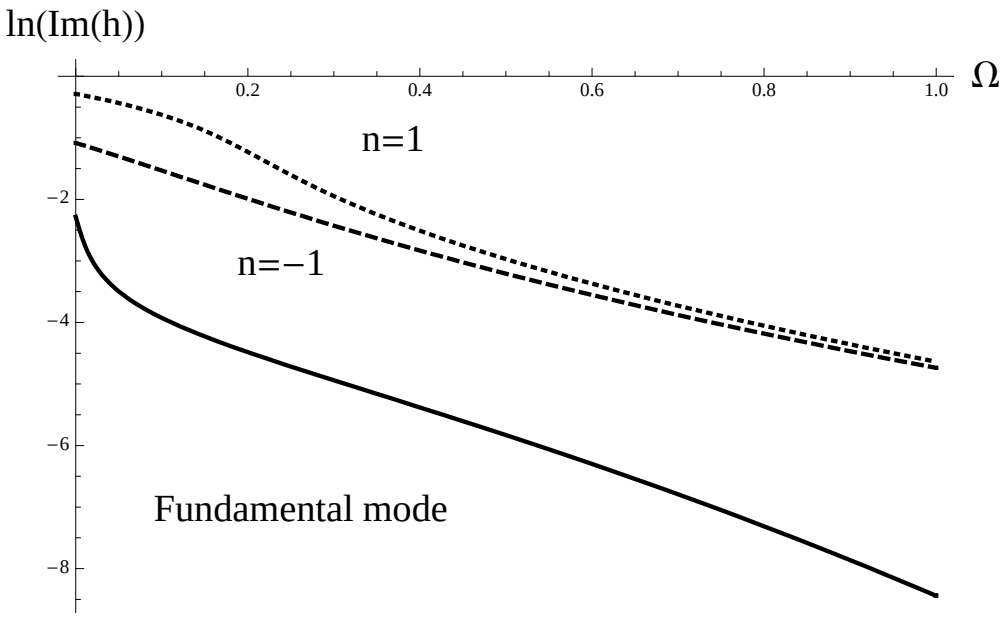

Fig. 26. The dispersion diagram of an open planar Bragg waveguide with a defect of periodicity for fundamental mode with $n = 0$ and modes with $n = \pm 1$. Diffraction losses $\ln(\mathrm{Im}h)$ as a function of the frequency shift form the cutoff $\Omega = 2k/\bar{h} - 1$.

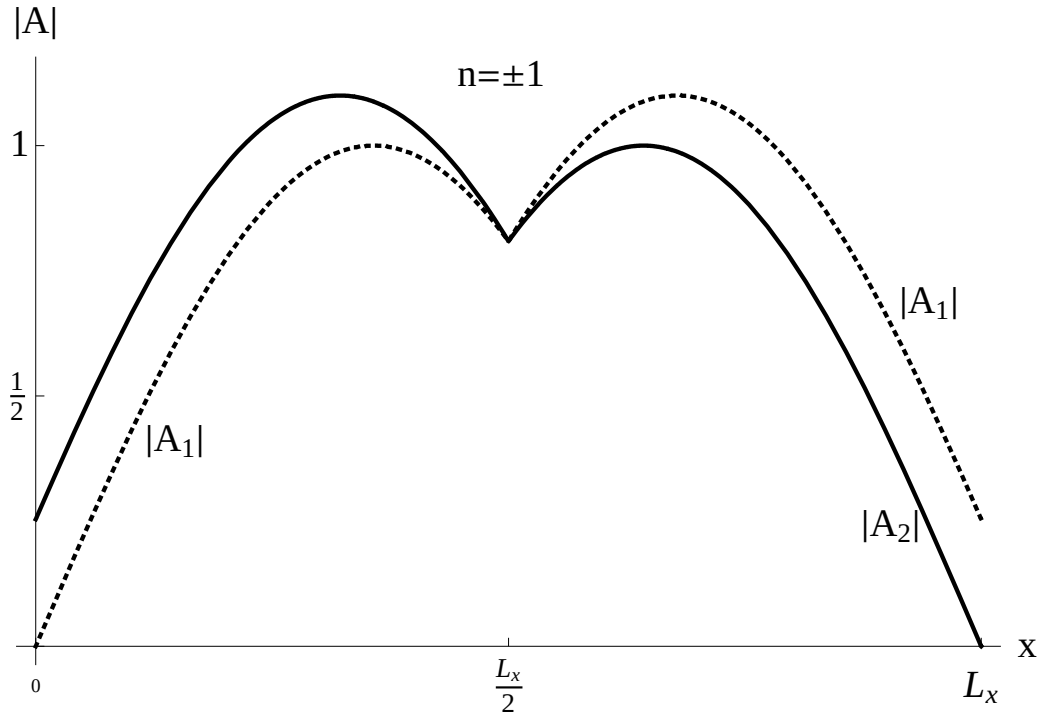

Fig. 27. The transverse structure of a waveguide mode with a defect of periodicity for $n = \pm 1$.

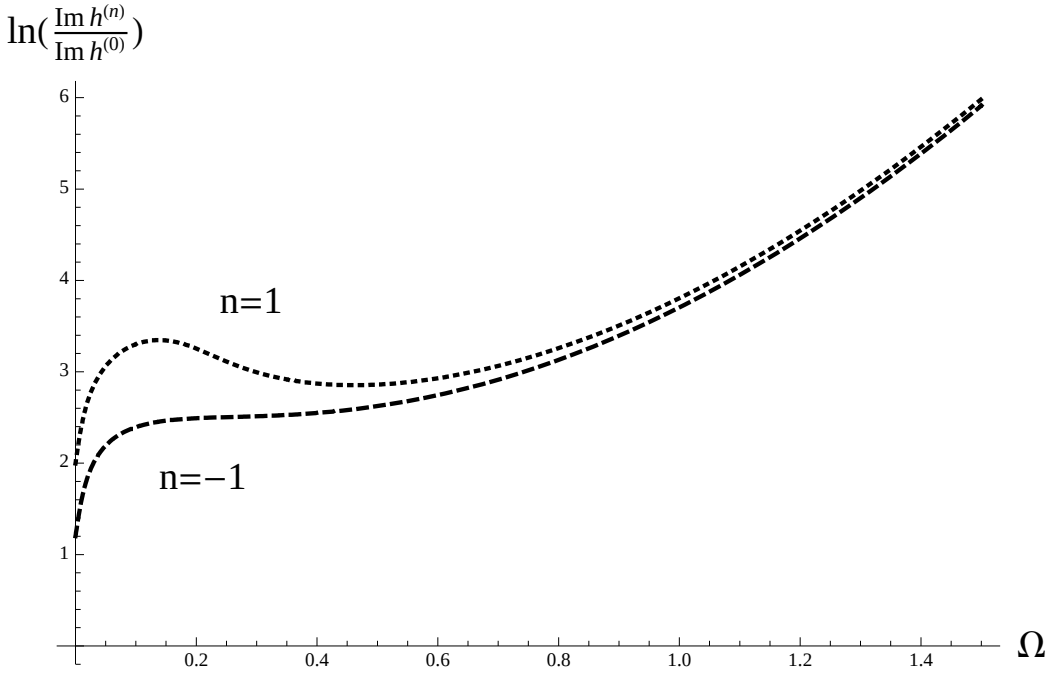

Fig. 28. Filtration coefficient (ratio of decrements of higher order modes to a decrement of the fundamental mode) as a function of the frequency shift form the cutoff $\Omega = 2k/\bar{h} - 1$.

where $h_0 = \sqrt{k^2 - \bar{h}^2/4}$. Expressions for Γ_n from Eq. (6.14) transform Eq. (6.15) for a regularly periodic problem as follows:

$$\mathrm{Re}h_n = h_0 - \alpha\frac{k}{h_0}\frac{n}{|n|}\left(1 + \frac{1}{2}\left(\frac{\pi n}{\alpha l_x}\frac{\bar{h}}{2k}\right)^2\right), \quad \mathrm{Im}h_n = -\alpha\frac{k}{h_0}\frac{1}{2}\frac{(\pi n)^2}{(\alpha l_x)^3}\left(\frac{\bar{h}}{2k}\right)^3, \quad (6.16)$$

and modify Eq. (6.9) for a problem with defect of periodicity as follows:

$$\mathrm{Re}h_n = h_0 - \alpha\frac{k}{h_0}\frac{n}{|n|}\left(1 + 2\left(\frac{\pi n}{\alpha l_x}\frac{\bar{h}}{2k}\right)^2\right), \quad \mathrm{Im}h_n = -\alpha\frac{k}{h_0}4\frac{(\pi n)^2}{(\alpha l_x)^3}\left(\frac{\bar{h}}{2k}\right)^3. \quad (6.17)$$

Close to the cut-off frequency expressions from Eq. (6.15) diverge. Formally it corresponds to the infinitely large diffraction losses and is caused by the violation of the applicability conditions.

Its worth noting that Eq. (6.15) can be obtained directly from the wave equation if one seeks a solution as a superposition of two partial waves propagating in the directions which form an angle ϕ between each other. As a result, the equation for the amplitude can be written as follows:

$$\frac{h_0}{k}\frac{dA_{1,2}}{dz} \mp \frac{\bar{h}}{2k}\frac{dA_{1,2}}{dx} + i\alpha A_{2,1} = 0. \quad (6.18)$$

Seeking a solution in the form $A_{1,2}(x,z)\exp(igx + i\Gamma z)$ one can obtain Eq. (6.15). It is important to mention that in the following section we will use this approximation to study the disperion relation for a planar waveguide with slight corrugation of the metal plates.

B. Planar Bragg waveguide with slightly corrugated plates

A discussed in the previous section Bragg waveguide based on a dielectric layer with the periodic modulation of the dielectric constant was important for us since it allows us to study the main properties of the mentioned waveguides. However, as in the

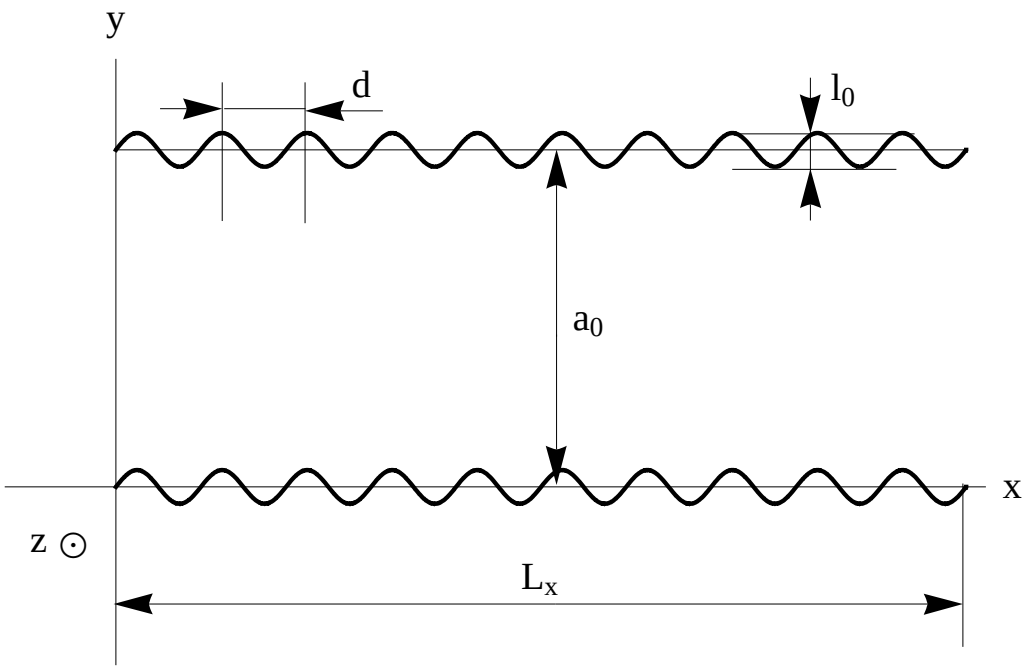

Fig. 29. The scheme of an open planar Bragg waveguide formed by two metal plates with a shallow corrugation. Wave propagates in z direction which is transverse to the lattice vector $\vec{\bar{h}} = \vec{x}^{(0)}\bar{h}$, $\bar{h} = 2\pi/d$. The transverse cross section.

case of Bragg resonators [37, 41, 42], for the relativistic electronics more practical is to introduce a waveguides which can be constructed by taking two metal plates with slightly corrugated walls.

Let us consider a planar waveguide (Fig. 29) with weakly corrugated walls:

$$l = l_0 \cos(\bar{h}x), \tag{6.19}$$

where $2l_0$ is a depth of corrugation. Let us assume that a lattice vector $\vec{\bar{h}} = \vec{x}^{(0)}\bar{h}$ is directed along the x-axis and its wavenumber is $\bar{h} = \frac{2\pi}{d}$, where d is period of corrugation. Coupling occurs for the TEM waves with x- and z- wavenumbers satisfying

Bragg resonance conditions (see Fig. 2):

$$h_{x_1} = -h_{x_2} = \bar{h}/2, \qquad h_{z_1} = h_{z_2} = h = \sqrt{k^2 - \left(\bar{h}/2\right)^2},$$

where $k = \omega/c$. Thus, the electric and magnetic fields can be presented as a linear combination of two TEM modes of a corresponding regular waveguide (Fig. 2)

$$\begin{cases} \vec{E} = \mathrm{Re}\left[\left(A_1(x,z)\vec{E}_1^{(0)}e^{i\frac{\bar{h}}{2}x} + A_2(x,z)\vec{E}_2^{(0)}e^{-i\frac{\bar{h}}{2}x}\right)e^{i\omega t - ihz}\right], \\ \vec{H} = \mathrm{Re}\left[\left(A_1(x,z)\vec{H}_1^{(0)}e^{i\frac{\bar{h}}{2}x} + A_2(x,z)\vec{H}_2^{(0)}e^{-i\frac{\bar{h}}{2}x}\right)e^{i\omega t - ihz}\right]. \end{cases} \tag{6.20}$$

Under an assumption that a corrugation depth is much less than a wavelength λ and a corrugation period, d: $l_0 << \lambda, d$, a perturbation of the waveguide plates can be treated by using the equivalent surface magnetic current [67]:

$$\vec{j^m} = \frac{c}{4\pi}\left[\vec{n}, \nabla(l(x)\vec{E}, \vec{n}) + i\frac{\omega}{c}l\left[\vec{n}, \vec{H}\right]\right], \tag{6.21}$$

where $\vec{n}$ is an external normal to the surface.

As a result for slowly varying (in the wavelength scale) partial waves amplitudes $A_{1,2}(x,z)$, one can write the coupling wave equations as follows:

$$\frac{h}{k}\frac{dA_{1,2}}{dz} \pm \frac{\bar{h}}{2k}\frac{dA_{1,2}}{dx} = -\frac{1}{N_{1,2}}\oint \vec{j^m}\vec{H}_{-1,2}d\sigma, \tag{6.22}$$

where integration in the right hand side of Eq. (6.22) is performed over the unperturbed contour of a waveguide, $N_{1,2} = \frac{c}{2\pi}\int \vec{E}_{1,2}^{(0)}\vec{H}_{-1,2}^{(0)}dS = ca_0/(2\pi)$ - norms of the interacting waves, a_0 is a distance between plates. Neglecting high frequency oscillating terms and terms of the high order with respect to $1/\lambda$ in the right hand side of Eq. (6.22) one can obtain the following equations:

$$\frac{h}{k}\frac{dA_{1,2}}{dz} \mp \frac{\bar{h}}{2k}\frac{dA_{1,2}}{dx} + i\alpha A_{2,1} = 0, \tag{6.23}$$

where

$$\alpha = \frac{l_0}{4a_0}\frac{\bar{h}^2}{2k} \tag{6.24}$$

is a coupling parameter, $k = 2\pi/\lambda$. If we introduce an angle ϕ between the partial waves propagation directions - $\sin\phi = \bar{h}/2k$, a coupling parameter can be represented as $\alpha = (l_0/4a_0)\bar{h}\sin\phi$. Therefore, in contrast with the case of medium with a periodic modulation of dielectric constant, in the planar waveguide a coupling parameter depends on the angle between partial waves.

The maximum value of a coupling parameter takes place when frequency tends to the cutoff frequency, $\omega \to \omega_c = c\bar{h}/2$ and wave vectors of two partial waves are counter directional ($\phi = \pi/2$). A coupling parameter and an angle ϕ decreases while a frequency shift from the cutoff increases.

By presenting a solution of Eqs. (6.23) as $A_{1,2}\exp(igx + i\Gamma z)$, we obtain the dispersion relation for the unbounded grating over x as follows:

$$\left(\frac{\bar{h}}{2}g\right)^2 = (k\Gamma)^2 - (k\alpha)^2, \tag{6.25}$$

where g and Γ are small amendments to the transverse and longitudinal wavenumbers, $|g| << \bar{h}/2$, $|\Gamma| << h_0$.

A defect of corrugation periodicity in the middle of a waveguide can be entered as π phase step of a waveguide corrugation phase in Eq. (6.19) which leads to a change of the sign of α in Eq. (6.23) at the point $x = l_x/2$:

$$\alpha = \alpha(x) = \begin{cases} -|\alpha|, x < l_x/2, \\ +|\alpha|, x > l_x/2. \end{cases} \tag{6.26}$$

Using expressions for coupled waves in Eqs. (6.23), one can find eigenmodes of an open in the x direction planar Bragg waveguide with a width l_x. In this case the

boundary conditions for the partial waves can be presented as follows:

$$A_1(0) = A_2(l_x) = 0. \tag{6.27}$$

From the wave coupling equation (Eq. (6.23)), taking into account Eq. (6.27) and field continuity condition on the step of corrugation, the dispersion relation for a Bragg waveguide can be presented in a form similar to that known in theory of Bragg resonators [37, 38, 41]:

$$2\alpha^2 = \left[\Gamma^2 - \Gamma\left(g\frac{\bar{h}}{2k}\right)\right]\exp(igl_x) + \left[\Gamma^2 + \Gamma\left(g\frac{\bar{h}}{2k}\right)\right]\exp(-igl_x). \tag{6.28}$$

Solution of Eqs. (6.28) can be found analytically in the assumption of a strong wave coupling ($\alpha l_x >> 1$). The spectrum of longitudinal wavenumbers includes a single mode at exact Bragg resonance with $\mathrm{Re}\Gamma = 0$ (which will be treated as fundamental mode with an index $n = 0$),

$$g_0 = \pm i\alpha\frac{2k}{\bar{h}}, \quad \mathrm{Re}\Gamma_0 = 0, \quad \mathrm{Im}\Gamma_0 = -2\alpha\frac{k}{h}\exp\left(-\alpha\frac{2k}{\bar{h}}l_x\right) \tag{6.29}$$

and a set of higher order modes:

$$g_n = \frac{\pi n}{l_x} - 2i\frac{\pi n}{\alpha l_x^2}\frac{\bar{h}}{2k},$$

$$\mathrm{Re}\Gamma_n = \alpha\frac{k}{h}\frac{n}{|n|}\left(1 + 2\left(\frac{\pi n}{\alpha l_x}\frac{\bar{h}}{2k}\right)^2\right), \qquad \mathrm{Im}\Gamma_n = -\alpha\frac{k}{h}4\frac{(\pi n)^2}{(\alpha l_x)^3}\left(\frac{\bar{h}}{2k}\right)^3, \tag{6.30}$$

where $n = \pm 1, \pm 2, \pm 3, ...$ are the mode indices.

Figs. 30 - 31 demonstrate the dispersion diagrams for a different mode numbers and the diffraction losses curves as a function of the frequency shift from the cutoff. It should be noted that expressions in Eqs. (6.29),(6.30) diverge at $h \to 0$, while frequency tends to the cutoff. These formally infinite diffraction losses appear when the applicability conditions of a perturbation theory fail to fulfill. Nevertheless, for a

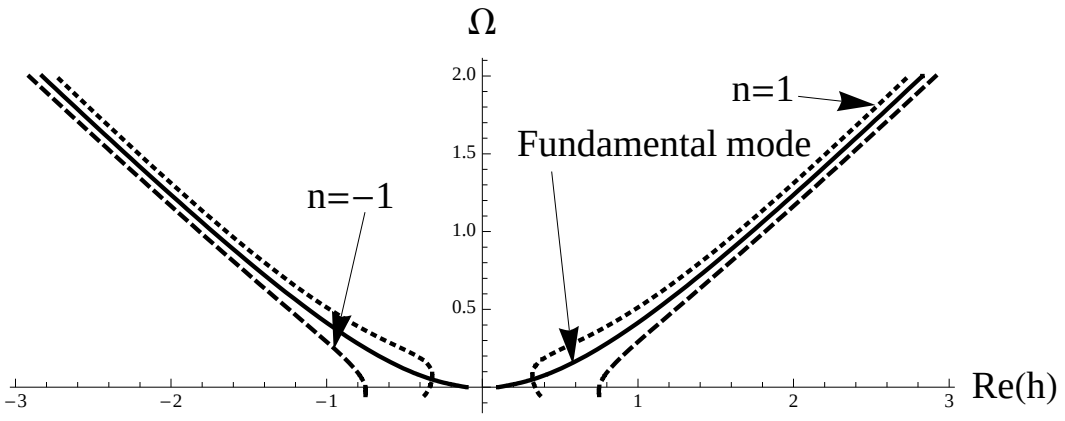

Fig. 30. The dispersion diagram of an open planar Bragg waveguide formed by two metal corrugated plates with a defect of periodicity for fundamental mode with $n = 0$ and modes with $n = \pm 1$. Real part of the longitudinal wavenumber Reh as a function of the frequency shift form the cutoff $\Omega = 2k/\bar{h} - 1$.

practical use of a Bragg waveguides, one needs to consider the case where group velocities of the waves are large, which corresponds to rather large detunings of radiation frequency from the cut-off (Bragg frequency) where expressions in Eqs. (6.29),(6.30) are non-divergent.

For $n > 0$ the transverse structure of n^{th} waveguide mode represents a distribution close to a standing wave with sine wave envelope having $|n|$ half-periods on the length l_x (Fig. 27), while the lowest mode distribution is localized near the defect and has the exponential transverse structure (Figs. 32, 33). A corresponding calculation was performed using a visualization environment of CST Microwave Studio package. Diffraction losses (ImΓ) of this mode are proportional to $\exp\left(-|2k\alpha l_x/\bar{h}|\right)$ and are very small at large l_x, while the higher order modes have significantly greater decrements (which decrease only as $1/l_x^3$) than the fundamental mode decrement. Thus, the outlined above Bragg structures can be used for highly selective waveguiding.

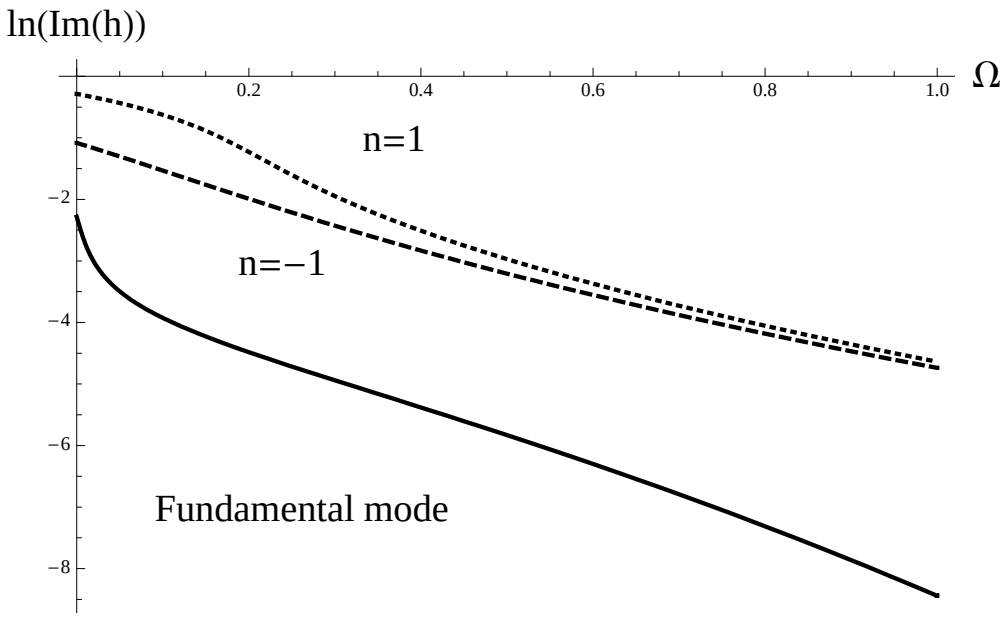

Fig. 31. The dispersion diagram of an open planar Bragg waveguide formed by two metal corrugated plates with a defect of periodicity for fundamental mode with $n = 0$ and modes with $n = \pm 1$. Diffraction losses $\ln(\mathrm{Im}h)$ as a function of the frequency shift form the cutoff $\Omega = 2k/\bar{h} - 1$.

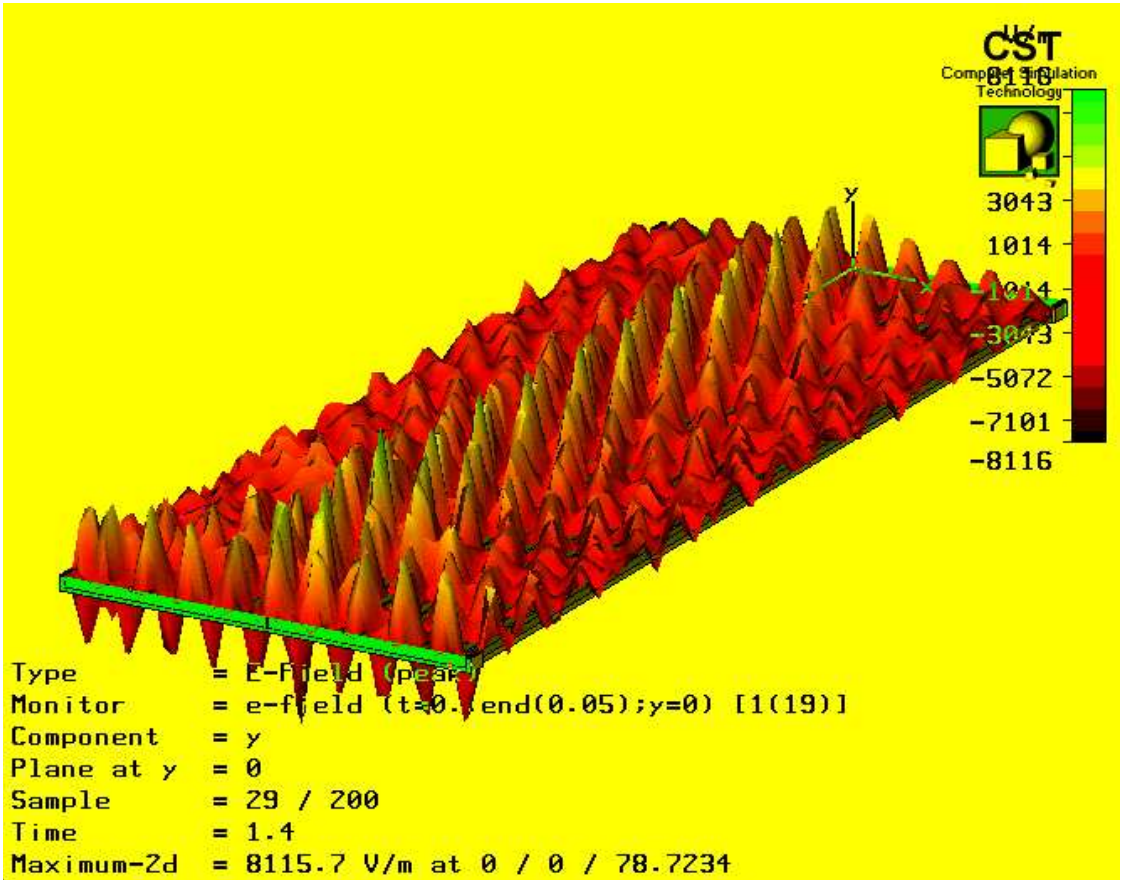

Fig. 32. The transverse structure of the principle mode for $n = 0$ localized in the vicinity of the defect. Simulation by Microwave Studio.

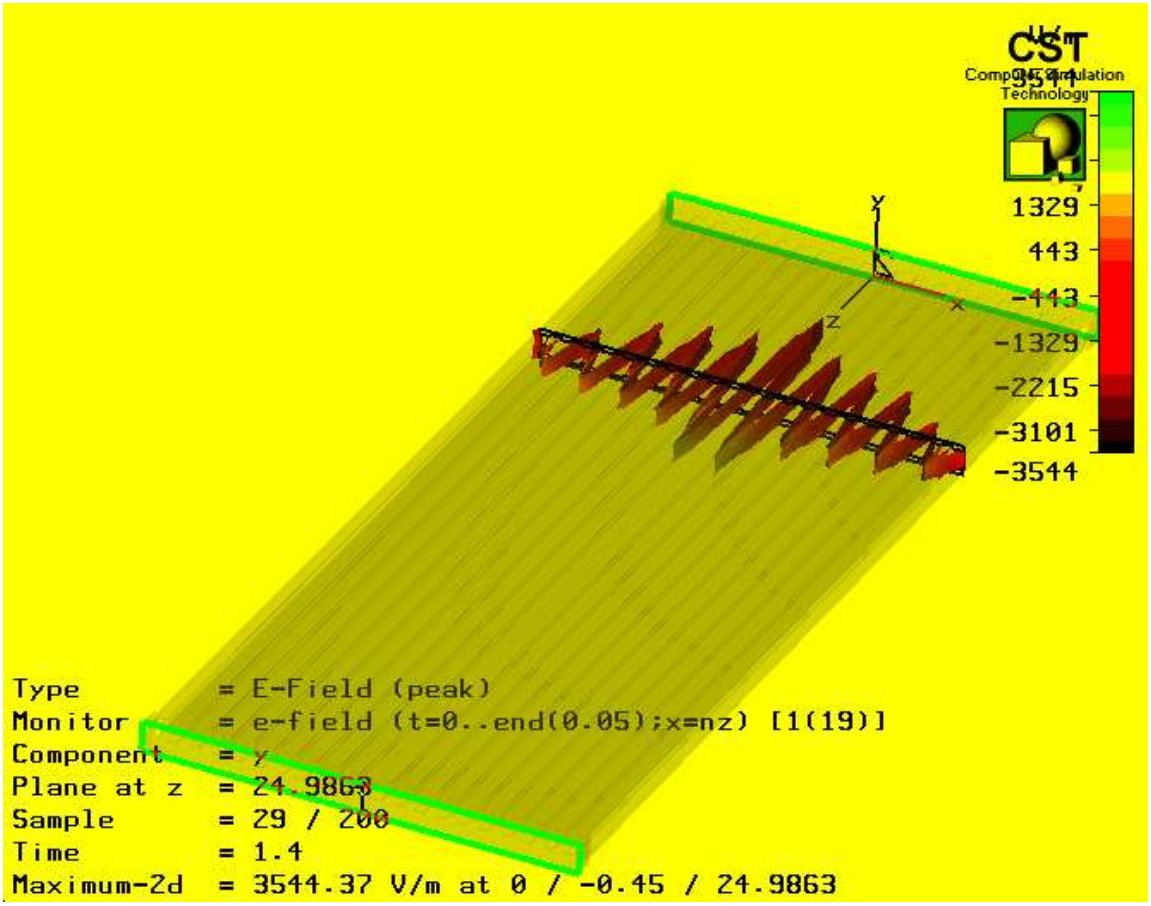

Fig. 33. The transverse structure of the principle mode for $n = 0$ localized in the vicinity of the defect. Transverse cross section view. Simulation by Microwave Studio.

CHAPTER VII

FREE ELECTRON LASER AMPLIFIERS BASED ON PLANAR BRAGG WAVEGUIDES

A. Free Electron Laser amplifier with Bragg waveguide

Let us consider amplifier scheme of a free electron laser (FEL) driven by a sheet electron beam with a waveguide system formed by a planar Bragg structure described in Chapter VI. Alongside with selectivity, the advantage of above structure is its compatibility with the beam transportation system. We assume that a thin, over the y coordinate, sheet electron beam moves in the undulator field

$$H_y = \mathrm{Re}\left(H_u e^{ih_u z}\right) \tag{7.1}$$

and is guided by a uniform magnetic field. This beam is synchronous to the fundamental mode of the waveguide described in Chapter VI, Section B under resonance condition:

$$\omega - h v_{||} \approx \Omega_b. \tag{7.2}$$

We assume that a bounce frequency $\Omega_b = 2\pi v_{||}/d_u$ (d_u is an undulator period) is far from a cyclotron synchronism with electrons: $|\Omega_b - \omega_H|T >> 2\pi$, where $\omega_{H_0} = eH_0/m_0 c\gamma_0$ is a cyclotron frequency, $v_{||}$ is a longitudinal velocity of electrons, $\gamma_0 = (1 - v^2/c^2)^{-1/2} >> 1$ is the relativistic factor, T is a characteristic time of interaction (a reverse gain).

Let us present the electromagnetic field as a Bragg waveguide mode:

$$\vec{E} = \vec{y}^{(0)} \mathrm{Re}\left(A(z) f(x) e^{i\omega t - ihz}\right), \tag{7.3}$$

where$f(x)$ is a transverse structure of the fundamental mode given by Fig. 24 (we

fix $f(l_x/2) = 1$). The process of a signal amplification can be described by equation of excitation of the waveguide mode:

$$\frac{dA}{dZ} + \tilde{\Gamma} A = \int_0^{L_x} I(X) f^*(X) dX, \tag{7.4}$$

by RF electron current $I(X) = (1/\pi) \int_0^{2\pi} e^{-i\theta(X)} d\theta_0$. This current can be found from the averaged electron motion equations [41]:

$$\frac{d^2\theta}{dZ^2} = \mathrm{Re}\left(A f(X) e^{i\theta}\right). \tag{7.5}$$

The boundary conditions for Eqs. (7.4) - (7.5) take the form:

$$\left.\frac{d\theta}{dZ}\right|_{X=0} = 0, \qquad \theta|_{X=0} = \theta_0 \in [0, 2\pi), \qquad A|_{Z=0} = A_0. \tag{7.6}$$

Here the following normalized variables and parameters have been used: $Z = Ckz$, $A = e\kappa\mu \mathrm{A}/(nc\omega\gamma C^2)$, θ is an electron phase, $C = \left((eI_0\mu c\kappa^2)/(mc^3 L_x \omega_c \gamma_0 N)\right)^{1/3}$ is a gain parameter, $\kappa = \Omega_b e H_u/(mc\omega_c\gamma_0(\Omega_b - \omega_H))$ is an electron-wave coupling parameter, $\mu \approx (1 + \Omega_b e^2 H_u^2/m^2c^2(\Omega_b - \omega_H)^3)\gamma_0^{-2}$ is an inertial bunching parameter, $N \approx h/(8\pi \mathrm{Im} g_0)$ is the fundamental mode norm, g_0 is given by Eq. (6.29), $\tilde{\Gamma} = \mathrm{Im}\Gamma_0/(kC)$, $\mathrm{Im}\Gamma_0$ is a diffraction losses parameter for the fundamental mode given by Eq. (6.29).

Fig. 34 demonstrates a dependence of amplification coefficient $\Gamma = |A(Z)|^2/A_0^2$ on a longitudinal coordinate found from numerical simulation of Eqs. (7.4), (7.5).

Using the presented analysis we can estimate a set of parameters for a 4 mm FEL that can be realized on the base of U2 high current accelerator at BINP RAS, Novosibirsk (a width of the beam is $\propto 15\ cm$, an energy of the electrons is $1\ MeV$, a current density is $j_0 = 1\ kA/cm$) [68]. We assume that an undulator period is $d_u = 3.6\ cm$, an undulator field amplitude $H_u = 2\ kOe$, a guiding magnetic field $H_0 = 10\ kOe$, $a_0 = 4\ cm$ (gain parameter is $C = 0.04$). The above parameters

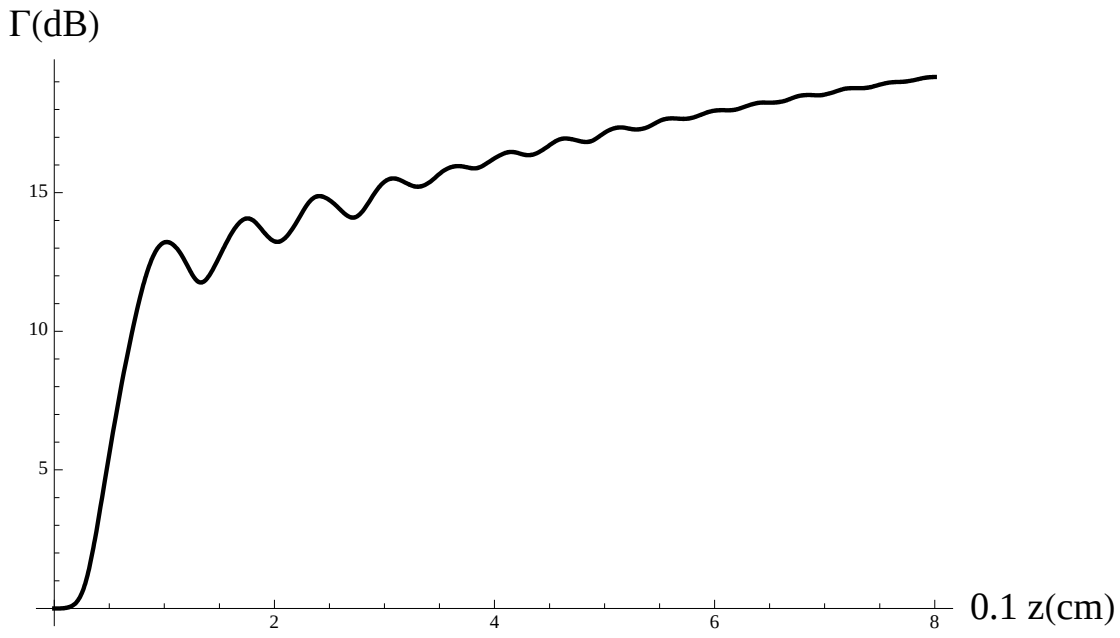

Fig. 34. The longitudinal dependence of an amplification coefficient for 4mm FEL amplifier. At the following parameters of the Bragg waveguide $l_0 = 0.4\ mm$, $d = 6\ mm$, $l_x = 15\ cm$, $l_z = 100\ cm$, one can get a gain up to 20 dB.

were selected in a way that facilitates the grazing regime of the interaction, which is beneficial for an increasing amplification frequency band. At the following parameters of a Bragg waveguide $l_0 = 0.4\ mm$, $d = 6\ mm$, $l_x = 15\ cm$, $l_z = 100\ cm$, one can get a gain up to 20 dB.

B. Laser amplifier with Bragg waveguide

A theory similar to the one developed above can be applied also to a medium with periodic modulation of dielectric constant:

$$\epsilon^{\text{Bragg}} = 1 + \tilde{\alpha}\cos(\bar{h}x). \tag{7.7}$$

In this case, like in previous one, a defect of periodicity is introduced and $\tilde{\alpha}$ is considered dependant on x (see Eq. (6.26)). The coupled waves equations (Eqs. (6.23)) with a wave coupling coefficient $\alpha = \tilde{\alpha}k/4$ are derived directly from the Helmholtz equation after substituting expressions for slow amplitudes from Eq. (6.5) and averaging over the space coordinates.

The modes of this structure with an open boundaries, described by boundary conditions in Eq. (6.27), are similar to those found in Eqs. (6.29)-(6.30) and have the following dependences (see Figs. 35, 36) of the longitudinal wavenumbers on frequency:

$$\text{Re}h_0 = h, \qquad \text{Im}h_0 = -2\alpha\frac{k}{h}\exp\left(-\alpha\frac{2k}{\bar{h}}l_x\right),$$
$$\text{Re}h_n = h - \alpha\frac{k}{h}\frac{n}{|n|}\left(1 + 2\left(\frac{\pi n}{\alpha l_x}\frac{\bar{h}}{2k}\right)^2\right), \qquad \text{Im}h_n = -\alpha\frac{k}{h}4\frac{(\pi n)^2}{(\alpha l_x)^3}\left(\frac{\bar{h}}{2k}\right)^3. \tag{7.8}$$

Let us consider a laser amplifier with this Bragg structure. We assume that the transition frequency is equal to the frequency of amplified signal and will describe an

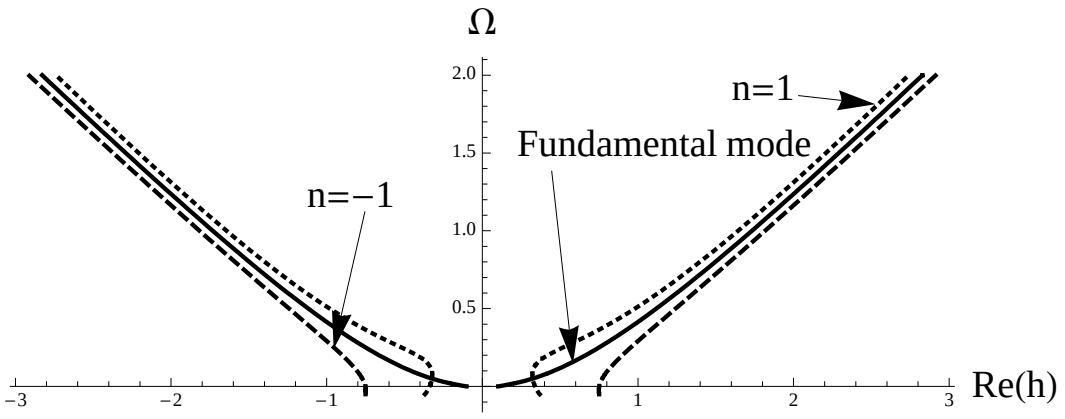

Fig. 35. The dispersion diagram of an open planar Bragg waveguide for a FEL formed by two metal corrugated plates with defect of periodicity for fundamental mode with $n = 0$ and modes with $n = \pm 1$. Real part of the longitudinal wavenumber Reh as a function of the frequency shift form the cutoff $\Omega = 2k/\bar{h} - 1$.

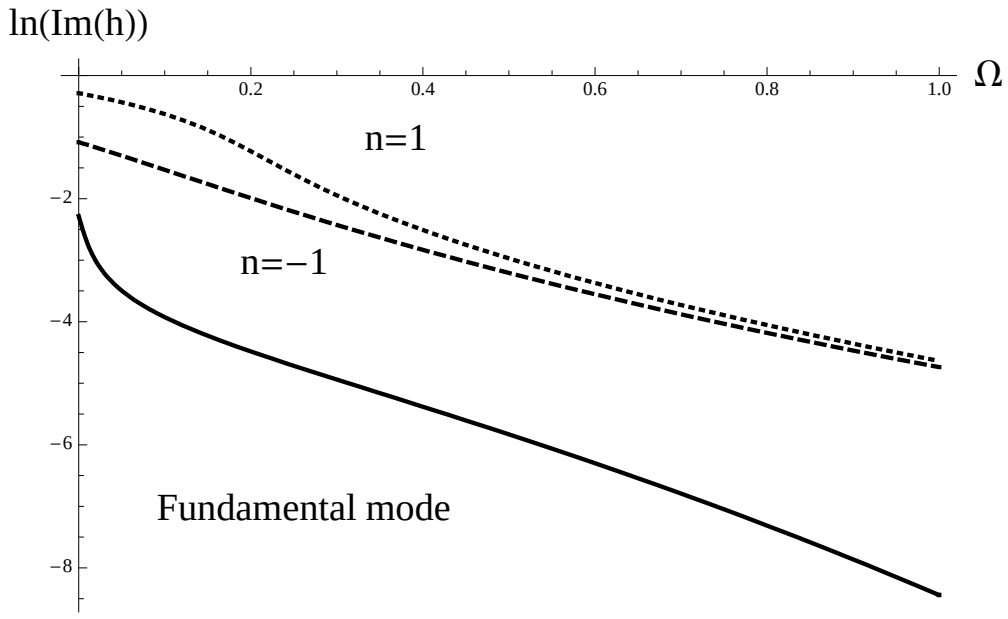

Fig. 36. The dispersion diagram of an open planar Bragg waveguide for FEL formed by two metal corrugated plates with defect of periodicity for fundamental mode with $n = 0$ and modes with $n = \pm 1$. Diffraction losses ln(Imh) as a function of the frequency shift form the cutoff $\Omega = 2k/\bar{h} - 1$.

active medium by a nonlinear negative conductance (an imaginary part of dielectric constant). In the simplest case, we can use cubic approximation:

$$\epsilon^{\text{active}} = 1 + i\nu(1 - p|E|^2). \tag{7.9}$$

Substituting electromagnetic field as a sum of the partial waves (see Eq. (6.5)), we obtain equations which describe, alongside with amplification, both linear and nonlinear wave coupling:

$$\begin{aligned} &\frac{\partial}{\partial Z}a_1 + \frac{\partial}{\partial X}a_1 + ia_2 - \tilde{\nu}\left(1 - \left(|a_1|^2 + 2|a_2|^2\right)\right)a_1 = 0, \\ &\frac{\partial}{\partial Z}a_2 - \frac{\partial}{\partial X}a_2 - ia_1 - \tilde{\nu}\left(1 - \left(|a_2|^2 + 2|a_1|^2\right)\right)a_2 = 0, \end{aligned} \tag{7.10}$$

where:

$$X = \frac{2\alpha k}{\bar{h}}, \quad Z = \frac{\alpha k}{h}, \quad a_{1,2} = \sqrt{p}A_{1,2}, \quad \tilde{\nu} = \frac{k\nu}{2\alpha}.$$

Boundary conditions for Eqs. (7.10) under an assumption that an input wave incident angle corresponds to a partial wave A_1 are as follows:

$$a_1(Z = 0) = a_0(Z), \quad a_2(Z = 0) = 0, \quad a_1(X = 0) = 0, \quad a_2(X = l_x) = 0. \tag{7.11}$$

The results of a simulation of Eqs. (7.10) are shown in Figs. 37, 38. A formation of the principal ($n = 0$) mode in Eq. (7.8) is clearly seen. The amplification factor is rather high, and the saturation for chosen parameters begins at $Z = 400$.

Thus, above analysis shows rather high gain of the novel amplification schemes with simultaneous discrimination of parasitic modes. However, a disadvantage of a described scheme of a laser and FEL amplifier is its rather low efficiency arising due to the standing wave transverse structure of the operating mode. Approximately half of the active medium (or electrons) is situated in the low (or zero) field and does not interact effectively with electromagnetic field.

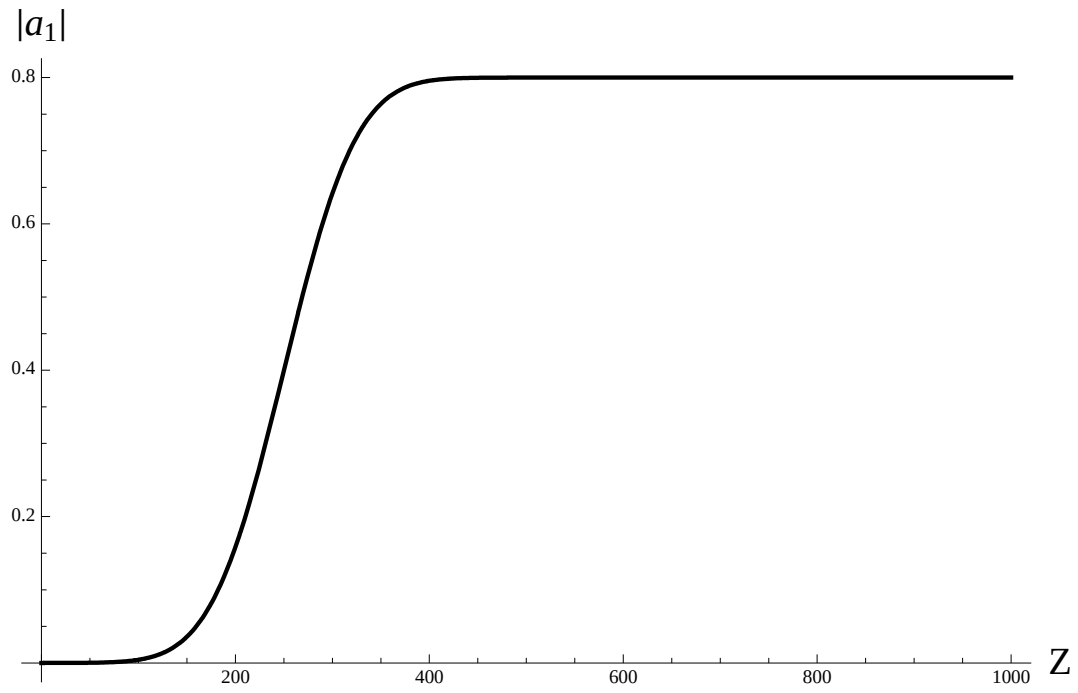

Fig. 37. The results of simulation of a laser amplifier for $k = \sqrt{2}\bar{h}(\phi = 45^o)$, $\alpha l_x = 8$, $\tilde{\nu} = 0.02$. The longitudinal dependence of the field amplitude.

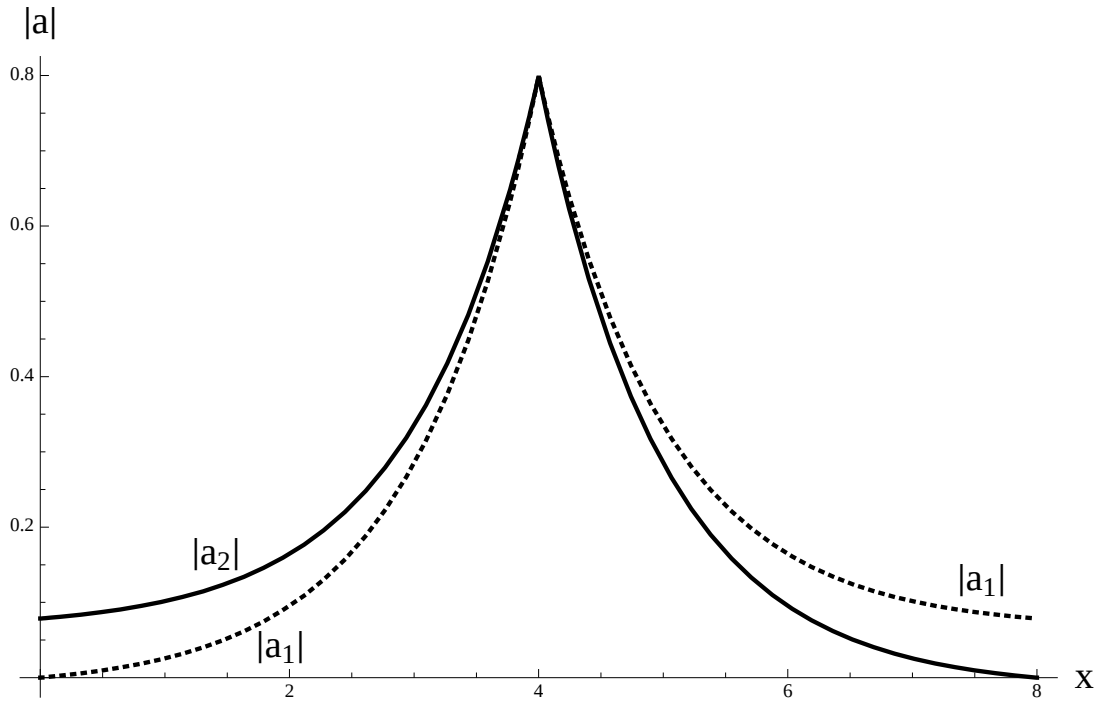

Fig. 38. The results of simulation of a laser amplifier for $k = \sqrt{2}\bar{h}(\phi = 45^o)$, $\alpha l_x = 8$, $\tilde{\nu} = 0.02$. The transverse distribution for the partial waves a_1 (solid line) and a_2 (dotted line) at $Z = 500$.

Nevertheless, for a FEL amplifiers there are some ways, which allow us to improve an operating performance. One possibility is based on the coupling between two TEM waves $A_{\pm}$ propagating at some angle to the axis and the wave B with higher y-index propagating directly along the system axis, which is synchronous to the beam propagating along the same axis. The coupling is provided by the regular corrugation under the following Bragg resonance condition: $\bar{h} = 2h_x$, where h_x is the transverse wavenumber of the TEM modes.

Another possible solution is a realization of so-called transverse current amplification scheme [45, 54–58]. In this scheme electron beam propagates in the described structure at angle ϕ to its axis so that a beam is synchronous with only one of the partial waves forming the waveguide mode. I will be considering this possibility in more details in the following section.

C. Transverse current FEL amplifier

Let us consider a propagating electromagnetic wave in a periodic Bragg structure, which is essentially a planar waveguide with periodic corrugation of the walls [54–56], which can be written as follows:

$$l = l_0 \cos(\bar{h}x + \psi(x)), \tag{7.12}$$

where $\bar{h} = 2\pi/d$, l_0 and d are amplitude and period of the corrugation respectively, $\psi(x)$ is a phase of corrugation. The wave propagation can be realized if both of coupled partial waves have a projection of the wavevector perpendicular to the lattice vector (see Fig. 39). The vector potential of the propagating wave can be written as follows:

$$\vec{\mathrm{A}}_s = \vec{y}^{(0)} \mathrm{Re}\left[\left(\mathrm{A}_+(x,z)e^{-i\bar{h}x/2} + \mathrm{A}_-(x,z)e^{i\bar{h}x/2}\right)e^{i\omega t - ihz}\right], \tag{7.13}$$

where $h = \sqrt{k^2 - \bar{h}^2/4}$, $k = \omega/c$. $A_{\pm}(x, z)$ are complex amplitude of the waves. In this case there is an electromagnetic energy flow (Poynting vector) directed along the corrugation (z-axis) and is perpendicular to the lattice vector respectively.

A Bragg waveguide has a full propagating mode spectrum, which differs by the transverse index (x -axis index). As in the case of Bragg resonators [42], the difference between diffraction losses of different modes depend upon a corrugation profile. The optimum filtration can be ahieved if a corrugation phase has a form of step-function along the transverse cross section of the waveguide (see Fig. 40):

$$\psi(x) = \begin{cases} 0, \text{ if } \quad 0 < x < l_x/2 \\ \pi, \text{ if } \quad l_x/2 < x < l_x. \end{cases} \tag{7.14}$$

In this case there exists a mode, which is localized in the vicinity of defect of the corrugation, which has significantly smaller diffraction losses comparing to other modes of the waveguide.

Assume that the direction of velocity of electrons, which oscillate in the field of a planar undulator coincide with the direction of wavevector for the partial wave A_+ [54–56]. The synchronism condition with this wave can be written in the following form: $\omega - kv_{||} \approx \Omega_b$, where $\Omega_b = 2\pi v_{||}/d_u$ is a frequency of electron oscillations in the undulator with period d_u, $v_{||} = \beta_{||} c$ is a velocity of particles. The resonance frequency is given by:

$$\omega = \Omega_b/(1 - \beta_{||}), \tag{7.15}$$

and for the relativistic beams can significantly exceed a bounce frequency Ω_b because of the Doppler effect. In contrast with the traditional FEL schemes, an angle between group velocity of the amplifying wave and particle velocity is quite large.

The process of monochromatic signal amplification in the transverse current FEL scheme can be described by equations similar to the nonstationary equations of tra-

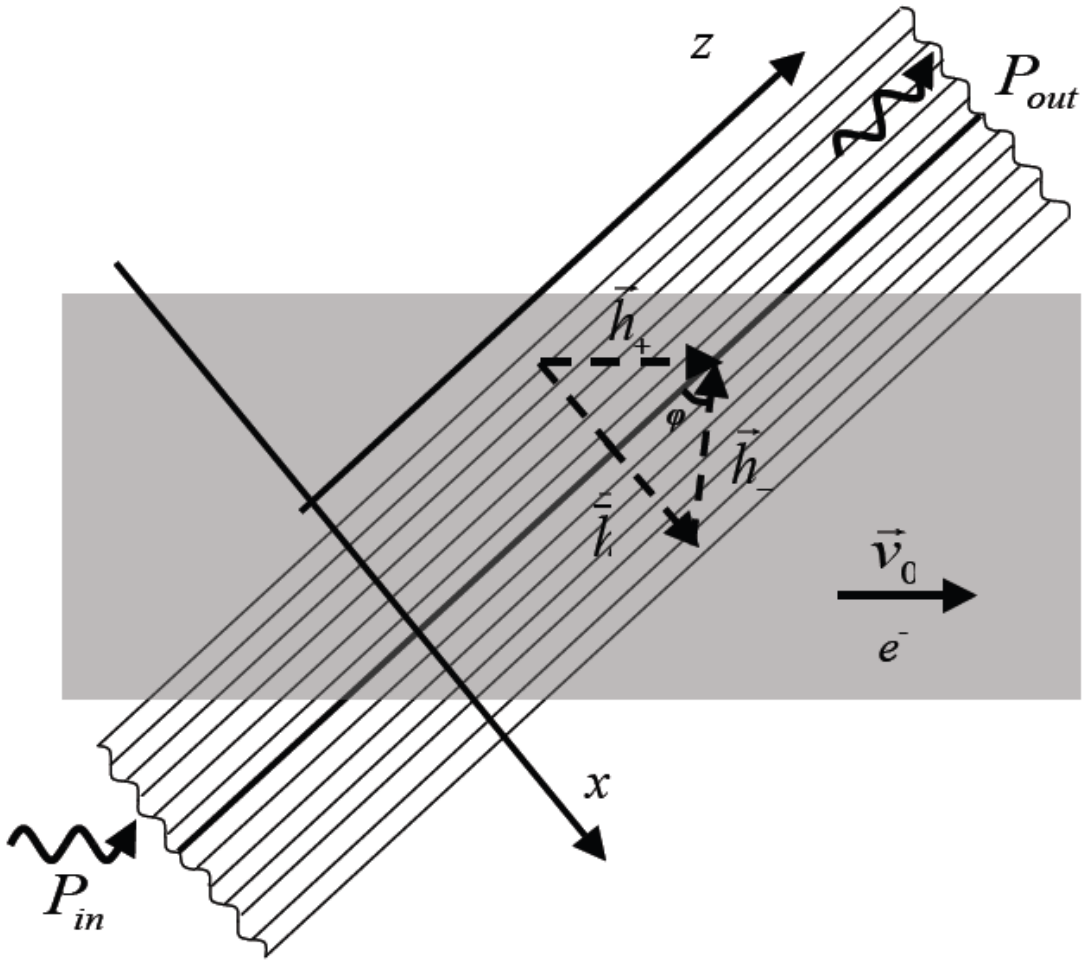

Fig. 39. FEL amplifier based on open planar Bragg waveguide: $\vec{h}$ is a lattice vector, $\vec{h}_\pm$ are wavevectors of partial waves $A_\pm$, which form a waveguide mode; sheet electron beam is collinear with a partial wave A_+.

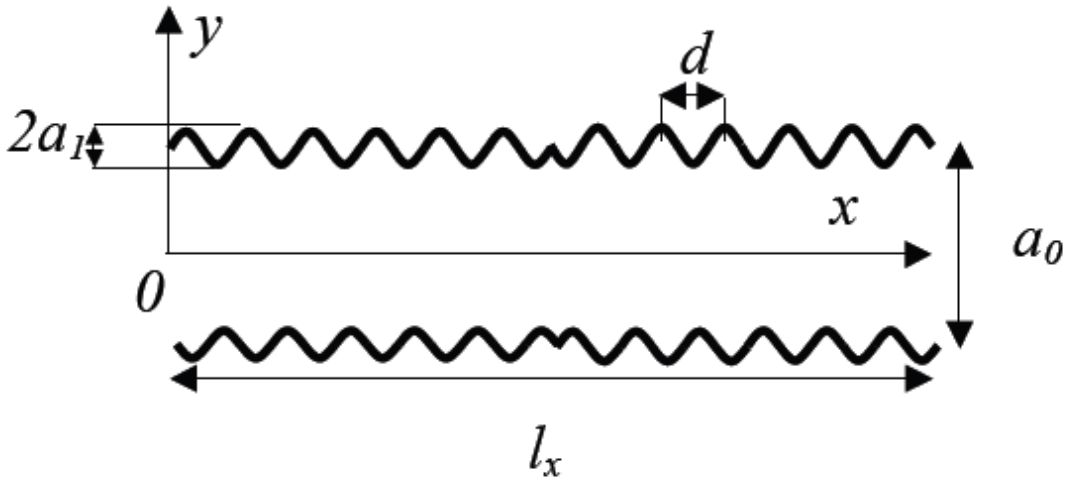

Fig. 40. Transverse cross section of a metal Bragg waveguide with a defect of corrugation periodicity at $x = l_x/2$.

ditional FEL with 1D Bragg resonator [42] with time variable replaced by spatial one (see Appendix D). These equations describe the formation of a transverse structure of the fields together with their longitudinal structure:

$$\frac{\partial A_+}{\partial Z} + \frac{\partial A_+}{\partial X} + i\alpha A_- = \frac{1}{\pi}\int_0^{2\pi} e^{-i\theta} d\theta_0, \qquad \frac{\partial A_-}{\partial Z} - \frac{\partial A_-}{\partial X} + i\alpha^* A_+ = 0, \qquad (7.16)$$

$$\left(\frac{\partial}{\partial Z} + \frac{\partial}{\partial X}\right)^2 \theta = \mathrm{Re}\left(A_+ e^{i\theta}\right),$$

where $Z = zCk^2/h$, $X = 2xCk^2/\bar{h}$, $L_z = l_z Ck^2/h$, $L_x = 2l_x Ck^2/\bar{h}$, $\tau = C\omega t$, $A_\pm = \mathrm{A}_\pm e\kappa\mu/\gamma mc\omega C^2$, $\kappa = \beta_\perp/\beta_{||}$ is electron-wave coupling parameter, $\beta_\perp$ is oscillatory velocity of particles in the undulator field, $\mu \approx \gamma^{-2}$ is bunching parameter, γ is relativistic mass-factor, I_0 is linear current density, θ is electron phase, $C = ((eI_0\lambda^2\mu\kappa^2)/(mc^3 8\pi\gamma a_0))^{1/3}$ is Pierce parameter (gain parameter). This parameter is a single dimensionless parameter in the system, which contains all the information about the system. It depends on the current, bunching parameter, wave

frequency, waveguide geometry. Compare to the case of longitudinal waveguiding discussed in Section A, Eqs. (7.4) - (7.5) one can see the difference due to the different geometry. Consequently the dimensionless coordinates in Eq (7.16) have additional wavenumber multipliers due to the different geometry [54–56]. Normalized wave coupling parameter is given by [43]:

$$\alpha(X) = \frac{l_0 \bar{h} e^{i\psi(X)}}{4ka_0 C} \sin\phi, \tag{7.17}$$

where $\phi = \arcsin(\bar{h}/2k)$ is an angle between a wavevector of the partial wave and waveguide axis, a_0 is distance between plates (see Fig. 40). For a given corrugation profile in Eq. (7.14) a coupling parameter changes its sign on the waveguide axis.

If initially an electron beam is not modulated, then the boundary conditions for the particle can be written as: $\theta|_{X=0} = \theta_0 \in [0, 2\pi)$, $(\partial/\partial Z + \partial/\partial X)\theta|_{X=0} = \delta$, where δ is a synchronism detuning between electrons and wave on the operating frequency. If the input signal is a wave packet $A_0(X)$ entering the system under an angle corresponding to the direction of propagation of partial wave A_+, then the boundary conditions for Eq. (7.16) take the form:

$$A_+|_{Z=0} = A_0(X), \quad A_-|_{Z=0} = 0, \quad A_+|_{X=0} = 0 \quad A_-|_{X=L_x} = 0. \tag{7.18}$$

Electronic efficiency is given by:

$$\eta = \frac{C}{\mu(1-\gamma_0^{-1})}\hat{\eta}, \qquad \hat{\eta} = \frac{1}{2\pi L_z}\int_0^{L_z}\int_0^{2\pi}\left(\frac{\partial\theta}{\partial X} - \delta\right)\Big|_{X=L_x} d\theta_0 dZ \tag{7.19}$$

According to the energy conservation law:

$$4\hat{\eta} = \frac{1}{L_z}(P_{\text{side}} + P(Z=L_z) - P(Z=0)), \tag{7.20}$$

a total power radiated by electron beam is distributed into the output power:

$$P(Z) = \int_0^{L_x} (|A_+(X,Z)|^2 + |A_-(X,Z)|^2) dX, \tag{7.21}$$

and energy losses in the sidewalls:

$$P_{\text{side}} = \int_0^{L_z} (|A_+(X = L_x, Z)|^2 + |A_-(X = 0, Z)|^2) dX. \tag{7.22}$$

The efficiency of the amplifier is determined by the amplification coefficient: $\Gamma(Z) = P(Z)/P(0)$ and wave efficiency: $P(z = L_z)/L_z$, which characterized the power radiated by an electron flow through the output cross section $Z = L_z$.

Figs. 41, 42 demonstrate the dependence of the amplification coefficient and electron efficiency on a beam width L_z, respectively, obtained by direct simulations of Eqs. (7.16). Simulations show that for an arbitrary shape of the input signal A_0 field distribution is close to the structure of the fundamental mode of the Bragg waveguide already at initial stage of interaction. This structure remains unchanged in the process of amplification because of its high quality and filtration properties (see Fig. 43). The amplification coefficient in the discussed example for the optimum detuning $\delta = 1.5$ reaches $30dB$. For the normalized waveguide width $L_x = 4$ the integral diffraction losses, caused by the radiation flows in the transverse direction of a waveguide P_{side} do not exceed 15%.

Lets estimate the realization of the discussed above FEL-amplifier in $4 - mm$ wavelength range based on 150 cm sheet electron beam formed by accelerator U-2 (BINP RAS): particle energy 1 MeV, sheet current density 1 kA/cm. For the oscillatory velocity in the undulator $\beta_\perp \approx 0.3$, undulator period 4.5 cm and the distance between plates 1 cm Pierce parameter is $C = 0.005$. It follows form Fig. 41 that the amplification coefficient $\Gamma = 30$ dB and maximum of efficiency reaches at $L_z \approx 20$. That is for a given Pierce parameter and an angle between a beam and a

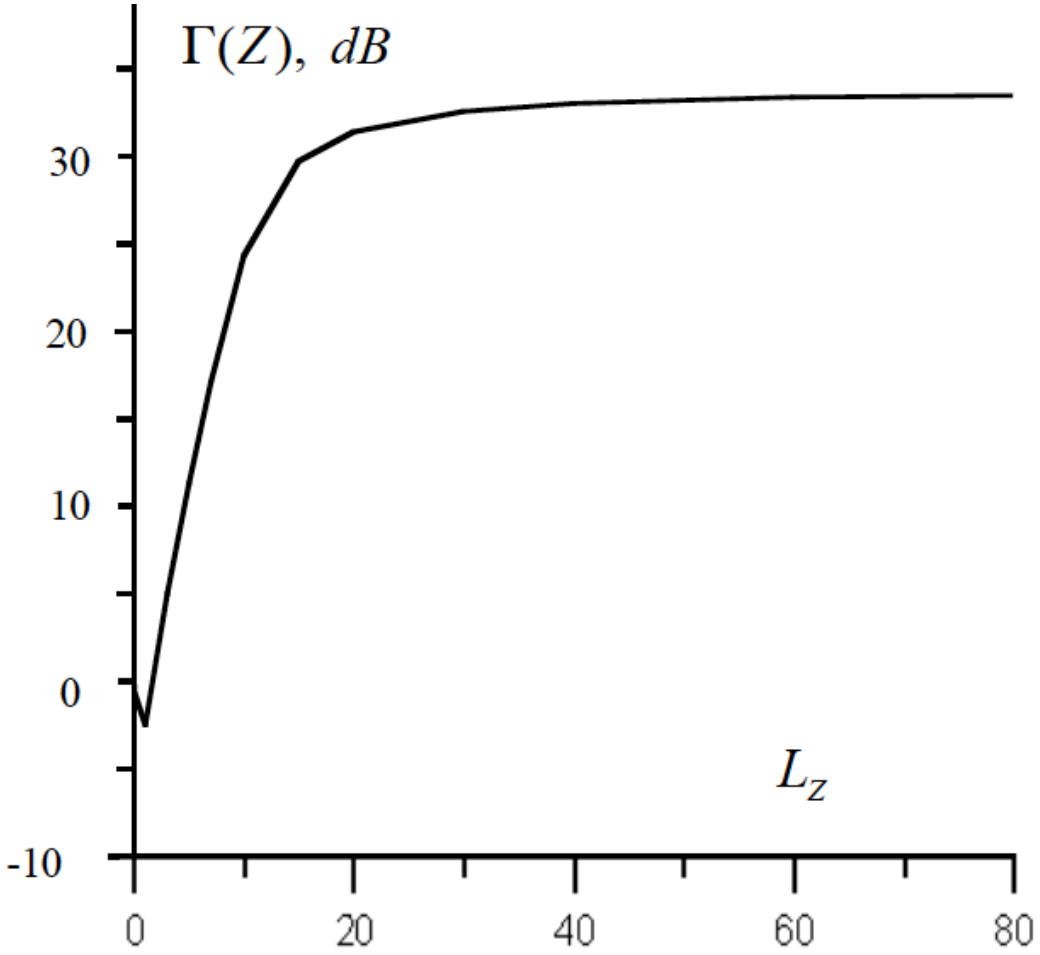

Fig. 41. Amplification coefficient of the transverse current FEL amplifier as a function of the width of electron beam: $L_x = 4$, $\delta = 1.5$, $|\alpha| = 1.5$.

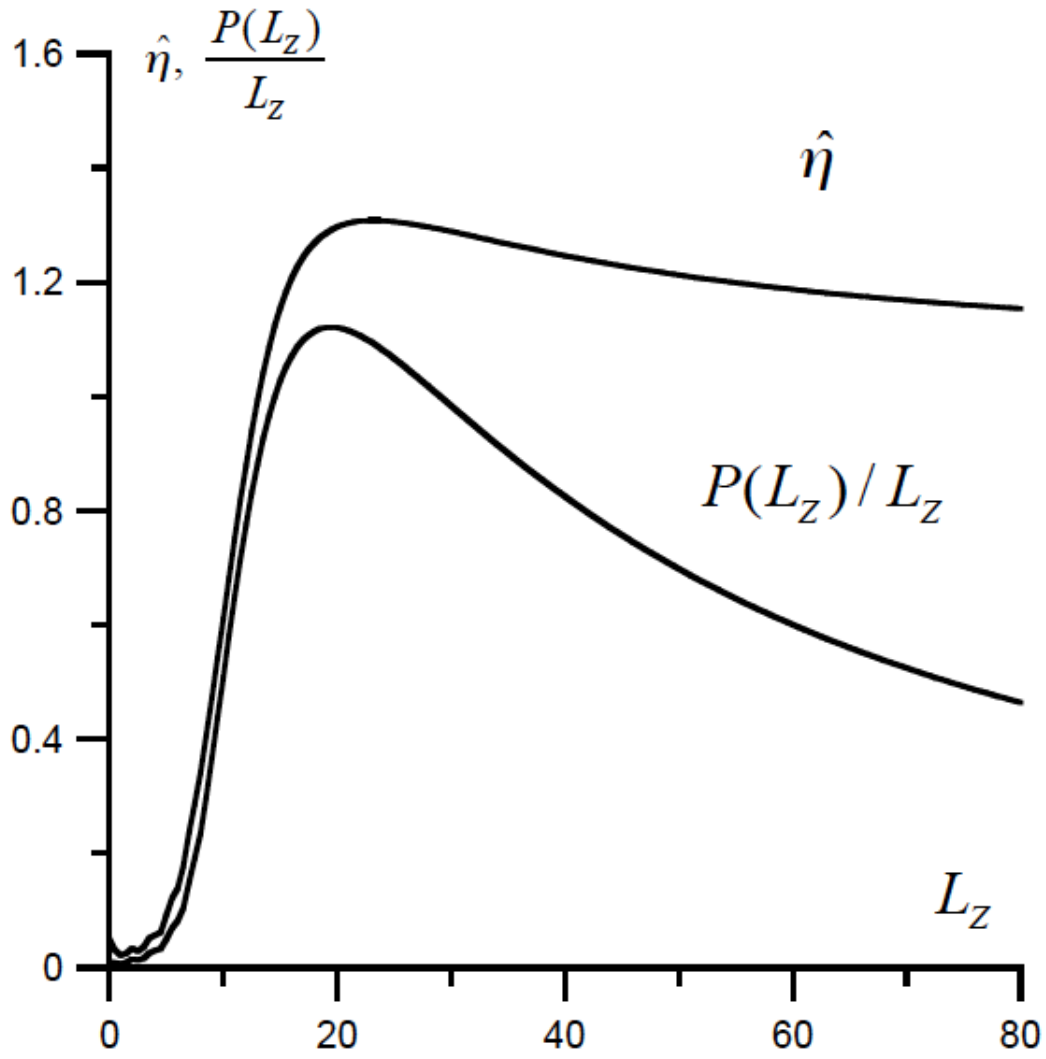

Fig. 42. Full and wave efficiency of the transverse current FEL amplifier as a function of the width of electron beam: $L_x = 4$, $\delta = 1.5$, $|\alpha| = 1.5$.

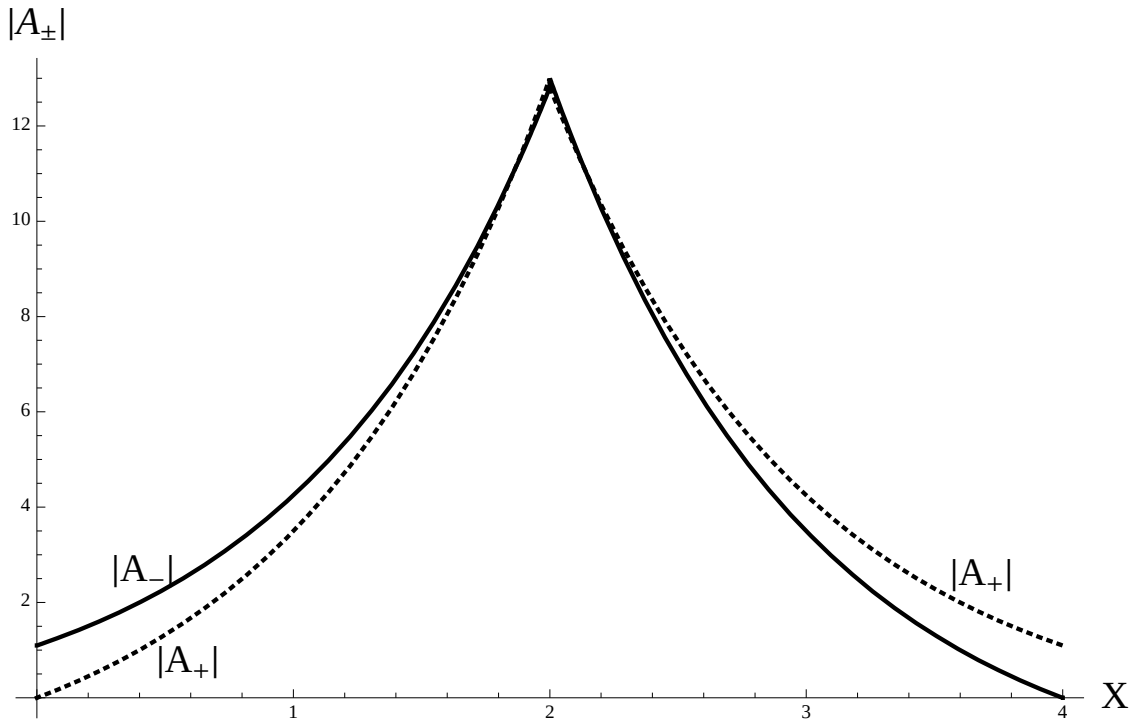

Fig. 43. Transverse structure of the partial waves at the output of amplifier: $L_x = 4$, $\delta = 1.5$, $|\alpha| = 1.5$, $L_z = 20$.

waveguide axis $\phi = 45^o$, which corresponds to the interaction length $l_z = 175\ cm$ and electron beam width 150 cm. Normalized waveguide width $L_x = 4$ corresponds to the physical size $l_x = 35\ cm$, the corrugation period is 0.57 cm. The normalized coupling parameter $\alpha = 0.5$ is realized for the corrugation depth 1.2 mm. Full efficiency is approximately 10% and, according to the diffraction losses, it corresponds to the output power 10 GW.

D. Other possible amplification schemes based on Bragg waveguides

Another variant of using of an open Bragg structure for provision of higher selectivity in FEL amplifier can be based on coupling between two TEM waves $A_\pm$ propagating at some angle to the axis and the wave B with a higher y-index propagating directrly along the system axis. The latter wave is synchronous to the beam propagating directly along the axis, while the former waves provide the synchronization of radiation over the x coordinate. The coupling is provided by the regular corrugation with the following Bragg resonance conditions $\bar{h} = 2h_x$, where h_x is the transverse wavenumber of TEM modes. This interaction is described by the following equations.

$$\frac{\partial A_\pm}{\partial Z} \pm \frac{\partial A_\pm}{\partial X} = i\alpha B$$

$$\frac{\partial B}{\partial Z} + \frac{i}{2}\frac{\partial^2 B}{\partial^2 Z} = -i\alpha(A_+ + A_-) + J$$

These equations are similar to those describing the excitation of the FEL oscillator based on coupling of the propagating and the trapped waves with excitation factor removed into the equations for the higher mode. Preliminary estimations show that in this case multiplication coefficient also should be rather high.

It is worth noting in the conclusion that a planar Bragg waveguide with a step of corrugation phase can be considered as one of the possible versions of more general

principle of radiation canalization in photonic crystals. The traditional photonic crystals are made from the system of parallel dielectric rods or plates, which contains a defect of periodicity [46, 47]. It is obvious that the advantage of a planar Bragg waveguide formed by corrugated metal plates is its compatibility with an intense electron beam transportation systems. Consequently, the presented above amplifier can be interpreted as the experimental possibility of use of photonic crystals in Free Electron Laser physics.

It is worth noting that the concept of two-dimensional distributed feedback (DF) has a huge innovational potential. A lot of radiation schemes can be based on this concept. The most important examples of radiational systems are based on Cherenkov radiation, sheet electron beams and two dimensional laser medium. The latter example of laser, but based on one dimensional DF, realized by means of one dimensional Bragg structures has vast applications in quantum electronics. A discussed above analysis shows a possibility of generalization of two-dimensional and, in principle, three-dimensional mechanism for obtaining a spatial-coherent radiation.

CHAPTER VIII

CONCLUSIONS

A. Summary of the main results on the BEC statistics

In this section I summarize an overall picture of mesoscopic BEC statistics and the main results of the Chapters II - V, most of which are presented in [63–66, 69].

The statistics of the BEC fluctuations in the ideal and weakly interacting gases in a box in the thermodynamic limit and in the systems with a finite number of particles is essentially the statistics of the sum of the noncondensed quasiparticles occupations $n_{\mathbf{k}}$, $n_0 = N - \sum_{\mathbf{k}\neq 0} n_{\mathbf{k}}$. This statistics is very different from the standard thermodynamics fluctuations and is strongly non-Gaussian. The latter is justified in this work by explicit calculations of the cumulants and central moments of all order in the properly reduced many-body Fock space.

1. The only approach that reveals the actual nature and universality of the BEC statistics is based on the study of canonical-ensemble quasiparticles in Chapter II, Section A. It allows us to analyze the condensate fluctuations as being complimentary to the cut off by the particle-number constraints fluctuations of the noncondensate quasiparticles both in the ideal and in the weakly interacting gases. In latter case the canonical quasiparticles are dressed by Bogoliubov coupling. The cut off in Eq. (2.35) of the probability distribution function of the unconstrained noncondensate occupation given by Eqs. (2.14) - (2.17) and (2.20) - (2.22) describes accurately and clearly the mesoscopic effects in BEC statistics of the ideal and weakly interacting Bose gases.

2. A direct numerical calculation of the characteristic function, such as in Eq. (2.41), followed by a Fast Fourier Transformation (FFT) technique for the evaluation

of the noncondensate occupation probability distribution is developed, used in the dissertation, and proven to be very effective numerical technique for the analysis of BEC statistics.

3. A multinomial expansion in Eq. (2.47) for the distribution function of the noncondensed atoms in both ideal and weakly interacting Bose gas in a box is introduced and analyzed. The difference in the coefficients of the expansion for the ideal and weakly interacting gases is caused by a two-mode squeezing due to Bogoliubov coupling between modes with equal in magnitude and opposite in direction momenta. The analytical formulas for the moments in Eqs. (2.48) - (2.50) explicitly obey the particle-number constraint and are in perfect agreement with the exact recursion relation in Eq. (2.51) [20]. The analysis indicates the suppression of the condensate fluctuations at high temperatures and their enhancement at low temperatures as compared to the case of an ideal gas. The low-temperature asymptotic formula (2.58) for the ideal gas coincides with the formula obtained previously in [21]. The high temperature asymptotics in Eq. (2.63), is consistent with the grand-canonical ensemble approximation for both ideal and weakly interacting gas since interaction is significantly suppressed at high temperature. In the case of moderate temperatures the fluctuations of weakly interacting gas can be written in terms of the fluctuations of the ideal gas by means of the crossover relations in Eqs. (2.76) - (2.77).

4. There exists a remarkable universality of the BEC statistics that is analyzed in the dissertation by means of the exact numerical simulations of the moments and cumulants for a wide range of the numbers of atoms in the trap, $N < 10^4$. Thereye are no doubts that a similar universality is valid for the ideal gas in any other traps and for other, than periodic boundary conditions. The particular shapes of the universal functions depend on a trap energy spectrum. The standard Landau mean-field theory does not resolve that universal structure of BEC statistics in the critical region.

5. An exactly solvable Gaussian model of BEC in a degenerate interacting gas, Eq. (3.11), is presented and elucidates on how the unconstrained Gaussian statistical distribution with vanishing higher-order cumulants ($\kappa_m^{(\infty)} = 0$ for all $m \neq 2$) results, via the constraint-cut-off mechanism, in the strongly non-Gaussian BEC fluctuations.

6.The simulations of the universal functions for the order parameter and all moments and cumulants for a relatively small mesoscopic system of a finite number of atoms constitutes an effective tool for the studies of BEC phase transition in the macroscopic systems in the thermodynamic limit.

In a general case of the interacting gas, the shapes of the universal functions for the moments and cumulants of the BEC fluctuations, in addition, depend on a deformation of the statistical distribution due to a feedback of the order parameter on the quasiparticle energy spectrum and correlations. These effects can be taken into account in a quite general, non-perturbative-in-fluctuations way using a theorem on the nonpolynomial averages in statistical physics and appropriate diagram technique [61–64]. These problems are outside the scope of the present dissertation and will be analyzed elsewhere.

7. A two-level trap model of BEC and its analytical solution for the distribution function and cumulants Eqs. (4.1) - (4.4) as well as their continuous approximation in Eqs. (4.6) - (4.8) are presented and allow us to analyze all details of the mesoscopic BEC statistics. The two-level trap model provides a basic block which allows us to construct a regular scheme for the approximation of the BEC statistics in any real traps, including all higher-order moments which are not given accurately by the quasithermal ansatz [21] since it comes to the cut-off Gaussian statistics in the thermodynamic limit.

8. An analytical solution within a three-level trap model (4.9) is presented and describes remarkably accurate all mesoscopic effects of BEC statistics.

9. An important conclusion is that the outlined universal constraint-cut-off mechanism so much dominates the origin of the strong non-Gaussian effects in BEC statistics that it predicts a qualitative behavior of all, including higher-order, moments in the critical region even on the basis of the simplest two-level trap model (quasithermal ansatz) or cut-off Gaussian model.

10. An analysis of the asymptotical behavior of the ground state occupation statistics in a box in the framework of the refined saddle-point approximation is fulfilled. It leads to the parabolic cylinder functions as a basis for the cumulants and other statistical moments. The complications of the present calculations for an ideal gas in a box compared to the studied earlier in [27] case of the harmonic trap originate from the degeneracies and symmetries of the boundaries. The obtained asymptotic formulas for the different regions of parameters, Eqs. (5.27) - (5.29), mainly agree with the results calculated via the FFT method in Chapter III. However in the critical and condensed regions the saddle-point method is unable to give an accurate result, apparently because due to a strong nonanalyticity of the cut-off probability distribution near the critical point, infinitely many orders in the saddle-point expansion have to be taken into account and resummed to yield the correct result.

Clearly, the mesoscopic effects in the Bose-Einstein condensate fluctuations constitute an important class of problems in the many-body physics.

B. Summary of the main results on the FEL electrodynamics

Below I summarize the main results of the Chapters VI - VII, most of which are presented in [43–45, 54–56].

1. An open planar metal waveguide with slightly corrugated walls and a defect of periodicity in the middle of the wall corrugation has a remarkable selectivity in the

transverse mode spectrum, as follows from the obtained dispersion relation in Eqs. (6.29) - (6.30). This system is very competitive in the case of microwave electronics and, in particular, it is compatible with the electron beam transportation systems.

2. Equations (7.4) - (7.5) describing a process of electromagnetic wave amplification in a basic FEL amplifier, scheme where electron beam moves along a waveguide axis [43], are derived and a longitudinal coordinate dependence of amplification coefficient (Fig. 34) is studied. The main effect is an increase of the effective size of operating mode in a structure with regular longitudinal corrugation that couples two partial waves, propagating at some angle to the axis, to the wave propagating directly along the axis. This wave, which is transformed into cutoff modes, is excited by the electron beam.

3. A mode excitation equations (7.10) and a dependence of field amplification on a longitudinal coordinate (Fig. 37) is obtained for an active medium which has a defect of a periodic modulation of a dielectric constant and a nonlinear negative conductance (an imaginary negative part of the dielectric constant).

4. A transverse current FEL amplifier [54–56], which is an alternative to the longitudinal device, is suggested and described by the equations (7.16) for the wave amplification and for the motion of an electron combinational phase, Simulations of the amplification coefficient (Fig. 41), as well as the full and electron efficiency (Fig. 42) for this system shows its advantage compare to the case of the longitudinal waveguiding.

5. It is important to mention that the discussed above models mostly cannot be considered as a full description of the certain sources of coherent radiation. Their purpose is to demonstrate a possibility of a construction of a device with unique parameters of the output radiation and development of the theoretical methods for the analysis of the complicated dynamics of two- or three-dimensional active medium.

Despite a usual tendency in the analysis of complicated stochastic dynamics based on very simple basic assumptions and models with minimum degrees of freedom, the purpose of this study is completely different, and constitutes a study of the relatively simple models of radiation in the complicated systems with large numbers of degrees of freedom. This analysis shows that different modifications of two-dimensional Bragg structures allow one to solve a problem of control of spatial-time radiation characteristics for large number of types of radiating systems.

REFERENCES

[1] A. Einstein, Sitzungsberichte der preussischen Akademie der Wissenschaften, XXII. Gesamtsitzung **10**, 261 (1924).

[2] A. Einstein, Sitzungsberichte der preussischen Akademie der Wissenschaften, XXII, I. Sitzung der physikalisch-mathematischen Klasse **8**, 3 (1925).

[3] S. N. Bose, Z. Phys. **26**, 178 (1924).

[4] L. Landau and E. M. Lifshitz, *Statistical Physics, Part 1* (Pergamon, Oxford, 1969).

[5] E. M. Lifshitz and L. P. Pitaevskii, *Statistical Physics, Part 2* (Pergamon, Oxford, 1981).

[6] A. Z. Patashinsky and V. L. Pokrovsky, Sov. Phys. JETP **37**, 733 (1974).

[7] P. Pitaevskii and S. Stringari, Rev. Mod. Phys. **71**, 463 (1999).

[8] H. Shi and A. Griffin, Phys. Rep. **304**, 1 (1998).

[9] M. Anderson, J. Ensher, M. Matthews, C. Wieman, and E. Cornell, Science **269**, 198 (1995).

[10] K. B. Davis, M.-O. Mewes, M. R. Andrews, N. J. van Druten, D. S. Durfee, D. M. Kurn, and W. Ketterle, Phys. Rev. Lett. **75**, 3969 (1995).

[11] C. C. Bradley, C. A. Sackett, J. J. Tollett, and R. G. Hulet, Phys. Rev. Lett. **75**, 1687 (1995).

[12] A. Leggett, Rev. Mod. Phys. **73**, 307 (2001).

[13] C.-S. Chuu, F. Schreck, T. P. Meyrath, J. L. Hanssen, G. N. Price, and M. G. Raizen, Phys. Rev. Lett. **95**, 260403 (2005).

[14] A. M. Dudarev, M. G. Raizen, and Q. Niu, Phys. Rev. Lett. **98**, 063001 (2007).

[15] T. P. Meyrath, F. Schreck, J. L. Hanssen, C.-S. Chuu, and M. G. Raizen, Phys. Rev. A **71**, 041604 (2005).

[16] C. D. J. Sinclair, E. A. Curtis, I. L. Garcia, J. A. Retter, B. V. Hall, S. Eriksson, B. E. Sauer, and E. A. Hinds, Phys. Rev. A **72**, 031603(R) (2005).

[17] Y.-J. Wang, D. Z. Anderson, V. M. Bright, E. A. Cornell, Q. Diot, T. Kishimoto, M. Prentiss, R. A. Saravanan, S. R. Segal, and S. Wu, Phys. Rev. Lett. **94**, 090405 (2005).

[18] G.-B. Jo, Y. Shin, S. Will, T. A. Pasquini, M. Saba, W. Ketterle, and D. E. Pritchard, Phys. Rev. Lett. **98**, 030407 (2007).

[19] S. Stringari, Phys. Rev. Lett. **86**, 4725 (2001).

[20] V. V. Kocharovsky, Vl. V. Kocharovsky, M. Holthaus, C. H. R. Ooi, A. Svidzinsky, W. Ketterle, and M. O. Scully, Advances in Atomic, Molecular and Optical Physics **53**, 291 (2006).

[21] V. V. Kocharovsky, Vl. V. Kocharovsky, and M. O. Scully, Phys. Rev. A **61**, 053606 (2000).

[22] A. A. Abrikosov, L. P. Gorkov, and I. E. Dzyaloshinskii, *Methods of Quantum Field Theory in Statistical Physics* (Prentice-Hall, Englewood Cliffs, NJ, 1963).

[23] A. L. Fetter and J. D. Walecka, *Quantum Theory of Many-Particle Systems* (McGraw-Hill, San Francisco, 1971).

[24] B. C. Crooker, B. Hebral, E. N. Smith, Y. Takano, and J. D. Reppy, Phys. Rev. Lett. **51**, 666 (1983).

[25] M. H. W. Chan, K. I. Blum, S. Q. Murphy, G. K. S. Wong, and J. D. Reppy, Phys. Rev. Lett. **61**, 1950 (1988).

[26] P. A. Crowell, F. W. V. Keuls, and J. D. Reppy, Phys. Rev. Lett. **75**, 1106 (1995).

[27] M. Holthaus and E. Kalinowski, Ann. Phys. (N.Y.) **276**, 321 (1999).

[28] V. V. Kocharovsky, M. O. Scully, S.-Y. Zhu, and S. Zubairy, Phys. Rev. A **61**, 23609 (2000).

[29] M. Abramowitz and I. A. Stegun, *Handbook of Mathematical Functions* (Dover, New York, 1972).

[30] M. Girardeau and R. Arnowitt, Phys. Rev. **113**, 755 (1959).

[31] M. Holthaus, K. T. Kapale, V. V. Kocharovsky, and M. O. Scully, Physica A **300**, 433 (2001).

[32] R. K. Pathria, *Statistical Mechanics, 2nd ed.* (Elsevier, Oxford, 1996).

[33] P. Pitaevskii and S. Stringari, *Bose-Einstein Condensation* (Clarendon, Oxford, 2003).

[34] R. M. Ziff, G. E. Uhlenbeck, and M. Kac, Phys. Rep. **32**, 169 (1977).

[35] V. V. Kocharovsky, Vl. V. Kocharovsky, and M. O. Scully, Phys. Rev. Lett. **84**, 11 (2000).

[36] S. Giorgini, L. P. Pitaevskii, and S. Stringari, Phys. Rev. Lett. **80**, 5040 (1998).

[37] A. Yariv, *Introduction to Optical Electronics* (Holt, Rinehart and Winston, New York, 1976).

[38] C. V. Kogelnik and J. Shank, Appl. Phys **43**, 2327 (1972).

[39] G. A. Turnbull, P. Andrew, and M. J. Jory, Phys. Rev. B **64**, 125122 (2001).

[40] S. Hansmann, H. Walter, H. Hillmer, and H. Burkhard, IEEE J. Quant. Electron. **30**, 2477 (1994).

[41] V. L. Bratman, G. G. Denisov, N. S. Ginzburg, and M. I. Petelin, IEEE J. Quant. Electron. **9**, 282 (1983).

[42] N. S. Ginzburg, A. S. Sergeev, and N. Y. Peskov, IEEE Trans. on Plasma Sci. **24**, 770 (1996).

[43] K. Dorfman, N. Ginzburg, A. Malkin, and A. Sergeev, Las. Phys. **17**, 1 (2007).

[44] K. Dorfman, N. Ginzburg, A. Malkin, and R. Rozental, in *Book of Abstracts, IRMMW-THz* (Shanghai, China, 2006).

[45] K. Dorfman, N. Ginzburg, A. Malkin, and R. Rozental, in *Proceedings of the 28th FEL Conference* (Berlin, Germany, 2006).

[46] R. J. Temkin, J. R. Sirigiri, and K. Kreischer, Phys. Rev. Lett. **86**, 5628 (2001).

[47] E. Yablonovitch, T. J. Gmitter, and K. M. Leung, Phys. Rev. Lett. **67**, 2295 (1991).

[48] V. Radisic, Y. Qian, and T. Itoh, IEEE Microw. Guid. Wave Lett. **8**, 13 (1998).

[49] A. V. Arzhanikov, N. S. Ginzburg, and N. Y. Peskov, in *Proceedings of the 14th FEL Conference* (Kobe, Japan, 1992).

[50] N. Ginzburg, N. Y. Peskov, and A. Sergeev, Opt. Comm. **96**, 254 (1993).

[51] N. Ginzburg, N. Y. Peskov, and A. Sergeev, Phys. Rev. E **60**, 935 (1999).

[52] I. V. Konoplev, A. Cross, and N. S. Ginzburg, in *Proceedings of Strong Microwaves in Plasmas Conference* (N. Novgorod, Russia, 2005).

[53] A. V. Arzhanikov, V. T. Astrelin, and A. V. Burdakov, JETP Lett. **77**, 426 (2003).

[54] V. Baryshev, K. Dorfman, N. Ginzburg, A. Malkin, N. Peskov, R. Rozental, A. Sergeev, and V. Zaslavsky, Applied Nonlinear Dynamics **14**, 123 (2006).

[55] K. Dorfman, N. Ginzburg, A. Malkin, and A. Sergeev, submitted to J. Tech Phys. (2009).

[56] K. Dorfman, N. Ginzburg, A. Malkin, and A. Sergeev (2006), presented at the Conf. Coherent Control of the Fund. Proc. in Opt. and X-ray Opt., Inst. of Appl. Phys. RAS. N. Novgorod, Russia.

[57] D. A. Dann, W. A. Harman, L. M. Field, and G. S. Kino, in *Proceedings of IRC* (1956).

[58] Y. V. Bikov, A. V. Gaponov, and M. I. Petelin, Radiofizika. **17**, 1219 (1974).

[59] M. D. Girardeau, Phys. Rev. A **58**, 775 (1998).

[60] N. L. Balazs and T. Bergeman, Phys. Rev. A **58**, 2359 (1998).

[61] V. V. Kocharovsky and Vl. V. Kocharovsky, Las. Phys. **17**, 700 (2007).

[62] V. V. Kocharovsky and Vl. V. Kocharovsky, J. Mod. Opt. **54**, 2491 (2007).

[63] K. Dorfman, V. V. Kocharovsky, and Vl. V. Kocharovsky (2009), presented at the Conf. 39th Winter Colloquium on the Physics of Quantum Electronics Snowbird, UT.

[64] K. Dorfman, V. V. Kocharovsky, and Vl. V. Kocharovsky (2009), presented at the Conf. TAMU PQE Workshop, Texas A&M University College Station, TX.

[65] V. V. Kocharovsky, Vl. V. Kocharovsky, and K. E. Dorfman, J. Mod. Opt. **56** (2009), (in print).

[66] V. V. Kocharovsky, Vl. V. Kocharovsky, and K. E. Dorfman, Radiophys. Quantum Electronics **52** (2009), (in print).

[67] N. F. Kovalev, I. M. Orlova, and M. I. Petelin, Radiofizika **11**, 783 (1968).

[68] A. V. Arzhanikov and V. S. Nikolaev, J. Appl. Phys. **72**, 1657 (1992).

[69] K. Dorfman, V. V. Kocharovsky, and Vl. V. Kocharovsky (2008), presented at the Conf. Texas & Four Corners Sections American Physical Society Joint Meeting, University of Texas El Paso, TX.

APPENDIX A

DERIVATION OF THE ANALYTICAL FORMULAS FOR THE DISTRIBUTION FUNCTION OF THE TOTAL NUMBER OF NONCONDENSED ATOMS IN AN IDEAL GAS. METHOD OF THE CHARACTERISTIC FUNCTION AND RESIDUES

I start with the defined in Chapter II distribution function in Eq. (2.14), written as a Fourier integral from the characteristic function:

$$\rho\left(n\right)=\frac{1}{2\pi}\int_{-\pi}^{\pi}e^{-inu}\Theta_{n}(u)\,du. \tag{A.1}$$

Making the transformation of variable $z=e^{iu}$ in Eq. (A.1), one will obtain the contour integral in the complex plane z, where the contour encircles the origin in the counterclockwise direction:

$$\rho(n)=\frac{1}{2\pi i}\oint_{|z|=1}\frac{\Theta\left(z\right)}{z^{n+1}}\,dz=\frac{1}{2\pi i}\oint_{|z|=1}\frac{1}{z^{n+1}}\prod_{\mathbf{k}\neq0}\frac{z_{\mathbf{k}}-1}{z_{\mathbf{k}}-z}\,dz, \tag{A.2}$$

where $\Theta(z)=\Theta_{n}(u)$ with $z=e^{iu}$. The integrand in Eq.(A.2) has an infinite number of poles at the positions $z=z_{\mathbf{k}}$ outside the contour, and the pole of the order of $n+1$ at the origin $z=0$. The order of the each external pole is equal to the degeneracy of of the $\mathbf{k}$ mode, i.e. $g_{\mathbf{k}}=6,8,12,24,48$. Therefore, the integration can be performed in two different ways.

First way is to sum up contributions from the residues in external poles. It is convenient if the number of particles is sufficiently large ($N>>48$). In this case the highest derivative, to be calculated is of the order of 47 and it does not depend on

the particle number. The result of this calculation yields:

$$\rho(n) = \sum_{\mathbf{p}\neq 0} \operatorname*{res}_{z=z_{\mathbf{p}}} \frac{\Theta(z)}{z^{n+1}} = \sum_{\mathbf{p}\neq 0} \frac{1}{(g_{\mathbf{p}}-1)!} \frac{d^{g_p-1}}{dz^{g_p-1}} \left(\frac{\Theta(z)}{z^{n+1}} (z-z_{\mathbf{p}})^{g_p} \right) \Big|_{z=z_{\mathbf{p}}}, \tag{A.3}$$

where an index $\mathbf{p}$ runs over different energy levels $\epsilon_{\mathbf{k}}$. Another way of calculation is to compute the $n+1$-st order residue at the origin. It looks more complicated in the sense of calculation higher order derivatives for large enough number of particles, but nevertheless I will present this result, since it leads to the closed form analytical expression for the distribution function useful in the analysis. Thus, one can find:

$$\rho(n) = \operatorname*{res}_{z=0} \frac{\Theta(z)}{z^{n+1}} = \frac{1}{n!} \frac{d^n}{dz^n} \Theta(z) \Big|_{z=0}, \tag{A.4}$$

which is exactly the n-th coefficient in the Taylor expansion of the characteristic function about the point $z = 0$.

APPENDIX B

INITIAL (NONCENTERED) MOMENTS

In this section I apply the result in Eq. (A.4) to obtain the closed form expressions for the noncentered moments of the distribution function following the same path as was used for the calculation the distribution function itself. The advantage of using the zero-residue calculation is that one can perform explicitly the summation over n first, and then calculate the residue. This is true for the moments of any order. To see that I start with the lowest order moment - the zeroth order, which is nothing but the normalization factor. The general expression for the initial moments is the following:

$$\alpha_m \equiv \langle n^m \rangle = \sum_{n=0}^{N} n^m \rho(n). \tag{B.1}$$

The integral expression for the normalization yields:

$$\alpha_0 \equiv \langle \theta(N-n) \rangle = \frac{1}{2\pi i} \oint_{|z|=1} \Theta(z) \sum_{n=0}^{N} \frac{1}{z^{n+1}}. \tag{B.2}$$

Performing the summation over n, using the geometric series, one obtains:

$$\sum_{n=0}^{N} \frac{1}{z^{n+1}} = \frac{1-z^{N+1}}{z^{N+1}(1-z)}. \tag{B.3}$$

Next step is to perform the contour integration with the pre-factor in Eq. (B.3) by evaluating the residue at the origin. The order of residue after the summation over n is $N+1$. The point $z=1$ in the denominator is a regular point, since there is a finite limit at $z \to 1$. Therefore, the resulting expression for the zeroth initial moment is:

$$\alpha_0 \equiv \langle \theta(N-n) \rangle = \frac{1}{2\pi i} \oint_{|z|=1} \Theta(z) \frac{1-z^{N+1}}{z^{N+1}(1-z)} = \operatorname*{res}_{z=0} \frac{1-z^{N+1}}{z^{N+1}(1-z)} \Theta(z) =$$

$$= \frac{1}{N!}\frac{d^N}{dz^N}\left(\frac{1-z^{N+1}}{1-z}\Theta(z)\right)\Big|_{z=0}. \tag{B.4}$$

All the higher moments can be written as a derivatives from the zeroth order

$$n^m = \left(-z\frac{d}{dz}\right)^m z^{-n}, \tag{B.5}$$

thus one can express the pre-factor of any moment in terms of the pre-factor of the zeroth order moment in Eq. (B.3). Therefore, for any noncentered moment of the distribution function one has:

$$\alpha_m = \frac{1}{N!}\frac{d^N}{dz^N}\left(F_m(z)z^{N+1}\Theta(z)\right)\Big|_{z=0}, \tag{B.6}$$

where the general form of the pre-factor is

$$F_m(z) = \left(-z\frac{d}{dz}\right)^m \frac{1-z^{N+1}}{z^{N+1}(1-z)}. \tag{B.7}$$

APPENDIX C

THE MULTINOMIAL EXPANSION

Let us go back to the characteristic function of the total number of noncondensed atoms. It can be written in different ways:

$$\Theta\left(z\right)=\prod_{\mathbf{k}\neq0}\frac{z_{\mathbf{k}}-1}{z_{\mathbf{k}}-z}=\prod_{\mathbf{k}\neq0}\frac{z_{\mathbf{k}}-1}{z_{\mathbf{k}}}\prod_{\mathbf{k}\neq0}\frac{1}{1-z/z_{\mathbf{k}}}=\Theta_0\exp\left(-\sum_{\mathbf{k}\neq0}\ln(1-z/z_{\mathbf{k}})\right), \tag{C.1}$$

where $\Theta_0\equiv\Theta(z=0)=\prod_{\mathbf{k}\neq0}(z_{\mathbf{k}}-1)/z_{\mathbf{k}}$ - the characteristic function at zero fugacity z. Now I employ the Taylor expansion of the logarithm under the summation about the point $z=0$, using the fact, that $|z|<|z_{\mathbf{k}}|$, thus:

$$\ln(1-z/z_{\mathbf{k}})=-(z/z_{\mathbf{k}})-\frac{(z/z_{\mathbf{k}})^2}{2}-\frac{(z/z_{\mathbf{k}})^3}{3}-...=-\sum_{m=1}^{\infty}\frac{1}{m}\left(\frac{z}{z_{\mathbf{k}}}\right)^m. \tag{C.2}$$

One can rewrite (C.1), as following:

$$\Theta(z)=\Theta_0\exp\left(\sum_{\mathbf{k}\neq0}\sum_{m=1}^{\infty}\frac{1}{m}\left(\frac{z}{z_{\mathbf{k}}}\right)^m\right). \tag{C.3}$$

Changing the order of summation and defining $f_m(z)\equiv\sum_{\mathbf{k}\neq0}\left(z-z_{\mathbf{k}}\right)^{-m}$ and $f_m(0)\equiv f_m$, one can obtain

$$\Theta(z)=\Theta_0\exp\left(\sum_{m=1}^{\infty}f_m z^m\right). \tag{C.4}$$

Comparison of Eq. (C.4) with the distribution function in Eq. (A.4) allows one to conclude, that $\rho(n)$is nothing else but the Taylor coefficient of the z^n term, since all the other terms are zero. All terms of the lower orders vanish because of the higher order of the derivative, and all the higher order terms will be cancelled, because we have to set $z=0$ in the end. Therefore, one can transform the expression for the characteristic function by replacing the infinite sum in the exponential power by

the finite, with the upper limit of N. I will leave the infinite sum, instead of the finite sum for the purpose of the more convenient definition, as will be explained later. Expanding the exponent in Taylor series with respect to z we are left with the following expression for the distribution function:

$$\rho(n) = \frac{\Theta_0}{n!}\frac{d^n}{dz^n}\left(\sum_{r=0}^{\infty}\frac{1}{r!}\left(\sum_{m=1}^{\infty} f_m z^m\right)^r\right)\Big|_{z=0}. \tag{C.5}$$

One can now employ the wonderful properties of the multinomial coefficients, which are defined by the following formula [29]:

$$\left(\sum_{m=1}^{\infty} f_m z^m\right)^r \equiv r!\sum_{n=r}^{\infty}\frac{z^n}{n!}\sum(n; a_1, a_2, a_3..., a_n)^* f_1^{a_1} f_2^{a_2} f_3^{a_3}...f_n^{a_n}, \tag{C.6}$$

summed over $a_1 + a_2 + a_3 + ... + a_n = r$ and $a_1 + 2a_2 + 3a_3 + .. + na_n = n$, where the multinomial coefficients have the following closed form expression:

$$(n; a_1, a_2, a_3..., a_n)^* = n!/1^{a_1}a_1!2^{a_2}a_2!3^{a_3}a_3!...n^{a_n}n! \tag{C.7}$$

with the same restricted summation $a_1 + 2a_2 + 3a_3 + .. + na_n = n$. The meaning of these coefficients is the number of permutations of $n = a_1 + 2a_2 + 3a_3 + .. + na_n$ symbols composed of a_k cycles of length k for $k = 1, 2, 3, ..., n$. The useful property of the multinomial coefficients which connects them to the Stirling numbers of the first kind is $\sum(n; a_1, a_2, a_3..., a_n)^* = (-1)^{n-m}S_n^{(m)}$, summed over $a_1 + a_2 + a_3 + ... + a_n = m$ and $a_1 + 2a_2 + 3a_3 + .. + na_n = n$.

One can apply the expression (C.6) to obtain the distribution function:

$$\rho(n) = \frac{\Theta_0}{n!}\frac{d^n}{dz^n}\left(\sum_{r=0}^{\infty}\sum_{n=r}^{\infty}\frac{z^n}{n!}\sum(n; a_1, a_2, ..., a_n)^* f_1^{a_1} f_2^{a_2}...f_n^{a_n}\right)\Big|_{z=0} \tag{C.8}$$

Now, changing the summation order and employing the discussed above conclusion, that n-th derivative is non zero only for the n-th term in the expansion, the result

can be written as

$$\rho(n) = \frac{\Theta_0}{n!} \sum_{m=0}^{n} \sum_{\left(\begin{array}{l} a_1 + a_2 + ... + a_n = m \\ a_1 + 2a_2 + ... + na_n = n \end{array} \right)} (n, a_1, a_2, ..., a_n)^* \prod_{j=1}^{n} f_j^{a_j}. \qquad \text{(C.9)}$$

The latter formula does not look very simple from the first sight. Nevertheless, it is very useful and, in particular, provides a convenient basis for the study of the limiting cases and asymptotical behavior, which are discussed in details in Section F of the Chapter II.

APPENDIX D

SELF-CONSISTENT SYSTEM OF EQUATIONS FOR TRANSVERSE CURRENT FEL AMPLIFIER

Consider a sheet electron beam with an infinitesimal thickness over a coordinate η which is moving in the undulator field and uniform magnetic field $\vec{H}_0 = H_0\vec{\xi}_0$. Electron beam is injected into a waveguide parallel to the direction of propagation of one of the partial waves. Interaction space is a planar waveguide which is formed by two parallel corrugated metal plates perpendicular to the axis η and a distance between plates a_0. Assume that electron beam excites TEM mode of the waveguide.

We seek a solution for vector-potential as a sum of a vector potential of operating mode and undulator field as follows:

$$\begin{cases} \vec{A}_s = \mathrm{Re}\left(A_s(\xi,\zeta)e^{i\omega t - ik\xi}\vec{\zeta}_0\right), \\ \vec{A}_u = \mathrm{Re}\left(A_u(\xi,\zeta)e^{ih_u\xi}\vec{\eta}_0\right), \end{cases} \tag{D.1}$$

where $A_s(\xi,\zeta)$ is slowly varying amplitude of the operating mode, which essentially is a combination of the amplitudes of two partial waves, $h_u = 2\pi/d_u$, d_u is undulator period, $k = \omega/c$, $\vec{\xi}_0$, $\vec{\eta}_0$, $\vec{\zeta}_0$ are unit vectors of the cartesian system of coordinates.

Consider an interacton between electron beam and electromagnetic field in the conditions of undulator synchronism: $\omega = \Omega_b + hv_{||}$, where $\Omega_b = h_u v_{||}$ is undulator frequency. Assume that electromagnetic wave and undulator field are far from the cyclotron resonance with electrons: $|\Omega_b - \omega_H|T >> 2\pi$, where $\omega_{H_0} = eH_0/m_0c\gamma_0$ is cyclotron frequency, $v_{||}$ is longitudinal velocity of electrons, $\gamma_0 = (1 - v^2/c^2)^{-1/2} >> 1$ is relativistic factor, T is characteristic time of an interaction (a reverse gain).

Equation of motion of a particle in electromagnetic fields has a form:

$$\frac{d\vec{p}}{dt} = e\vec{E} + \frac{e}{c}\left[\vec{v}, \vec{H}\right], \tag{D.2}$$

where electric and magnetic fields are functions of a total vector-potential and driving uniform magnetic field $\vec{H}_0$:

$$\vec{E} = -\frac{1}{c}\frac{\partial \vec{A}}{\partial t}, \vec{H} = \vec{H}_0 + \vec{\nabla} \times \vec{A}. \tag{D.3}$$

Introducing new variables: $p_\pm = p_\zeta \pm i p_\eta$, $p_{||} = p_\xi$, $\theta_s = \omega t - k\xi$, $\theta_u = h_u \xi$, one can obtain a system of equations where for the transverse components of momentum one has the following expressions:

$$p_\pm = -\frac{e\Omega}{c}\left(\frac{A_s e^{i\theta_s}}{\Omega \pm \omega_H} \pm i\frac{A_u e^{i\theta_u}}{\Omega \pm \omega_H}\right). \tag{D.4}$$

Taking into account Eq. (D.4) and starting from equation for energy:

$$\frac{d\epsilon}{dt} = e(\vec{v}_\perp \vec{E}_\perp), \tag{D.5}$$

after averaging, Eq. (D.5) can be written as follows:

$$\frac{dW}{d\tilde{\xi}} = -\left(\frac{1}{W-q} - \frac{1}{W+q}\right) \mathrm{Re}\left(\tilde{A}_u \tilde{A}_s e^{i\theta}\right), \tag{D.6}$$

where $W = \gamma/\gamma_0$ is dimensionless energy, $\tilde{\xi} = k\xi/2\gamma_0^2$ is dimensionless longitudinal coordinate, $q = \omega_{H_0}/\Omega$, $\tilde{A}_{u,s} = eA_{u,s}/\sqrt{2}mc^2$ is dimensionless amplitude of vector-potential, $\tilde{\theta} = \theta_s - \theta_u = \omega t - (k + h_u)\xi$ is a combinational phase obeys the following equation of motion:

$$\frac{d\tilde{\theta}}{d\tilde{\xi}} = \frac{\omega}{v_{||}} - (k + h_u). \tag{D.7}$$

Employing Eq. (D.4) and averaging Eq. (D.7) one has the following equation for the

combinational phase:

$$\frac{d\tilde{\theta}}{d\tilde{\xi}} = \frac{1}{W^2} + \frac{|\tilde{A}_u|^2 + |\tilde{A}_s|^2}{2}\left(\frac{1}{(W-q)^2} + \frac{1}{(W+q)^2}\right) -$$

$$- \left(\frac{1}{(W-q)^2} - \frac{1}{(W+q)^2}\right) \mathrm{Im}\left(\tilde{A}_u \tilde{A}_s e^{i\tilde{\theta}}\right) - \tilde{\Delta}, \qquad \text{(D.8)}$$

where $\tilde{\Delta} = 2\gamma_0^2 h_u/k$. The boundary conditions to Eqs. (D.6), (D.8) have the form:

$$W|_{\tilde{\xi}=0} = 1, \quad \tilde{\theta}|_{\tilde{\xi}=0} = \tilde{\theta}_0 \in [0, 2\pi). \qquad \text{(D.9)}$$

One can obtain FEL system of equations in x, y, z coordinates, where electron beam is not collinear to any of the axes (see Fig. 39). A coordinate transformation can be written as follows:

$$\xi = \frac{h}{k}x + \frac{\bar{h}}{2k}z, \qquad \zeta = \frac{\bar{h}}{2k}x - \frac{h}{k}z, \qquad \text{(D.10)}$$

where index s in the wavenumbers of the operating mode is understood, $h = \sqrt{k^2 - \bar{h}^2/4}$, $k = \omega/c$. This transformation illustrates a collinearity of the electron beam and a partial wave A_+. Eqs. (D.6), (D.8) in x, z coordinates have the following form:

$$\frac{\partial A_+}{\partial Z} + \frac{\partial A_+}{\partial X} + i\alpha A_- = \frac{1}{\pi}\int_0^{2\pi} e^{-i\theta} d\theta_0, \qquad \frac{\partial A_-}{\partial Z} - \frac{\partial A_-}{\partial X} + i\alpha^* A_+ = 0, \qquad \text{(D.11)}$$

$$\left(\frac{\partial}{\partial Z} + \frac{\partial}{\partial X}\right)^2 \theta = \mathrm{Re}\left(A_+ e^{i\theta}\right),$$

where

$$\tilde{\theta} = \omega t - hz - \bar{h}x/2 - h_u\left(\frac{h}{k}x + \frac{\bar{h}}{2k}z\right), \qquad \Delta = 2\gamma_0^2\left[\left(\frac{\bar{h}^2}{4h^2} + \frac{h_u}{k}\right)\tilde{\Delta} + \frac{h_u}{k}\right] \qquad \text{(D.12)}$$

$$\tilde{z} = \frac{k}{h}\frac{kz}{2\gamma_0^2}, \qquad \tilde{x} = \frac{2k}{\bar{h}}\frac{kx}{2\gamma_0^2}.$$

We seek a field of the operating mode as a sum of two partial waves coupled on a

lattice, where one of them is amplified by an electron beam (compare with Eq. (6.5)):

$$\vec{\mathrm{A}}_s = \vec{y}^0 \mathrm{Re}\left[\left(\mathrm{A}_+(x,z)e^{-i\bar{h}x/2} + \mathrm{A}_-(x,z)e^{i\bar{h}x/2}\right)e^{i\omega t - ihz}\right], \tag{D.13}$$

where $\mathrm{A}_\pm(x,z)$ are slowly varying function of their arguments. Equation of mode excitation can be written as follows:

$$\left(\frac{h}{k}\frac{dA_\pm}{dz} \pm \frac{\bar{h}}{2k}\frac{dA_\pm}{dx}\right)e^{i(\omega t - hz)\pm i\frac{\bar{h}}{2}x} = \left\langle \frac{1}{N_\pm}\oint\left(\vec{j^e}\vec{E}^*_\pm - \vec{j^m}\vec{H}^*_\pm\right)d\sigma\right\rangle\Big|_T, \tag{D.14}$$

where j^m is magnetic current (see Eq. (6.21)), j^e is electric current caused by an interaction between electron beam and partial wave A_+. Both currents do not contribute to equation for A_-. Integration in the right hand side of Eq. (D.14) is performed over the contour of unperturbed waveguide, $N_\pm$ are the mode norms. After time averaging one can write the system of the following equations:

$$\frac{h}{k}\frac{\partial A_+}{\partial z} + \frac{\bar{h}}{2k}\frac{\partial A_+}{\partial x} + i\tilde{\alpha}A_- = \frac{1}{2\pi}\int_0^{2\pi} j^e e^{-i\tilde{\theta}}d\tilde{\theta}_0, \quad \frac{h}{k}\frac{\partial A_-}{\partial z} - \frac{\bar{h}}{2k}\frac{\partial A_-}{\partial x} + i\tilde{\alpha}^*A_+ = 0, \tag{D.15}$$

where $\tilde{\alpha} = (l_0/4a_0)(\bar{h}^2/2k)$ is a coupling coefficient. The right hand side of Eq. (D.15) is averaged over the phase of injected electrons, $j^e = \rho v_\perp$, where ρ is a volume charge density. After employing charge conservation law ($\rho v_{||} = \rho_0 v_{||0}$) and introducing dimensionless variables from Eq. (D.12), Eq. (D.15) can be rewritten as follows:

$$\frac{\partial \tilde{A}_+}{\partial \tilde{z}} + \frac{\partial \tilde{A}_+}{\partial \tilde{x}} + i\tilde{\alpha}\tilde{A}_- = \frac{eI_0}{2mc^3\gamma a_0}\tilde{A}_u\int_0^{2\pi}\left(\frac{1}{W-q} - \frac{1}{W+q}\right)e^{-i\tilde{\theta}}d\tilde{\theta}_0,$$

$$\frac{\partial \tilde{A}_-}{\partial \tilde{z}} - \frac{\partial \tilde{A}_-}{\partial \tilde{x}} + i\tilde{\alpha}^*\tilde{A}_+ = 0, \tag{D.16}$$

where I_0 is linear current density.

Consider an approximation of inertial bunching where particle energy does not change much relatively to its initial value: $W = 1 + w$, $w << 1$. Introducing a Pierce parameter $C = \left((eI_0\lambda^2\mu\kappa^2)(mc^3 8\pi\gamma a_0)\right)^{1/3}$, one can write equations of mode

excitation and equation of motion as follows:

$$\frac{\partial A_+}{\partial Z}+\frac{\partial A_+}{\partial X}+i\alpha A_-=\frac{1}{\pi}\int_0^{2\pi}e^{-i\theta}d\theta_0,\qquad \frac{\partial A_-}{\partial Z}-\frac{\partial A_-}{\partial X}+i\alpha^* A_+=0, \tag{D.17}$$

$$\left(\frac{\partial}{\partial Z}+\frac{\partial}{\partial X}\right)^2\theta=\mathrm{Re}\left(A_+e^{i\theta}\right),$$

where $Z=zCk^2/h$, $X=2xCk^2/\bar{h}$, $L_z=l_zCk^2/h$, $L_x=2l_xCk^2/\bar{h}$, $\tau=C\omega t$, $A_\pm=\mathrm{A}_\pm e\kappa\mu/\gamma mc\omega C^2$, $\kappa=\beta_\perp/\beta_{||}=2q\tilde{A}_u/(1-q)$ is electron-wave coupling parameter, $\beta_\perp$ is oscillatory velocity of particles in the undulator, $\mu\approx\gamma^{-2}$ is bunching parameter, γ is relativistic mass-factor, I_0 is linear current density, θ is electron phase. I assume exact synchronism condition: $\Delta=1$. The normalized wave coupling parameter is given by [43]:

$$\alpha(X)=\frac{l_0\bar{h}}{4ka_0C}\sin\phi, \tag{D.18}$$

where $\phi=\arcsin\frac{\bar{h}}{2k}$ - angle between the wavevector of the partial wave and waveguide axis, a_0 - distance between plates (see Fig. 2). For the given corrugation profile in Eq. (7.12) the coupling parameter changes its sign on the waveguide axis, which results in adding phase factor $e^{i\psi(X)}$ into Eq. (D.18).

If initially an electron beam is not modulated, then the boundary conditions for the particle can be written as: $\theta|_{X=0}=\theta_0\in[0,2\pi)$, $(\partial/\partial Z+\partial/\partial X)\theta|_{X=0}=\delta$, where δ is a synchronism detuning between electrons and wave on the operating frequency. If the input signal is a wave packet $A_0(X)$ entering the system under the angle corresponding to the direction of propagation of the partial wave A_+, then the boundary conditions for Eq. (D.17) have the form:

$$A_+|_{Z=0}=A_0(X),\quad A_-|_{Z=0}=0,\quad A_+|_{X=0}=0\quad A_-|_{X=L_x}=0 \tag{D.19}$$

It is worth noting that Eq. (D.15) is equivalent to equation for FEL generator with 1D Bragg resonator by replacing a time variable by a spatial one [42]. In contrast

with previous works this system of equation allows one to describe both: longitudinal (Z-axis) and transverse (X-axis) field structures.

VITA

Konstantin Dorfman was born in Gorky, USSR. In September 2002, he entered Nizhny Novgorod State University and received his Bachelor of Science in physics in June 2006. In August 2006, he entered Texas A&M University and received his Master of Science degree in physics in August 2008. In September 2008 he entered Texas A&M University and completed the requirements for the Doctor of Philosophy degree in physics in May 2009. He may be reached at Department of Physics, Texas A&M University, College Station, Texas, 77843-4242.

The typist for this dissertation was Konstantin Dorfman.